REPORT 1336

AN INVESTIGATION OF SINGLE- AND DUAL-ROTATION PROPELLERS AT POSITIVE AND NEGATIVE THRUST, AND IN COMBINATION WITH AN NACA 1-SERIES D-TYPE COWLING AT MACH NUMBERS UP TO 0.84 [1]

By Robert M. Reynolds, Robert I. Sammonds, and John H. Walker

SUMMARY

An investigation has been made to determine the aerodynamic characteristics of the NACA 4-(5)(05)-041 four-blade, single-rotation propeller and the NACA 4-(5)(05)-037 six- and eight-blade, dual-rotation propellers in combination with various spinners and NACA D-type spinner-cowling combinations at Mach numbers up to 0.84. Propeller force characteristics, local velocity distributions in the propeller planes, inlet pressure recoveries, and static-pressure distributions on the cowling surfaces were measured for a wide range of blade angles, advance ratios, and inlet-velocity ratios. Included are data showing: (a) the effect of extended cylindrical spinners on the characteristics of the single-rotation propeller, (b) the effect of variation of the difference in blade angle setting between the front and rear components of the dual-rotation propellers, (c) the negative- and static-thrust characteristics of the propellers with 1-series spinners, and (d) the effects of ideal- and platform-type propeller-spinner junctures on the pressure-recovery characteristics of the single-rotation propeller-spinner-cowling combination. All tests were made at an angle of attack of 0°, and, except for the static-thrust data, were made at Reynolds numbers of 1.5 and 1.0 million per foot, respectively, for the single- and dual-rotation propeller-spinner-cowling combinations. A description of the 1000-horsepower propeller dynamometer used to obtain the data is also included in the report.

The highest Mach number at which the propellers with the NACA 1-series spinners operated without marked compressibility losses was about 0.7. The maximum efficiencies of the propellers at this Mach number were 79, 83, and 82 percent, respectively, for the four-, six-, and eight-blade propellers at a blade angle of 65°. The results indicate that for operation of the propellers at Mach numbers greater than about 0.8, highest efficiencies would be obtained at lower advance ratios and lower blade angles.

Substantially higher efficiencies were obtained for the NACA 4-(5)(05)-041 propeller with extended cylindrical spinners as compared to those obtained for the propeller with an NACA 1-series spinner, amounting to as much as 15 percent at the highest Mach number and blade angle of the tests. Due to the apparent increase in propeller thrust associated with favorable interference effects of the cowling on the flow field at the propeller, maximum efficiencies obtained with the single- and dual-rotation propellers operating in the presence of the cowlings were higher at all Mach numbers and blade angles than those for the isolated propeller-spinner combinations.

Addition of the propellers, with platform-type propeller-spinner junctures, to the spinner-cowling combinations resulted in a considerable decrease in pressure recovery at the inlet. At a Mach number of 0.8 and at the design inlet-velocity ratios, ram-recovery ratios of about 0.87 were obtained for the various propeller-spinner-cowling combinations, as compared to recovery ratios of about 0.96 with the propeller removed.

INTRODUCTION

Possible application of the turbine-propeller type of power plant for moderately high-speed long-range airplanes has led to a need for data concerning the characteristics of propellers and propeller-spinner-cowling combinations suitable for use with large turbine engines in this speed regime. Two general problems are involved, that of obtaining satisfactory propeller performance, and that of providing efficient air induction to the turbine engines.

Propellers driven by modern high-power gas-turbine engines must perform satisfactorily throughout a wide speed range, from static and near static conditions to high subsonic speeds, at either positive or negative thrust. The large thrust at low speed, resulting in a reduction in take-off run, constitutes one of the greatest advantages of the turbine-propeller combination over other means of aircraft propulsion. Interest in propeller performance in the negative-thrust range stems from the desire to utilize the negative thrust for landing and maneuvering, and to calculate and provide controls for the alleviation of the large drag forces which result in the event of an engine failure. Many investigations have been conducted in recent years, such as those reported in references 1 to 5, to determine the effects of compressibility, blade thickness ratio, and camber on the high-speed performance of two-blade, single-rotation propellers with cylindrical spinners. However, the data from these tests do not permit the assessment of the effects on performance of either practical spinner installations or the high solidities required to absorb large horsepowers. High-solidity, dual-rotation propellers, in spite of the advantages of smaller diameter, absence of reaction torque,

[1] Summarizes the results of NACA RM's A54J22 by Robert I. Sammonds and Robert M. Reynolds, 1955; A54G13 by John H. Walker and Robert M. Reynolds, 1954; A53B06 by Robert M. Reynolds, Robert I. Sammonds, and George C. Kenyon, 1953; A52D01a by Robert I. Sammonds, and Ashley J. Molk, 1952; A52I19a by Robert M. Reynolds, Donald A. Buell, and John H. Walker, 1952.

less noise, and theoretically greater efficiency over single-rotation propellers capable of absorbing equal power, have received only limited research effort, such as the investigation reported in reference 6 for a high advance-ratio design. Data on the static- and negative-thrust characteristics of propellers are also somewhat limited. The most recent data on the static characteristics of a two-blade, single-rotation propeller are reported in reference 7, and the results of previous investigations of numerous single- and dual-rotation propellers are correlated in reference 8. A number of reports relating to the performance of propellers operating at negative thrust are available, but most of the data, such as those reported in reference 9, are for propellers of older design and were obtained only at low speeds.

The efficiency of the air-induction system has a large effect on the power and fuel economy of a gas-turbine engine, as analyzed in reference 10. In the case of the propeller-spinner-cowling combination, the induction efficiency can be quite low as a result of interference effects of the propeller blade shanks and pressure losses in the spinner boundary layer. Reference 11 presents a procedure, from the results of tests at low speed, for the selection of D-type spinner-cowling combinations for specific high-speed requirements, the validity of which has been subsequently shown for high speeds in reference 12. The only data available showing the effects of propeller operation and propeller-spinner-juncture configuration on the internal-flow characteristics of spinner-cowling combinations of this type have been reported in references 13 and 14.

An investigation has been made in the Ames 12-foot pressure wind tunnel to provide additional data useful in the design and development of propellers and propeller-spinner-cowling combinations for application at high subsonic speeds. Presented herein are force-test results for the following configurations: (a) the NACA 4–(5)(05)–041 four-blade, single-rotation propeller and the NACA 4–(5)(05)–037 six-, and eight-blade, dual-rotation propellers operating at positive thrust with NACA 1-series spinners and with NACA D-type spinner-cowling combinations, (b) the NACA 4–(5)(05)–041 propeller at positive thrust with extended cylindrical spinners, and (c) the NACA 4–(5)(05)–041 and 4–(5)(05)–037 propellers with NACA 1-series spinners operating at negative thrust and at near static conditions. Included are results of measurements of the internal pressure-recovery characteristics of the propeller-spinner-cowling combinations, surface pressure distributions on the cowlings, and local velocity distributions in the propeller planes of the combinations.

The tests were conducted at Mach numbers up to 0.84, for a wide range of blade angles and inlet-velocity ratios. All tests were made at an angle of attack of 0° and, except for the static-thrust data, were made at Reynolds numbers of 1.5 and 1.0 million per foot, respectively, for the single- and dual-rotation propeller-spinner-cowling combinations.

SYMBOLS

a	speed of sound,[2] ft/sec
b	blade width, ft
B	number of blades
c_{l_d}	blade-section design lift coefficient
C_p	pressure coefficient, $\frac{p_l-p}{q}$
C_P	power coefficient, $\frac{P}{\rho n^3 D^5}$
C_T	thrust coefficient, $\frac{T}{\rho n^2 D^4}$
d	spinner diameter, in.
D	propeller diameter, ft
h	maximum thickness of blade section, ft
HP	horsepower
J	advance ratio, $\frac{V_e}{nD}$
M	Mach number, $\frac{V}{a}$
M_t	tip Mach number, $M\sqrt{1+\frac{\pi^2}{J^2}}$
n	propeller rotational speed, rps
p	static pressure,[2] lb/sq ft
p_t	total pressure,[2] lb/sq ft
$\frac{p_{t_1}-p}{p_t-p}$	ram-recovery ratio
P	power, ft-lb/sec
q	dynamic pressure, $\frac{\rho V^2}{2}$, lb/sq ft
r	radius from center of rotation
R	propeller tip radius, ft
S	propeller disc area, sq ft
T	thrust, lb
T_c	thrust coefficient, $\frac{T}{\rho V^2 D^2}$
V	air-stream velocity,[2] ft/sec
V_e	equivalent free-air velocity (air-stream velocity corrected for tunnel-wall constraint on the propeller slipstream), ft/sec
$\frac{V_1}{V}$	inlet-velocity ratio
x	distance along the longitudinal axis from any reference, such as the leading edge of the spinner or cowl, in.
X	total length along the longitudinal axis of any component of the model, such as the spinner or cowl, in.
β	propeller blade angle at 0.75 R
β_d	design propeller section blade angle
$\Delta\beta$	difference in blade angle between the front and rear components of the dual-rotation propellers, $\beta_F-\beta_R$
η	efficiency, $\frac{C_T}{C_P}J$
ρ	mass density of air,[2] slugs/cu ft

SUBSCRIPTS

1	rake location in cowling inlet
c	cowl
cr	critical, corresponding to a local Mach number of 1.0
F	front component of dual-rotation propeller
i	cowling inner lip

[2] As used herein, values of p, p_t, V, a, and ρ appearing without subscripts refer to conditions in the wind-tunnel air stream at a datum velocity that is uncorrected for wind-tunnel-wall constraint on the propeller slipstream but is corrected for blockage when the cowling is installed.

l	local
max	maximum
R	rear component of dual-rotation propeller
s	spinner

APPARATUS

PROPELLER DYNAMOMETER

Sketches, coordinates, and photographs of the 1000-horsepower propeller dynamometer with the NACA 1-series and extended cylindrical spinners used in these tests in the Ames 12-foot pressure wind tunnel are presented in figure 1. A detailed description of the dynamometer, including a discussion of the results of calibrations of the thrust gages, torquemeters, and tunnel air stream in the vicinity of the dynamometer, is given in the appendix.

PROPELLERS

The geometric characteristics of the NACA 4-(5)(05)-041 four-blade, single-rotation propeller and the NACA 4-(5)(05)-037 six- and eight-blade, dual-rotation propellers were established, through use of the charts of reference 15, for minimum induced energy losses for operation at advance ratios of 3.7 and 4.2, respectively. NACA 16-series blade sections were employed for all three propellers. The numer-

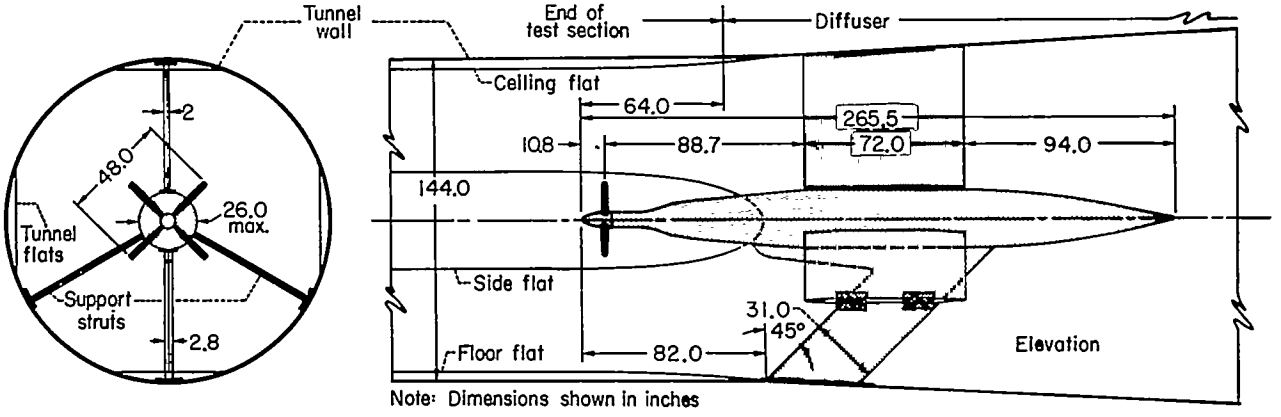

(a)

COORDINATES OF THE DYNAMOMETER WITH THE 7.20-INCH-DIAMETER, 1-SERIES SPINNER
(Coordinates in inches)

Distance from nose of spinner, x	Radius from center of rotation, r	Distance from nose of spinner, x	Radius from center of rotation, r	Distance from nose of spinner, x	Radius from center of rotation, r	Distance from nose of spinner, x	Radius from center of rotation, r
0.000	0.000	3.996	2.593	29.413	3.626	48.63	8.65
.096	.336	5.076	2.888	29.913	3.675	50.21	8.81
.270	.597	6.048	3.122	30.413	3.749	95.96	13.00
.486	.827	7.992	3.437	30.913	3.850	99.46	13.00
.864	1.145	8.856	3.523	31.413	3.978	171.46	13.00
1.296	1.443	9.936	3.587	31.892	4.126	191.46	12.47
1.729	1.688	10.584	3.599	40.986	7.188	211.46	10.78
2.052	1.847	[1]10.800	3.600	42.850	7.650	231.46	8.00
2.484	2.040	28.691	3.600	44.770	8.050	251.46	4.05
3.024	2.256	28.913	3.603	46.690	8.380	265.46	0.00

[1] End of 1-series spinner profile; cylindrical portion of spinner extends to x = 13.73.

(b)

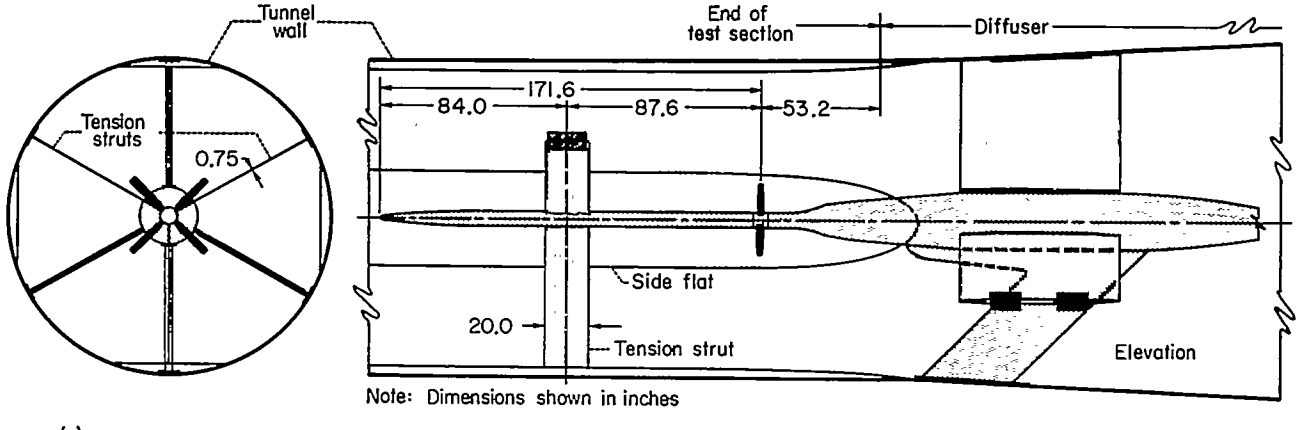

(c)

(a) General arrangement.
(b) Coordinates of the dynamometer with the 7.2-inch-diameter, 1-series spinner.
(c) Dynamometer with extended cylindrical spinner.

FIGURE 1.—Sketches, coordinates, and photographs of the 1000-horsepower propeller dynamometer in the Ames 12-foot pressure wind tunnel.

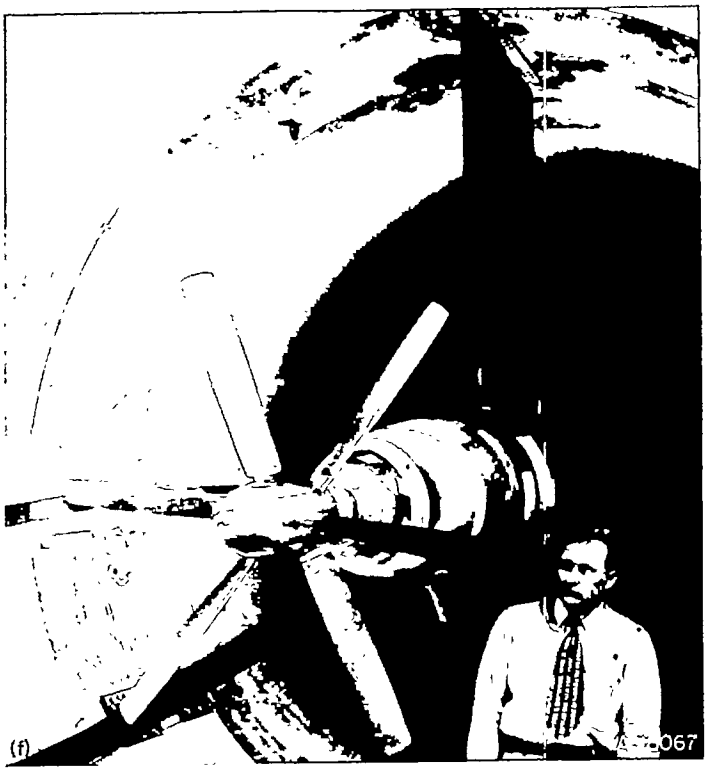

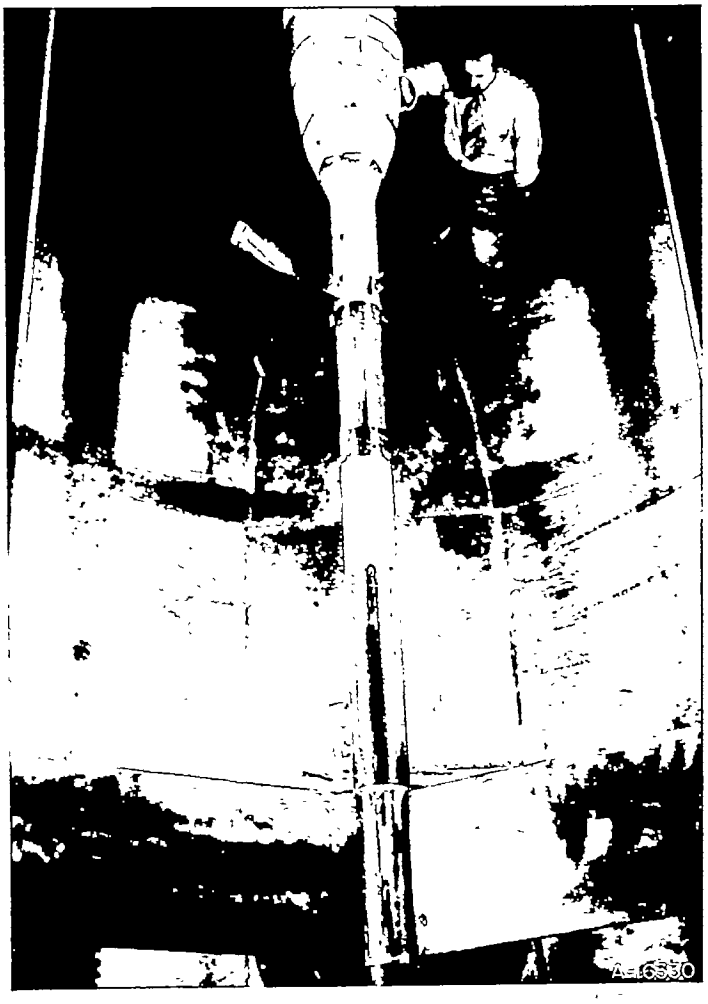

(d) Four-blade propeller and 7.2-inch-diameter, 1-series spinner installed on dynamometer.

(e) Four-blade propeller and extended cylindrical spinner installed on dynamometer.

(f) Six-blade propeller and 6.51-inch-diameter, 1-series spinner installed on dynamometer.

FIGURE 1.—Concluded.

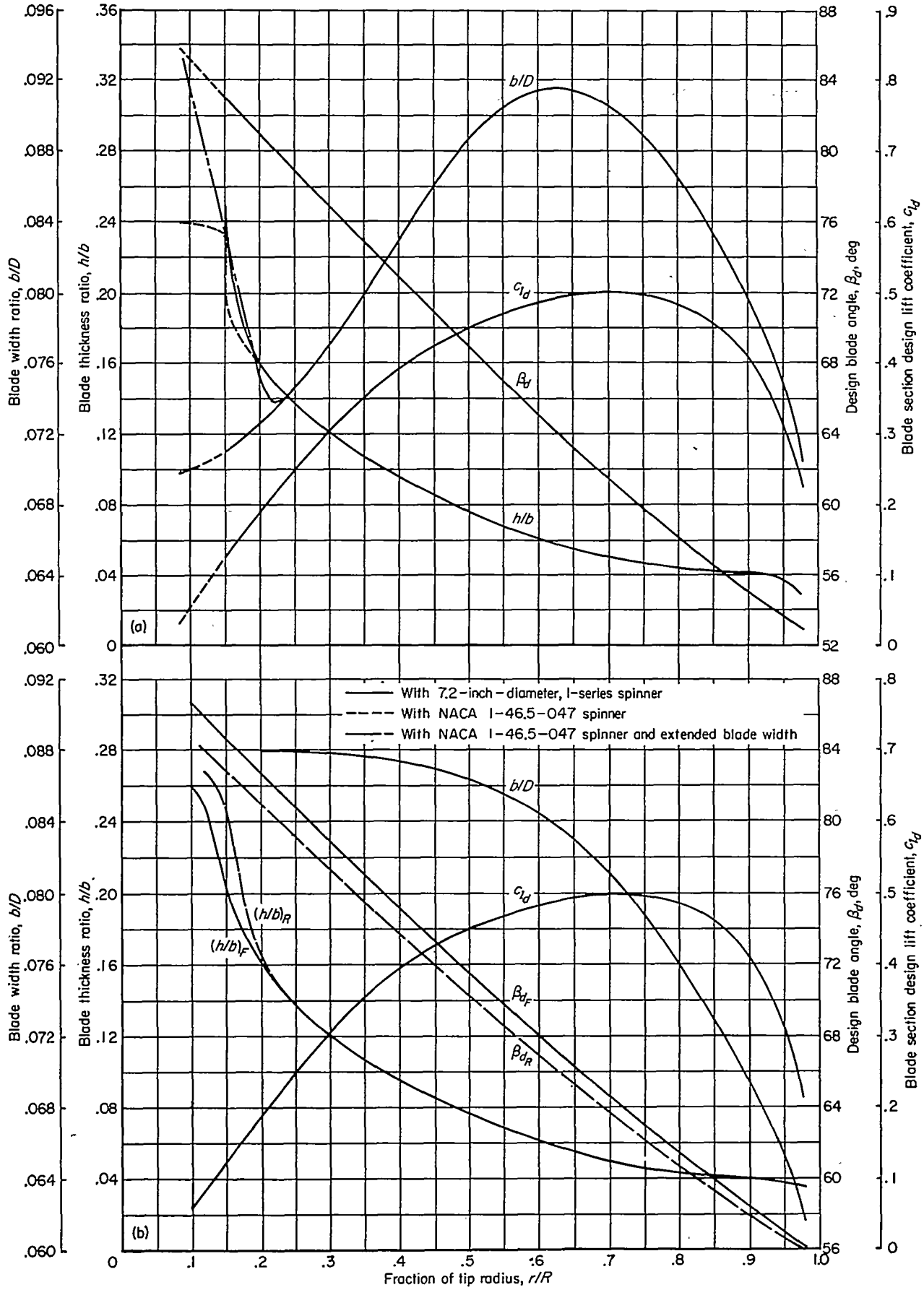

(a) NACA 4-(5)(05)-041 four-blade, single-rotation propeller.
(b) NACA 4-(5)(05)-037 six- and eight-blade, dual-rotation propellers.
FIGURE 2.—Propeller blade-form curves.

cal designations of the propellers are associated with the characteristics of the blade section at 0.70 of the tip radius. For example, the designation NACA 4–(5)(05)–041 for the four-blade, single-rotation propeller indicates a 4-foot-diameter propeller having a section design lift coefficient of 0.50, a section thickness ratio of 0.05, and a section solidity per blade of 0.041 at 0.70 tip radius. The blade-width ratios, thickness ratios, section design lift coefficients, and twist distributions for the three propellers are shown by the blade-form curves in figure 2. The broken curves in figure 2, for the four-blade propeller, indicate modifications made to the inboard portions of the blades to adapt them to various spinners.

Except for total solidity, the NACA 4–(5)(05)–037 six-blade, dual-rotation propeller was identical to the eight-blade propeller.

SPINNERS AND SPINNER-COWLING COMBINATIONS

For tests of the propellers alone, that is, without cowlings, spinners with NACA 1-series nose sections (ref. 11) and cylindrical afterbodies were used in an attempt to provide a nearly uniform stream for the inboard sections of the blades. The spinner used with the four-blade propeller had a maximum diameter of 7.2 inches and a total length of 13.73 inches, with a 10.8-inch-long nose section contoured to the NACA 1-series profile. The dual-rotation propellers were tested with a spinner having a maximum diameter of 6.51 inches and a total length of 22.71 inches, with a 9.77-inch-long nose section contoured to the NACA 1-series profile. Sketches of these spinners, designated respectively as the 7.2-inch-diameter and 6.51-inch-diameter, 1-series spinners, are shown in figure 3.

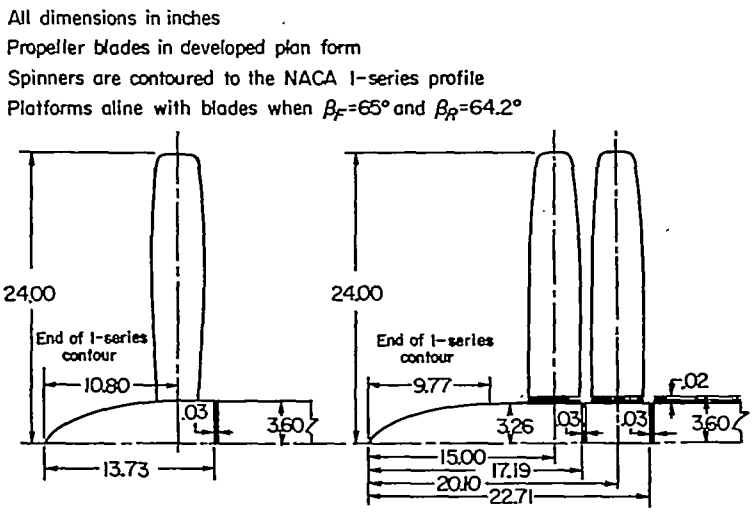

FIGURE 3.—Sketches of the propellers with NACA 1-series spinners.

The four-blade, single-rotation propeller was also tested in combination with two cylindrical spinners, extended approximately 14 feet ahead of the propeller as shown in figure 1. These spinners were 7.2 and 12.0 inches in diameter, and are designated as the 7.2- and 12.0-inch-diameter, extended cylindrical spinners. The nose portions of these spinners were NACA 1-series bodies of revolution having lengths equal to three times the maximum spinner diameters.

NACA 1-series, D-type spinner-cowling combinations for use with the single- and dual-rotation propellers were selected for a critical Mach number of 0.75 using the charts and designation of reference 11. The following combinations were chosen:

Propeller	Spinner	Cowling
Single rotation	NACA 1–46.5–047	NACA 1–62.8–070
Dual rotation	NACA 1–46.5–085	NACA 1–62.8–070

The NACA 1–62.8–070 cowlings were selected to operate at inlet-velocity ratios of 0.42 and 0.50 for the single- and dual-rotation cowlings, respectively. Both cowlings incorporated NACA 1-series inner-lip fairings to avoid separation of the air flow from the inner lip at high inlet-velocity ratios. The NACA 1–46.5–047 and 1–46.5–085 spinners were chosen as the smallest spinners that would enclose, respectively, representative single- and dual-rotation propeller hub assemblies. Sketches, coordinates, and photographs of the propeller-spinner-cowling combinations are shown in figure 4.

PROPELLER-SPINNER JUNCTURES

Two types of propeller-spinner junctures, designated as ideal and platform junctures, were used in these tests. The ideal type of juncture was formed by extending the propeller blade with filler blocks to the surface of the spinner and sealing all gaps. This type of juncture required a separate set of filler blocks for each blade-angle setting. The platform-type juncture consisted of airfoil-shaped lands mounted integrally with the spinner at a fixed angle and of sufficient height to place the gap between the land and the propeller blade outside the spinner boundary layer.

Sketches of the platform junctures used in these tests are shown in figures 3 and 4. It may be noted that the surfaces of the platform and propeller blade that bound the gap on the single-rotation propeller with the NACA 1–46.5–04 spinner and on the dual-rotation propellers with the 6.51-inch-diameter, 1-series spinner were formed by planes transverse to the blade axis. In contrast, for the dual-rotation propellers with the NACA 1–46.5–085 spinner, the surfaces of the platform and propeller blade that bound the gap were formed by rotating the surface element defined by the platform coordinates, tabulated in figure 4, about the axis of the propeller blade in order that the gap between the platform and blade remain unchanged as the blade angle was varied. The platforms were set to aline with the propeller blade sections at a blade angle setting of 60° for the single-rotation propeller, and at blade angle settings of 65° and 64.2°, respectively, for the front and rear components of the dual-rotation propellers.

SPINNER-COWLING INSTRUMENTATION

Four total-head rakes and two static-pressure rakes located in the cowling as shown in figure 4, were used to measure the inlet total and static pressures used in computing ram-recovery and inlet-velocity ratios. The total-head rakes were located 90° apart in the inlet and were shielded against circumferential flow components by means of cambered airfoils, as described in reference 16, spanning the annular duct. The static-pressure rakes were located 180° apart

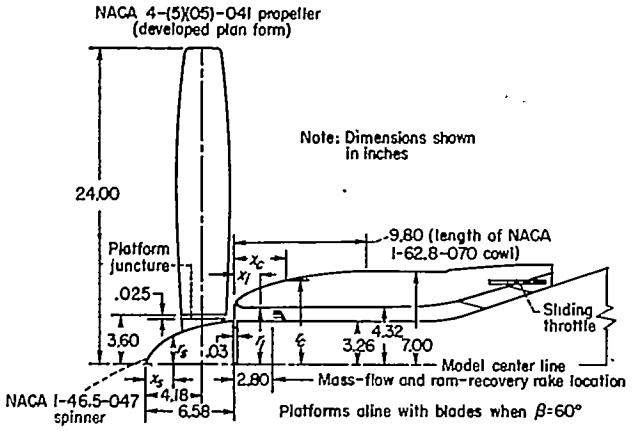

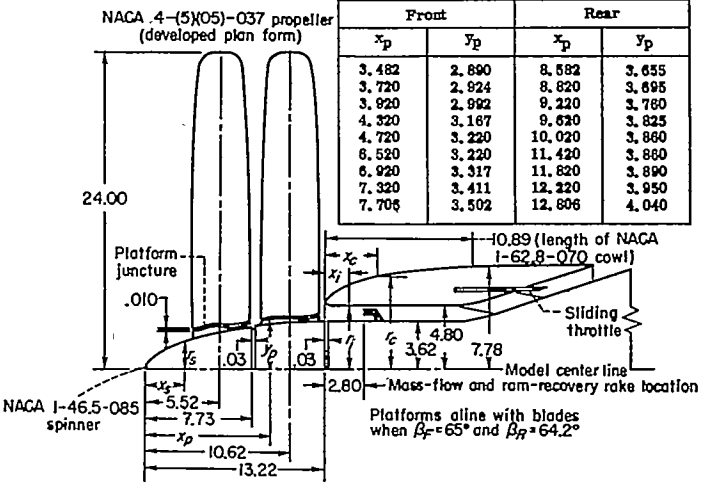

Platform coordinates			
Front		Rear	
x_p	y_p	x_p	y_p
3.482	2.890	8.582	3.655
3.720	2.924	8.820	3.695
3.920	2.992	9.220	3.760
4.320	3.167	9.620	3.825
4.720	3.220	10.020	3.860
6.520	3.220	11.420	3.860
6.920	3.317	11.820	3.890
7.320	3.411	12.220	3.950
7.705	3.502	12.806	4.040

Single-rotation propeller-spinner-cowling

Distance from leading edge of spinner, x_s	NACA 1-46.5-047 spinner, radius, r_s	Distance from leading edge of cowl, x_c	NACA 1-62.8-070 cowl, radius, r_c	Distance from leading edge of cowl, x_l	NACA 1-series inner lip, radius, r_l
0	0	0	4.460	0	4.460
.013	.156	.020	4.581	.008	4.439
.026	.216	.039	4.628	.017	4.429
.039	.264	.059	4.668	.034	4.415
.066	.338	.098	4.723	.050	4.403
.132	.479	.196	4.834	.087	4.394
.197	.596	.294	4.925	.084	4.386
.263	.699	.392	5.005	.101	4.378
.329	.793	.490	5.078	.118	4.372
.526	1.035	.784	5.268	.134	4.366
.790	1.305	1.176	5.478	.168	4.355
1.053	1.528	1.568	5.651	.202	4.346
1.316	1.715	1.960	5.798	.244	4.337
1.579	1.885	2.352	5.931	.277	4.331
1.842	2.040	2.744	6.052	.311	4.326
2.106	2.182	3.136	6.162	.344	4.323
2.369	2.313	3.528	6.265	.378	4.320
2.632	2.433	3.920	6.359	.420	4.320
2.895	2.544	4.312	6.445	---	---
3.158	2.645	4.704	6.524	---	---
3.553	2.781	5.292	6.630	---	---
4.080	2.938	6.076	6.751	---	---
4.606	3.058	6.860	6.846	---	---
5.132	3.151	7.644	6.918	---	---
5.659	3.214	8.428	6.968	---	---
6.185	3.250	9.212	6.996	---	---
6.580	3.255	9.800	7.000	---	---

Dual-rotation propeller-spinner-cowling

Distance from leading edge of spinner, x_s	NACA 1-46.5-085 spinner, radius, r_s	Distance from leading edge of cowl, x_c	NACA 1-62.8-070 cowl, radius, r_c	Distance from leading edge of cowl, x_l	NACA 1-series inner lip, radius, r_l
0	0	0	4.955	0	4.955
.053	.240	.022	5.091	.005	4.939
.106	.337	.044	5.142	.009	4.932
.198	.460	.065	5.184	.019	4.921
.331	.589	.109	5.248	.028	4.913
.463	.721	.218	5.371	.037	4.905
.595	.830	.327	5.472	.047	4.899
.793	.977	.436	5.561	.070	4.884
1.058	1.151	.544	5.643	.093	4.873
1.454	1.380	.871	5.853	.117	4.863
1.851	1.579	1.198	6.032	.140	4.854
2.248	1.751	1.524	6.188	.187	4.838
2.644	1.906	1.851	6.321	.234	4.826
3.173	2.095	2.178	6.443	.280	4.816
3.702	2.267	2.613	6.590	.327	4.808
4.231	2.424	3.049	6.724	.374	4.803
4.760	2.570	3.484	6.847	.420	4.800
5.289	2.704	3.920	6.961	.467	4.799
5.818	2.827	4.356	7.065	---	---
6.347	2.939	4.791	7.161	---	---
7.140	3.091	5.227	7.249	---	---
8.198	3.265	5.880	7.367	---	---
9.255	3.398	6.751	7.503	---	---
10.313	3.501	7.840	7.630	---	---
11.371	3.571	8.711	7.703	---	---
12.429	3.612	9.800	7.761	---	---
13.222	3.617	10.889	7.778	---	---

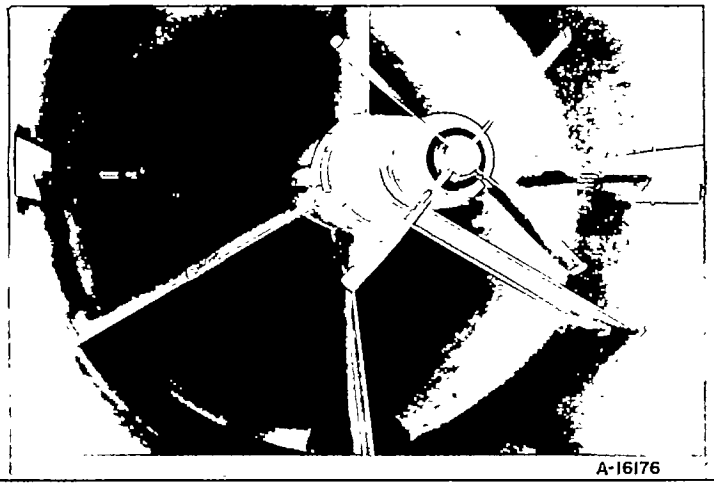

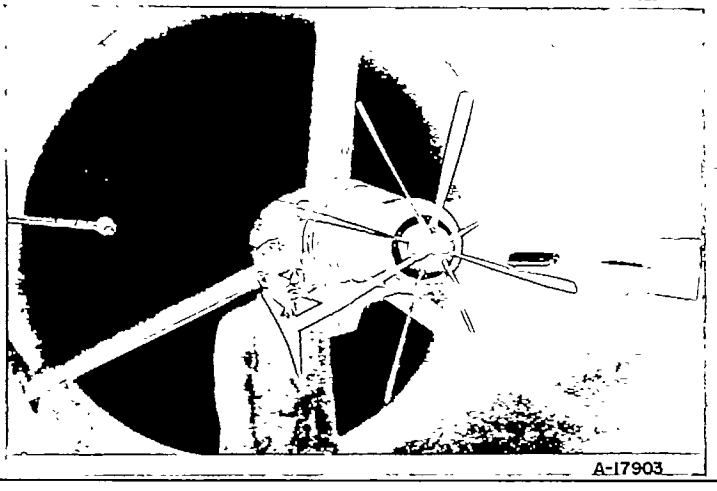

FIGURE 4.—Sketches, coordinates, and photographs of the single- and dual-rotation propeller-spinner-cowling combinations.

intermediate to the total-head rakes, and were constructed with the static tubes alternately displaced circumferentially to prevent flow interference between adjacent tubes. The total- and static-pressure rakes each contained eight tubes disposed radially across the duct in a manner such that the annular area between adjacent tubes was one-eighth of the total inlet area, and the annular area between the tubes at the extremities of the rake and the duct boundaries was one-sixteenth of the total inlet area. Calibrations of the total-head rakes indicated that the error in the measured total pressure was less than 1.0 percent at angles of attack, with respect to the shielding, up to 40° for Mach numbers up to 0.85. The static-pressure rakes were not calibrated.

The cowling used with the single-rotation propeller contained 29 flush static-pressure orifices located longitudinally with respect to the leading edge of the cowl as listed below:

External surface, in.					Inner-lip surface, in.
0	0.59	1.96	5.88	10.80	0.10
.10	.78	2.45	6.86	11.80	.20
.20	.98	2.94	7.84	12.80	.29
.29	1.18	3.92	8.82	13.80	.39
.39	1.57	4.90	9.80	14.80	------

The survey rake used to determine the local velocities in the propeller planes of the spinner-cowling combinations contained 24 static-pressure tubes spaced with respect to the innermost tube as follows:

Velocity-survey rake, in.			
0	2.00	7.00	19.00
.25	2.50	9.00	21.00
.50	3.00	11.00	23.00
.75	4.00	13.00	25.00
1.00	5.00	15.00	27.00
1.50	6.00	17.00	29.00

TESTS

The quantities measured and the range of the parameters investigated for the various combinations are given in table I. All of the tests were conducted at an angle of attack of 0°. Each run of the propeller tests was made at a fixed tunnel Mach number and blade angle, and also at a fixed throttle setting with the cowlings installed, and the dynamometer rotational speed varied to provide a suitable range of advance ratios. Each run was initiated near the zero-thrust condition and the rotational speed was increased (or decreased for negative thrust) until either the maximum capacity of the thrust gages or torquemeters, or the maximum rotational speed permitted by the structural characteristics of the propeller, or aural indication of stalling of the propellers was attained.

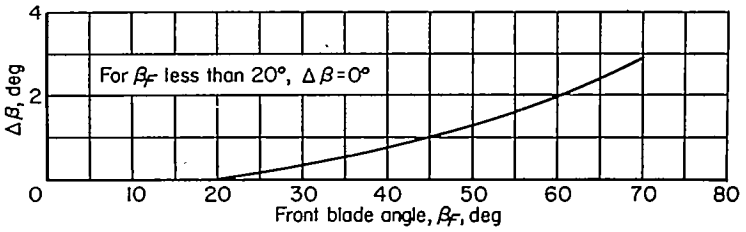

FIGURE 5.—The difference between the front and rear blade angles used for the optimum setting of the dual-rotation propellers.

Preliminary tests of the six-blade, dual-rotation propeller were made to determine the blade-angle setting of the rear component of the propeller required for equal division of power between the front and rear components of the propeller when operating near the advance ratio for maximum efficiency. The optimum blade angle difference, $\Delta\beta$, determined from these tests is shown in figure 5 as a function of the blade angle of the front component of the propeller. Subsequently, tests were made, as listed in table I, of the dual-rotation propellers at both the optimum blade-angle settings and the design blade-angle settings with $\Delta\beta=0.8°$.

REDUCTION OF DATA

MACH NUMBER AND AIR-STREAM VELOCITY

As discussed in the appendix, the test Mach numbers given in this report are the average Mach numbers over the disc area of the propeller, determined by velocity surveys made with the dynamometer and extended cylindrical spinners installed in the wind tunnel (fig. 1). Neither the test Mach numbers nor propeller tip Mach numbers were corrected for the effects of tunnel-wall constraint on the propeller slipstream. For tests made with the cowlings installed, however, the test Mach numbers, local Mach numbers, and corresponding dynamic pressures were corrected for the solid-blockage effects of the cowlings by the method of reference 17. In no case did the magnitude of these solid-blockage corrections exceed 1 percent of the uncorrected values.

For the computation of propeller advance ratios and efficiencies, the air-stream velocities were corrected for wind-tunnel-wall constraint on the propeller slipstream in accordance with the theory of reference 18. However, these tunnel-wall corrections to the stream velocity were neglected in the computation of inlet-velocity ratio for the spinner-cowling combinations with operating propellers. The ratio of the equivalent free-air velocity to the tunnel air-stream velocity determined experimentally using the method of reference 1 is compared in figure 6 with the theoretical values computed using the theory of reference 18. These data were obtained only for the four-blade, single-rotation propeller operating with the 7.2-inch-diameter, 1-series spinner. The good agreement, even at negative thrust, between the experimentally determined values and the theoretical values confirms the validity of the method. For the tests made with the cowlings installed, the air-stream velocities were also corrected for the solid-blockage effects of the cowlings, again by the method of reference 17.

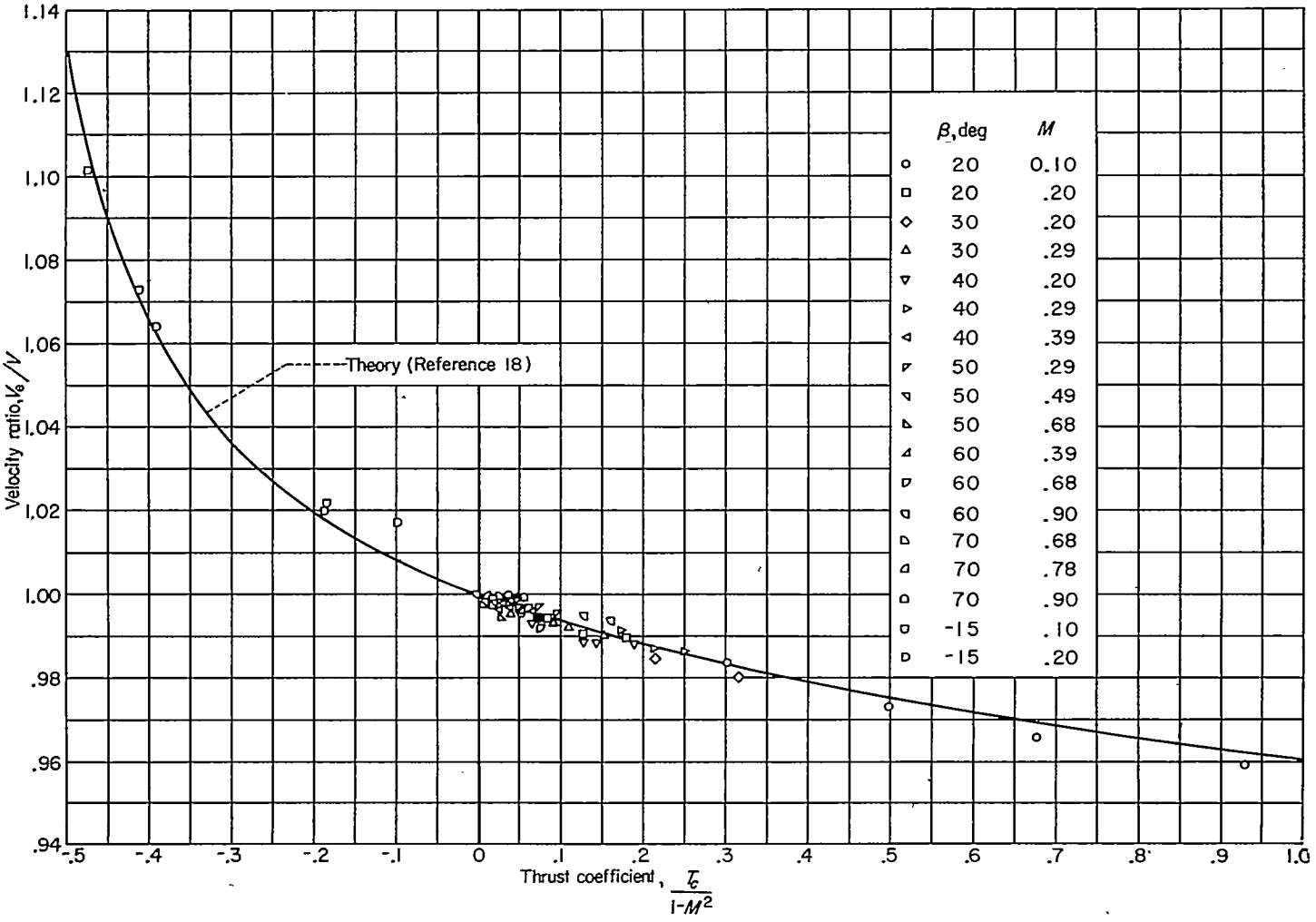

FIGURE 6.—Tunnel-wall-interference correction for a 4-foot-diameter propeller in the Ames 12-foot pressure wind tunnel.

PROPELLER THRUST AND TORQUE

Propeller thrust, as used herein, is the algebraic difference between the longitudinal force produced by the propeller-spinner combination, operating either alone or in the presence of the cowling, and the longitudinal force produced by the spinner, similarly alone or in the presence of the cowling, at the same air velocity, density, and cowling inlet conditions. The longitudinal forces on the spinner and the thrust forces due to pressures acting between the fixed and supported members of the dynamometer were measured and treated in the manner discussed in the appendix. It may be noted that the resultant longitudinal forces acting on the spinners at all test conditions, that is, either with or without a propeller and either for the spinner alone or in the presence of the cowling, were adjusted for computational purposes to correspond to a spinner base pressure equal to the static pressure of the free stream. This procedure determined the magnitude of the spinner drag tare forces but had no influence on the propeller thrust.

The torque produced in the propeller shafts was measured directly by means of calibrated inductance-type torquemeters described in the appendix. The measured torque was corrected for the small tare torque due to the friction of pressure seals and shaft roller bearings, as determined by calibrations with the propeller removed. Total torque for the dual-rotation propellers is the sum of the absolute values of the torques measured for the front and rear components of the propellers.

COWLING FLOW SURVEYS

Inlet-velocity ratios for the tests made with the cowlings installed were calculated by the method of reference 19. Conversion of inlet-velocity ratio, V_1/V, to mass-flow ratio, m_1/m, may be easily done, if desired, by use of figure 4 of reference 19.

The ram-recovery ratio presented as a function of radial location in the inlet is the arithmetic average of the recoveries from the four total-pressure tubes at each of the radial locations. All other values of ram-recovery ratio presented herein were computed as an arithmetic average of the recoveries at the 32 total-pressure tubes, and are equivalent to an area-weighted average because of the distribution of the tubes within the duct.

The surveys of the air stream in the vicinity of the dynamometer indicated the presence, at radii up to 30 inches from the tunnel center line, of adverse longitudinal pressure gradients (due to the dynamometer body) in the region where the cowling was to be located. To determine the magnitude of this effect of the dynamometer body on the cowling pressure distribution, tests were made with the spinner-cowling combination located both at its normal position on the dynamometer and extended 2 feet upstream of this position. The small differences in pressure coefficients, generally less

than about 0.05 over the length of the cowling, obtained with the cowling in the two positions were used as corrections to the pressure coefficients on the cowling for subsequent tests of the spinner-cowling combination in its normal location.

The data obtained in surveys of the local velocities in the propeller planes of the spinner-cowling combinations were corrected for small irregularities indicated by rake-alone calibrations and for the radial velocity gradient in the tunnel due to the influence of the dynamometer body.

ACCURACY

Analysis of the accuracy of the separate measurements of thrust, torque, rotational speed, and air-stream velocity indicates that errors in the propeller efficiencies reported herein are probably less than 2 percent.

As noted previously, the test Mach numbers were not corrected for the wind-tunnel-wall constraint on the propeller slipstream. In the exact use of the data, the test Mach number may be corrected to the equivalent free-air Mach number, by use of the ratio given in figure 6, wherever small changes in Mach number produce large changes in the results.

It may be noted that in reducing the data obtained in the velocity surveys in the propeller planes, no attempt was made to correct the static pressures indicated by the tubes of the survey rake immediately adjacent to the spinner surface. As a result, the values of local velocity obtained at low inlet-velocity ratios may be somewhat in error due to local angularity of the flow with respect to the rake.

RESULTS AND DISCUSSION

POSITIVE-THRUST CHARACTERISTICS OF PROPELLER-SPINNER COMBINATIONS

The variation, with advance ratio, of the propeller thrust coefficient, power coefficient, efficiency, and tip Mach number for the various propeller-spinner combinations operating at positive thrust at Mach numbers up to 0.84 are presented in figures 7 and 8. The characteristics of the NACA 4–(5)(05)–041 four-blade, single-rotation propeller and the NACA 4–(5)(05)–037 six- and eight-blade, dual-rotation propellers with the NACA 1-series spinners, and with an optimum $\Delta\beta$ for the dual-rotation propellers are presented in figure 7. Figure 8 presents the characteristics of the NACA 4–(5)(05)–041 propeller in combination with the 7.2- and 12.0-inch-diameter, extended cylindrical spinners. The effects of Mach number, advance ratio, tip Mach number, and spinner shape on the maximum efficiency of the propeller-spinner combinations at positive thrust, as derived from figures 7 and 8, are summarized in figures 9 to 12. The characteristics of the NACA 4–(5)(05)–037 propellers with the 1-series spinners, and with $\Delta\beta$ at the design value of 0.8°, are shown in figures 13 and 14.

Effect of Mach number on maximum efficiency.—The effects of Mach number on the maximum efficiency of the various propeller-spinner combinations, as shown in figures 9, 11, and 14, are similar to the results reported in references 1 to 3 for two-blade propellers. Propeller efficiency losses due to compressibility effects occur with increasing Mach number, resulting in a reduction in the envelope efficiencies from the relatively high values obtained at low speeds. For the propellers of these tests, the envelope efficiencies at low speeds, say at a Mach number of 0.4, were nearly equal at about 86 percent. Efficiency losses due to compressibility effects were small and accrued gradually up to a Mach number of about 0.7. At this Mach number, the efficiencies were about 79, 83, and 82 percent, respectively, for the four-, six-, and eight-blade propellers at a blade angle of 65°. At Mach numbers greater than about 0.7, severe compressibility losses, associated with supersonic resultant section Mach numbers and consequent reduced section lift-drag ratios, occurred for the propellers at the blade angles of these tests, and the rate of loss of efficiency increased with increasing blade angle.

As shown in figure 10, which presents the variation of maximum efficiency with tip Mach number for the propellers with 1-series spinners, the marked losses in efficiency due to compressibility effects began at about the same tip Mach number, approximately 0.8, regardless of the number of propeller blades or of the blade angles.

Effect of advance ratio on maximum efficiency.—The effects of advance ratio on the maximum efficiency of the propellers with 1-series spinners, shown for constant Mach numbers in figures 9, 11, and 14, were also similar to results reported in references 1 to 3 for two-blade propellers. As shown in figures 9, 11, and 14, highest efficiencies were obtained at relatively high advance ratios for operation of the propellers at subcritical Mach numbers. In contrast, it appears that for operation of the propellers at supercritical Mach numbers, highest efficiencies would be obtained at lower advance ratios and lower blade angles.

Effect of spinner on maximum efficiency.—Values of the maximum efficiency of the NACA 4–(5)(05)–041 four-blade propeller with 1-series and extended cylindrical spinners, from the data of figures 9 and 11, are compared in the following table (values in parentheses are estimated by extrapolation):

M	β=55°			β=60°			β=65°		
	1-series spinner	Extended cylindrical spinners		1-series spinner	Extended cylindrical spinners		1-series spinner	Extended cylindrical spinners	
	d=7.2	d=7.2	d=12.0	d=7.2	d=7.2	d=12.0	d=7.2	d=7.2	d=12.0
0.60	0.82	0.86	0.86	0.81	0.84	0.85	0.79	0.85	0.85
.70	.73	.80	.80	.76	.82	.83	.79	.82	.83
.75	.64	(.69)	(.72)	.67	.76	.76	.68	.78	.79
.80	----	----	----	.59	(.67)	(.69)	.57	.70	.72
.84	----	----	----	----	----	----	.51	(.61)	(.66)

It is evident that the maximum efficiencies of the propeller with the extended cylindrical spinners were considerably higher than those for the propeller with the 1-series spinner, and that the highest efficiencies were obtained with the largest cylindrical spinner. The increment in efficiency between the 1-series and cylindrical spinners generally increased with either increasing Mach number for a given blade angle or increasing blade angle for a given Mach number, amounting to as much as 15 percent at the highest Mach number and blade angle.

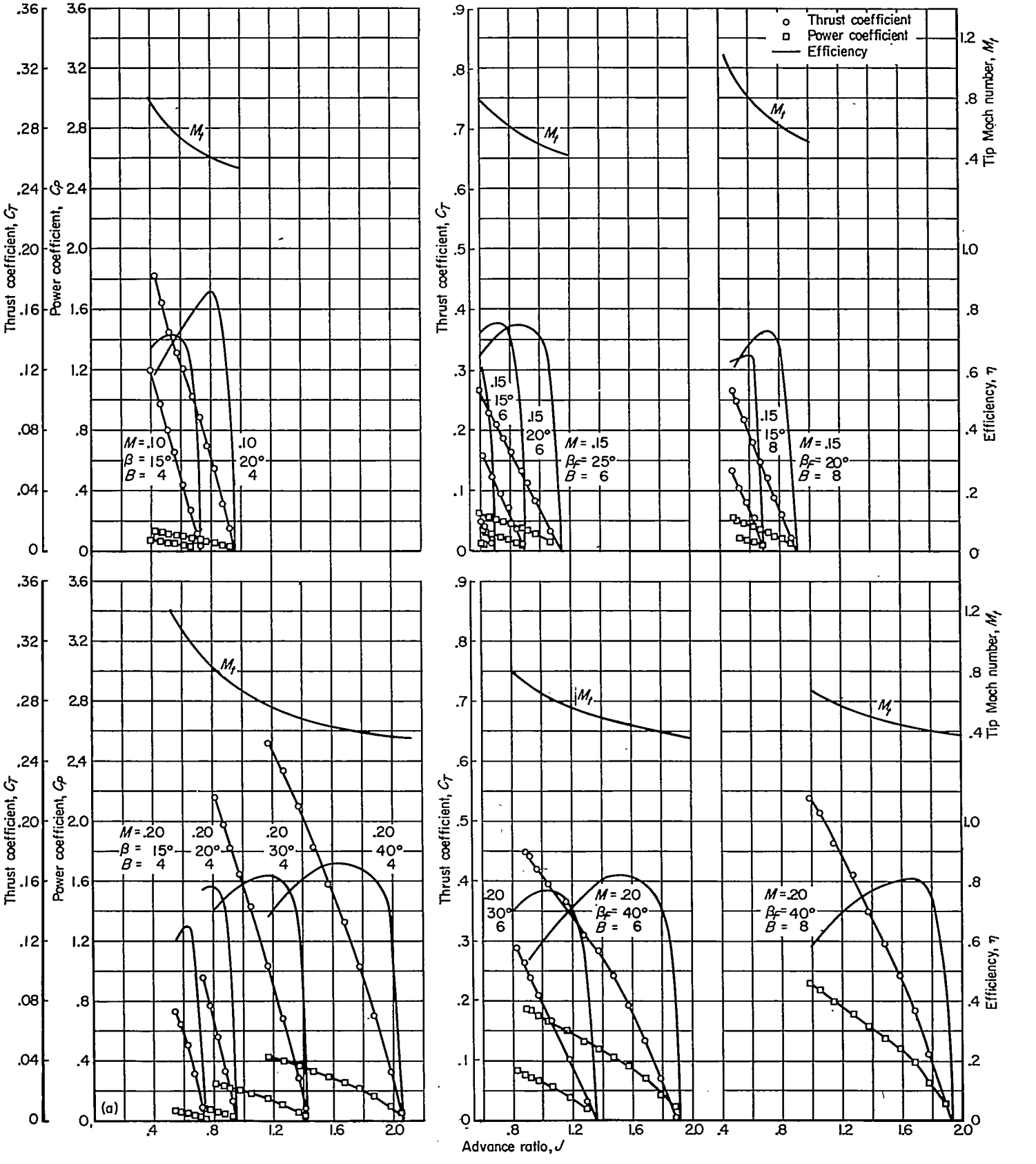

(a) $M \cong 0.10$ to 0.20

FIGURE 7.—Positive-thrust characteristics of the NACA 4–(5)(05)–041 four-blade, single-rotation propeller and the NACA 4–(5)(05)–037 six- and eight-blade, dual-rotation propellers (optimum $\Delta\beta$) with NACA 1-series spinners.

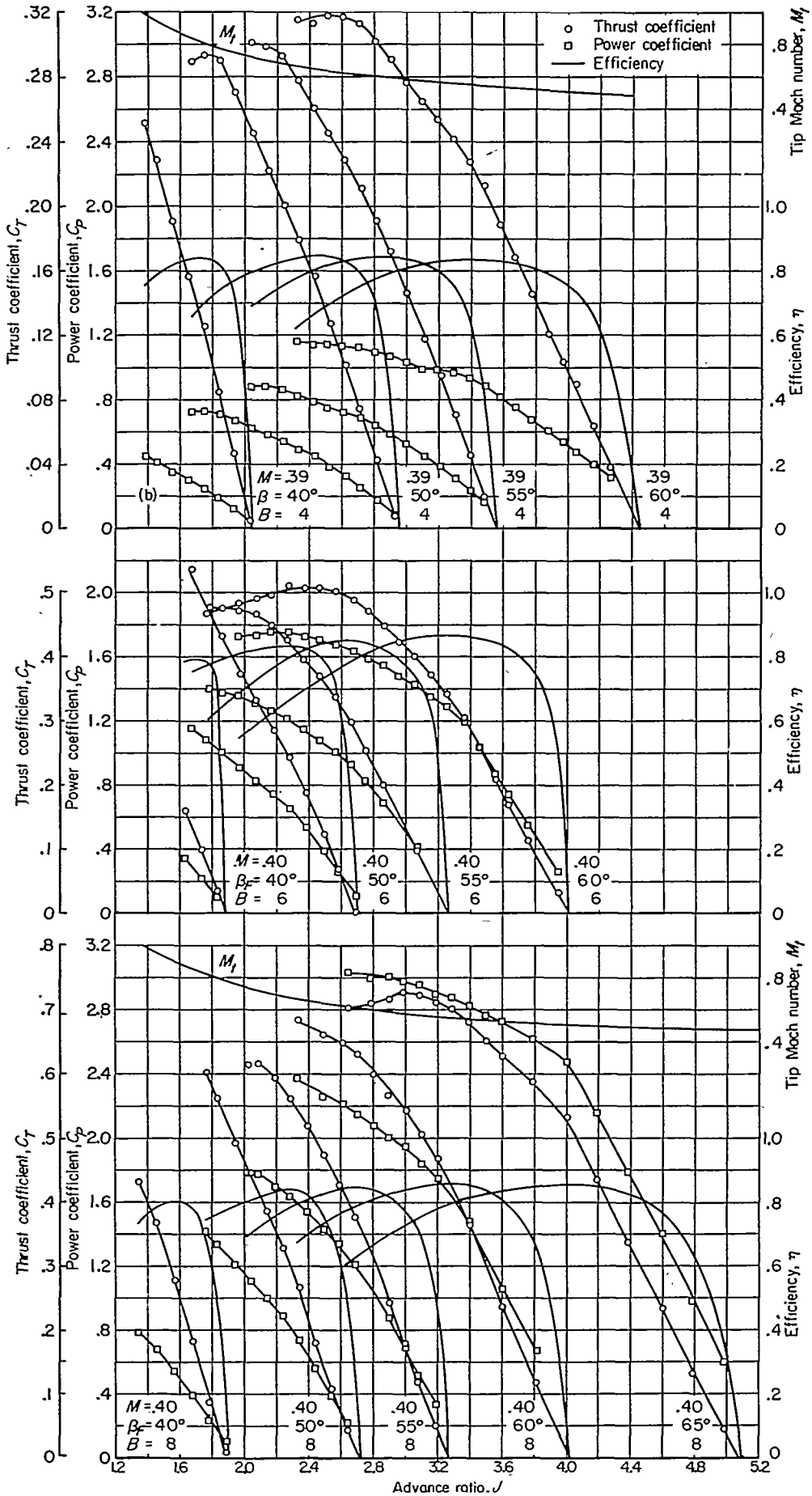

(b) $M \cong 0.40$

FIGURE 7.—Continued.

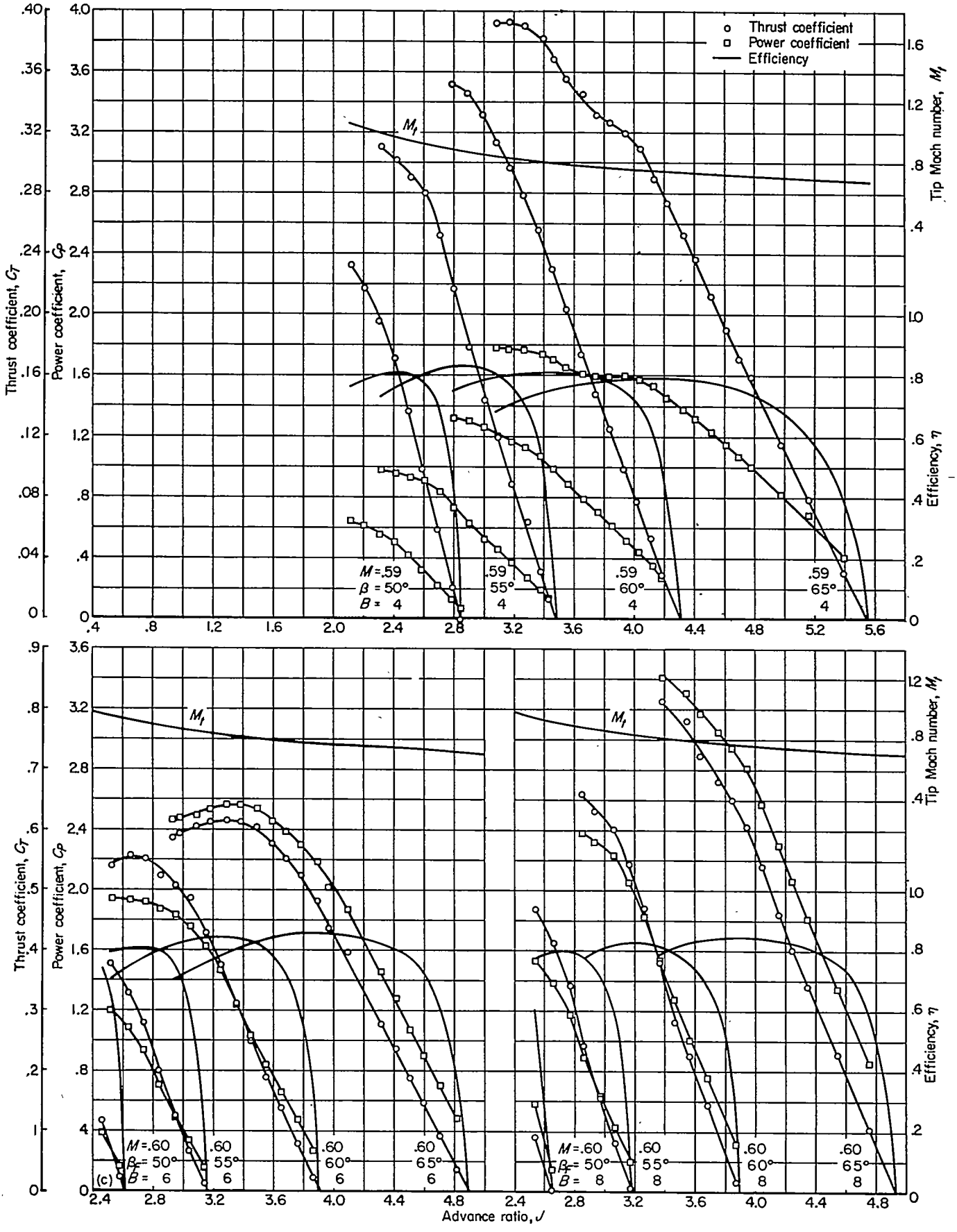

(c) $M \cong 0.60$

FIGURE 7.—Continued.

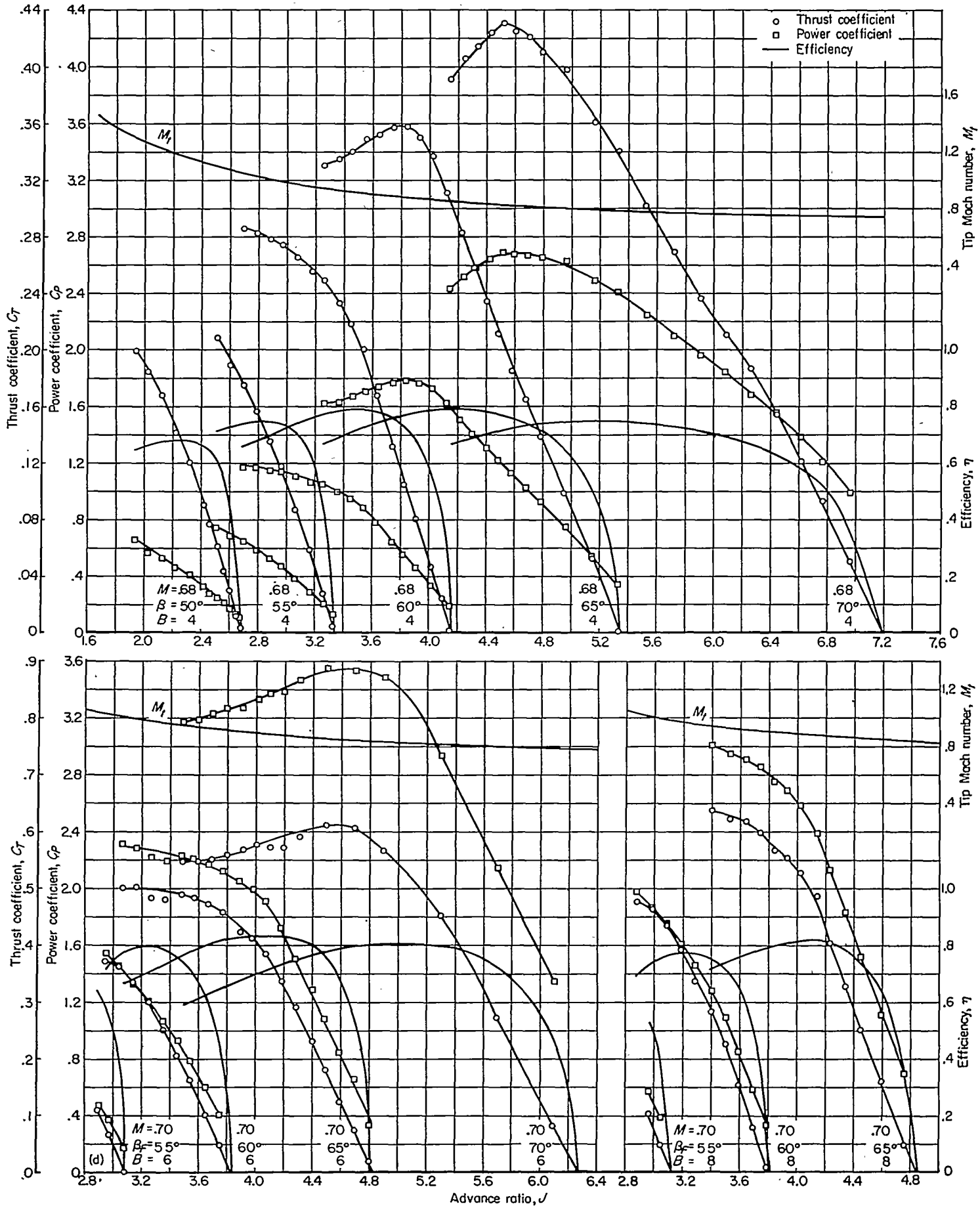

(d) $M \cong 0.70$

FIGURE 7.—Continued.

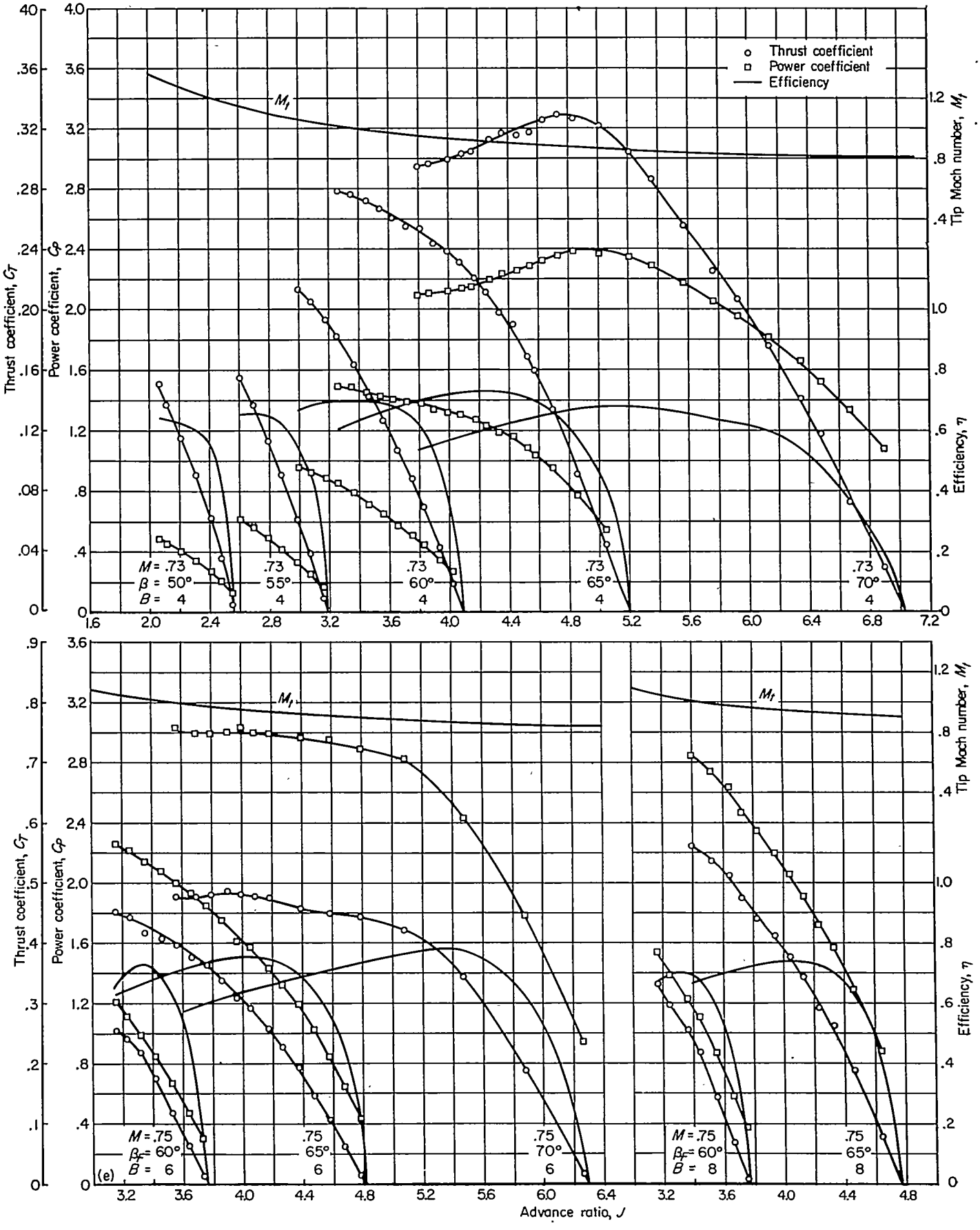

(e) $M \cong 0.75$

FIGURE 7.—Continued.

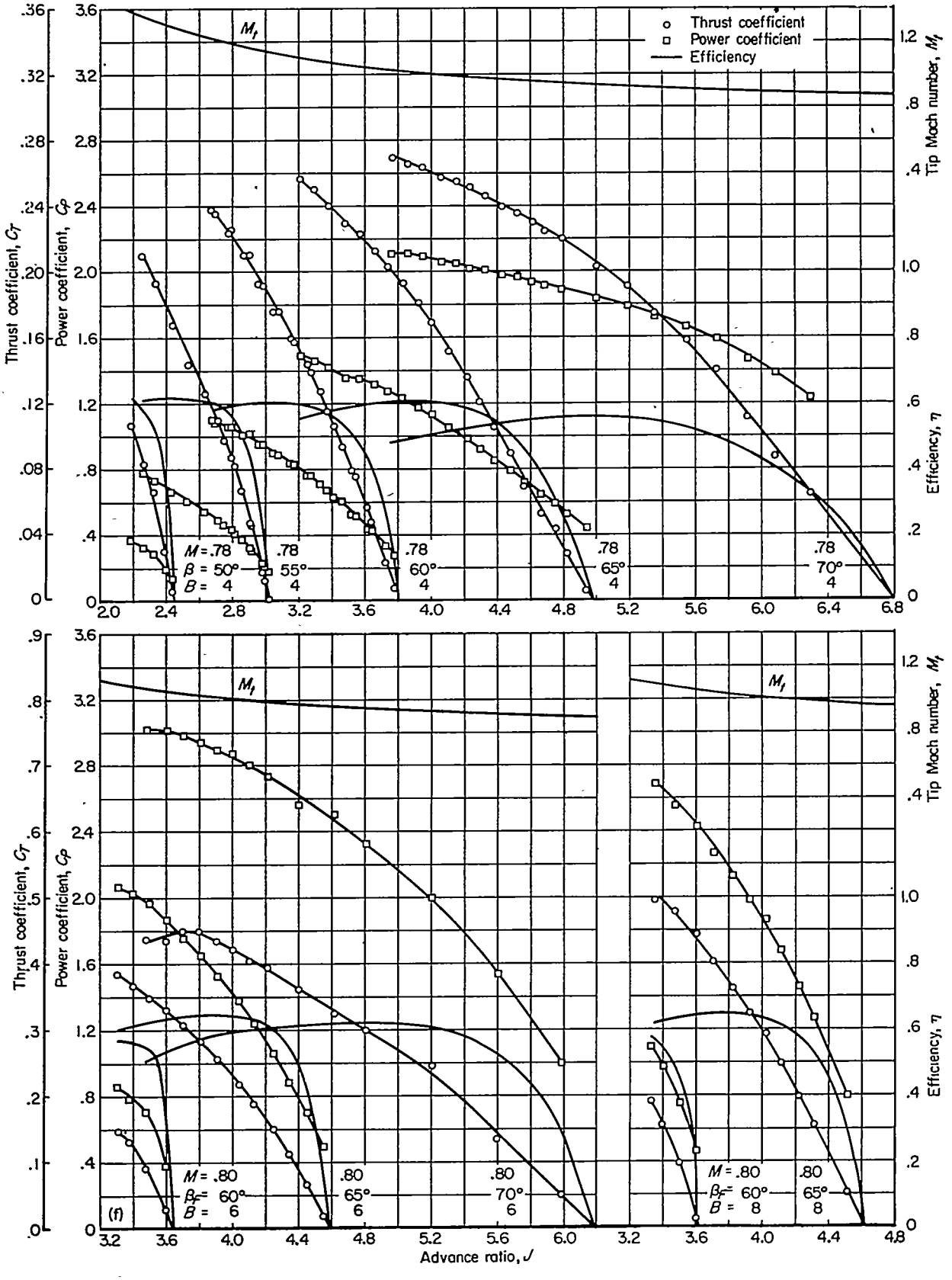

(f) $M \cong 0.80$

FIGURE 7.—Continued.

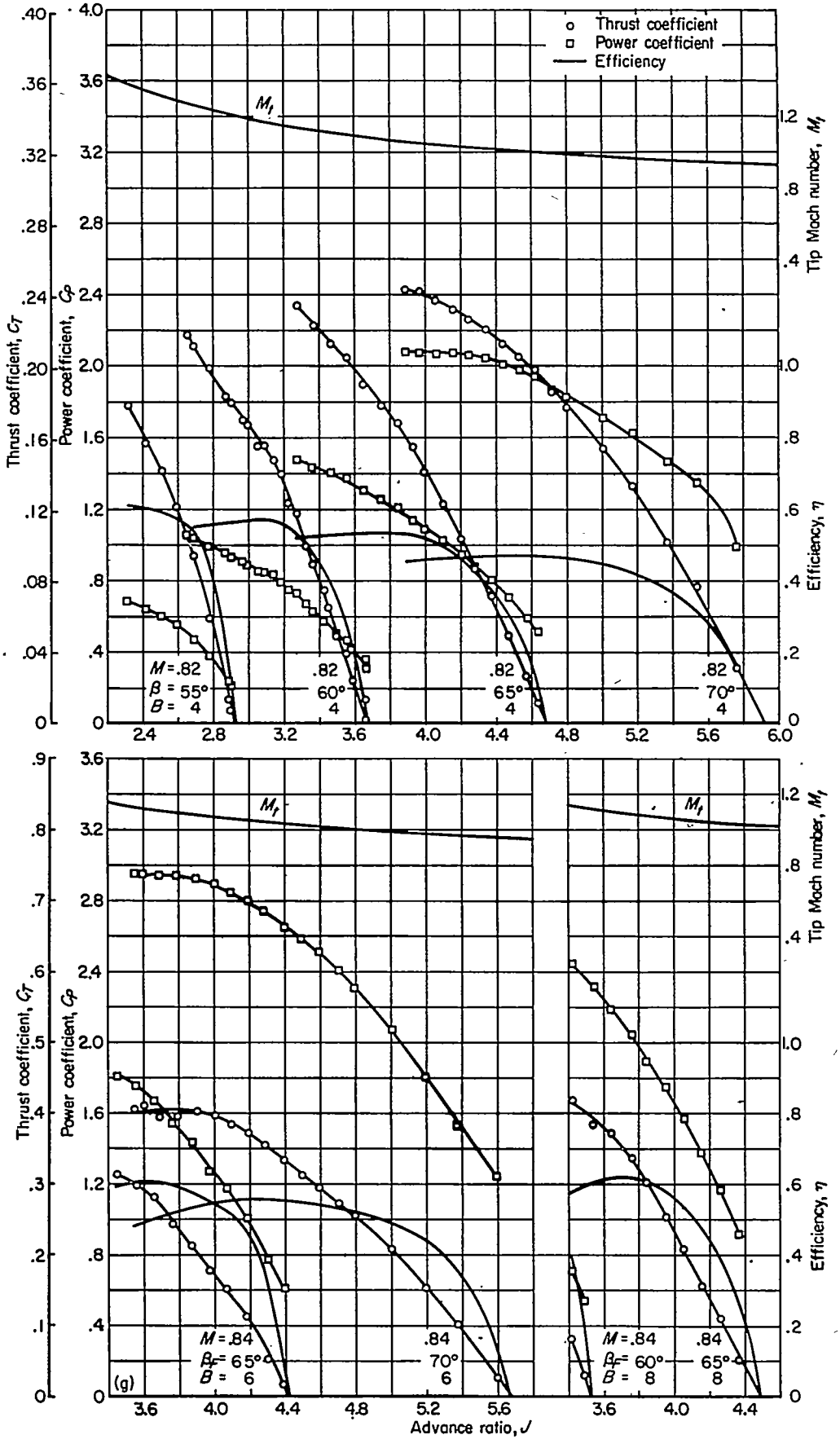

(g) $M \cong 0.84$

FIGURE 7 —Concluded.

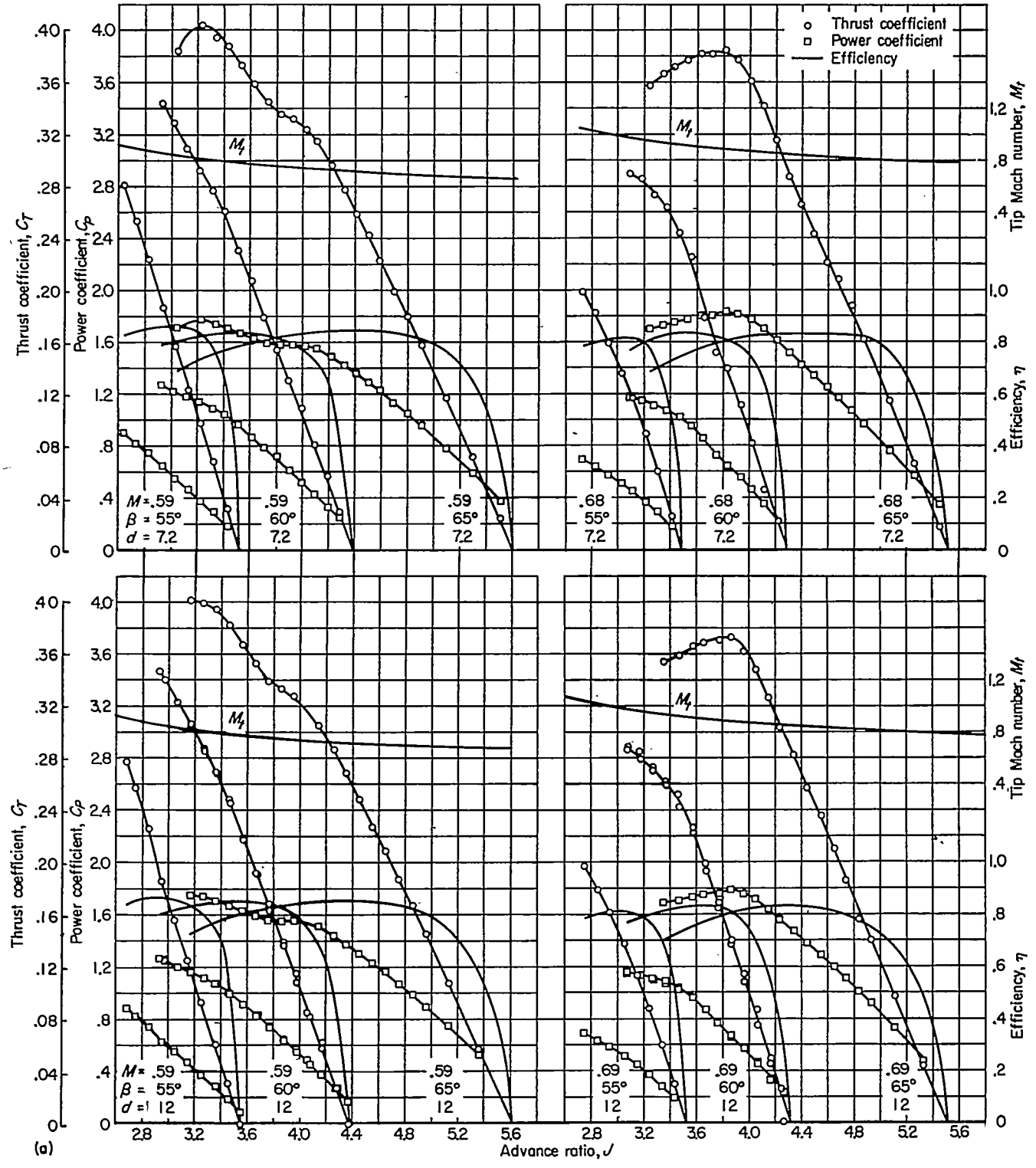

(a) $M \cong 0.60$ and 0.70

FIGURE 8.—Positive-thrust characteristics of the NACA 4–(5)(05)–041 four-blade propeller with the 7.2-inch- and 12.0-inch-diameter, extended cylindrical spinners.

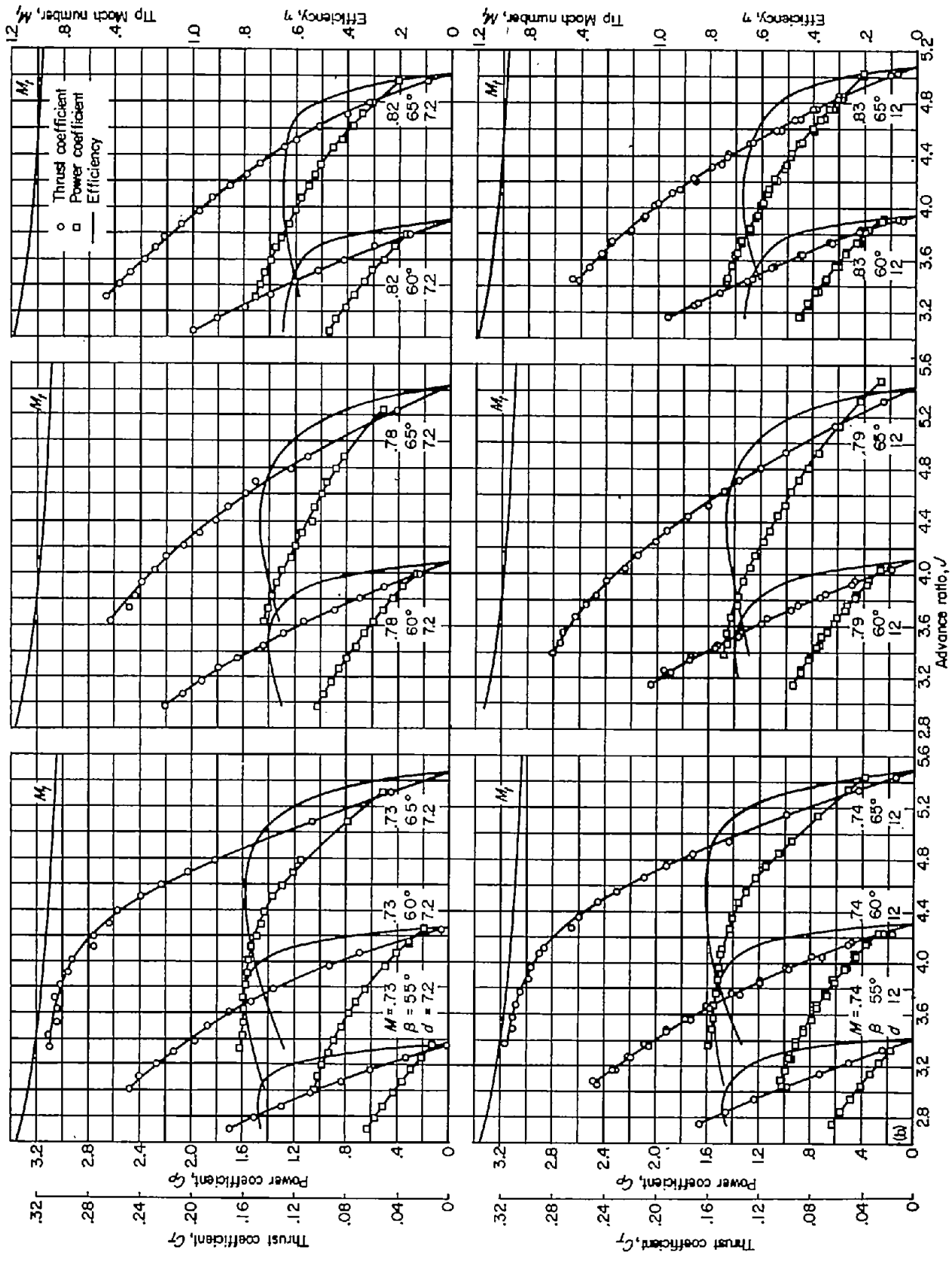

(b) M_t=0.74, 0.79, and 0.83
FIGURE 8.—Concluded.

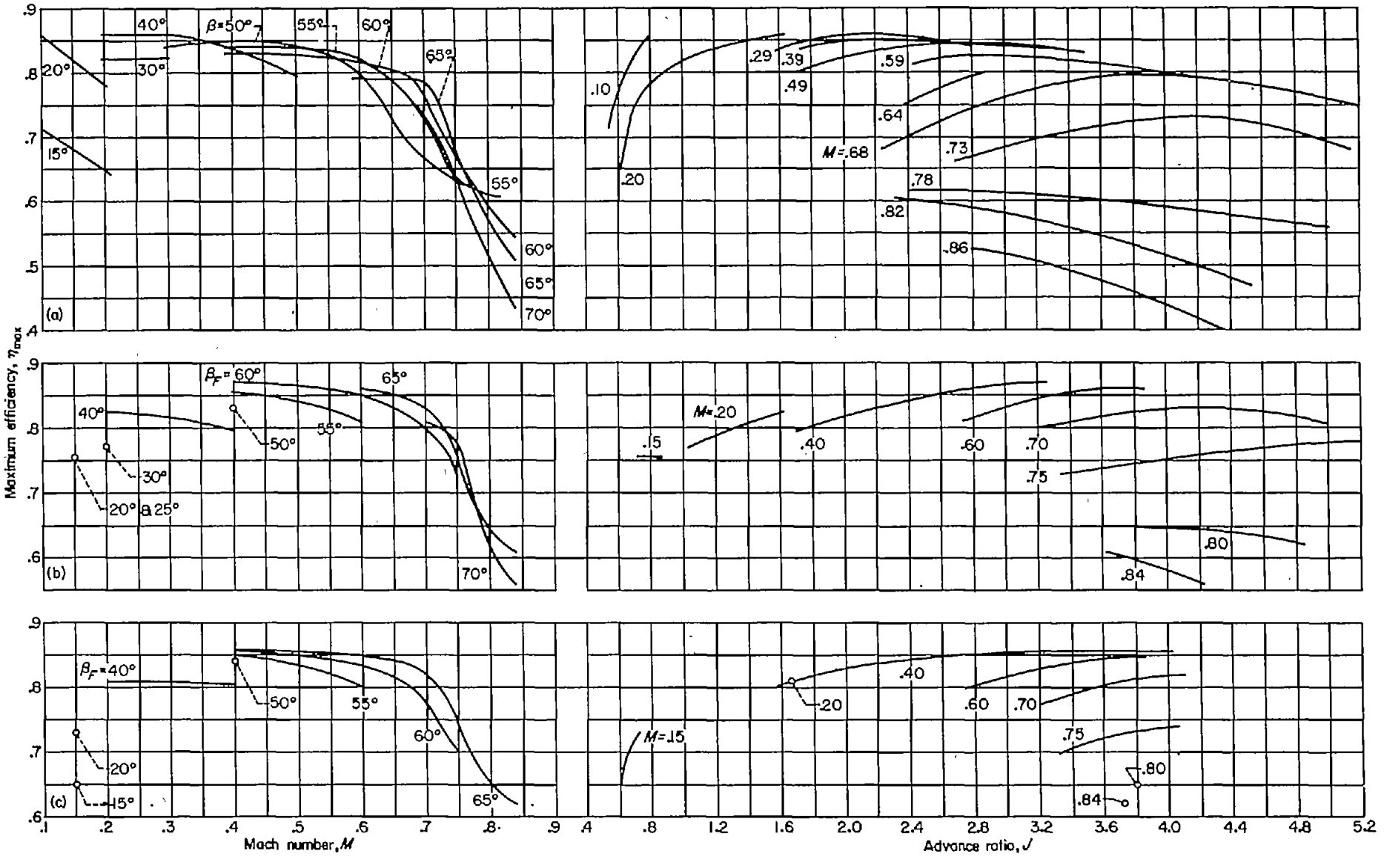

(a) NACA 4–(5)(05)–041 four-blade, single-rotation propeller.
(b) NACA 4–(5)(05)–037 six-blade, dual-rotation propeller.
(c) NACA 4–(5)(05)–037 eight-blade, dual-rotation propeller.

FIGURE 9.—The effect of Mach number and advance ratio on the maximum efficiency of the propellers with NACA 1-series spinners.

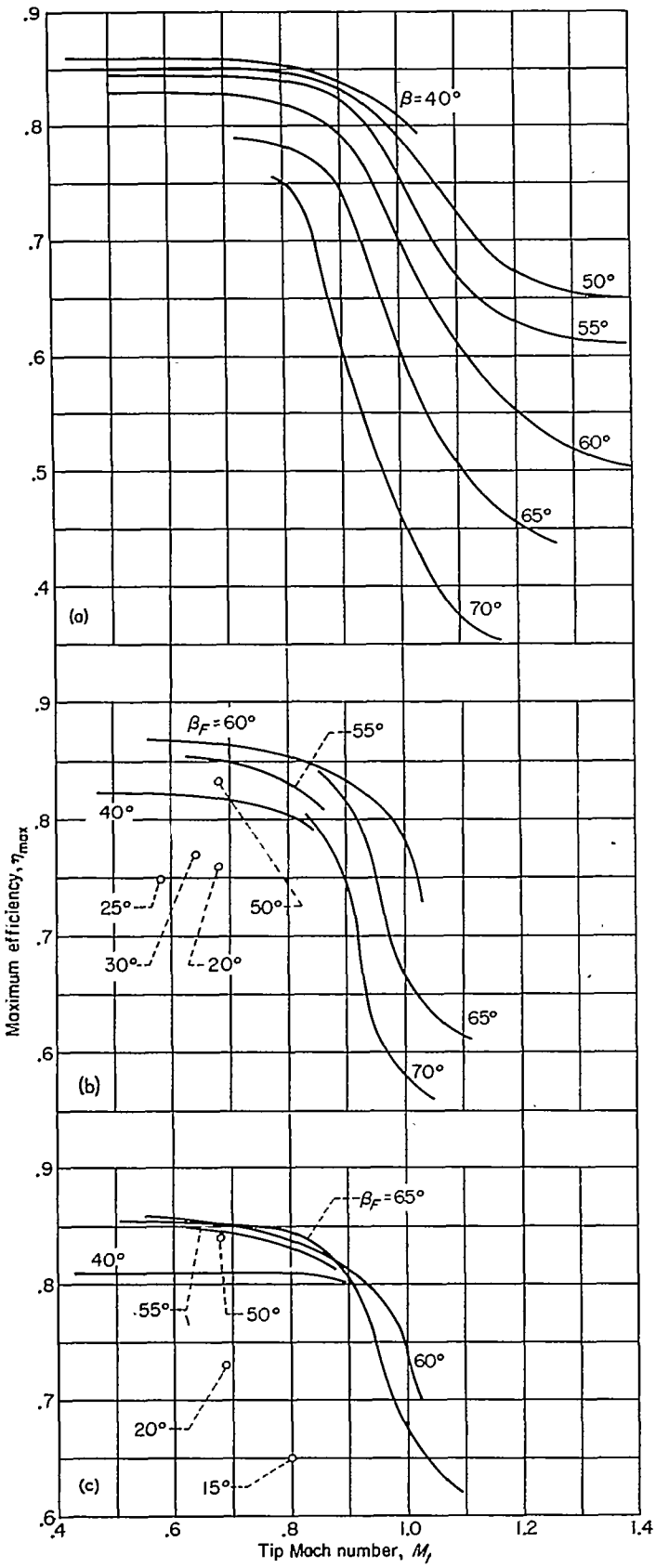

(a) NACA 4–(5)(05)–041 four-blade, single-rotation propeller.
(b) NACA 4–(5)(05)–037 six-blade, dual-rotation propeller.
(c) NACA 4–(5)(05)–037 eight-blade, dual-rotation propeller.

FIGURE 10.—The effect of tip Mach number on the maximum efficiency of the propellers with NACA 1-series spinners.

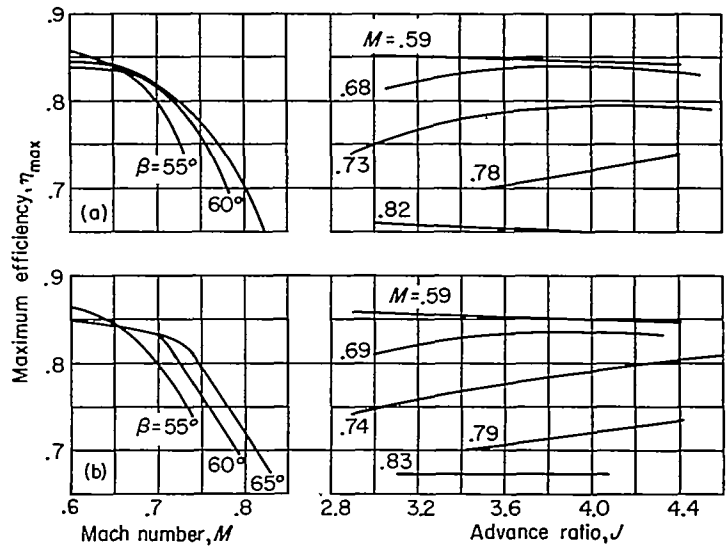

(a) Propeller with 7.2-inch-diameter spinner.
(b) Propeller with 12.0-inch-diameter spinner.

FIGURE 11.—The effect of Mach number and advance ratio on the maximum efficiency of the NACA 4–(5)(05)–041 four-blade, single-rotation propeller with extended cylindrical spinners.

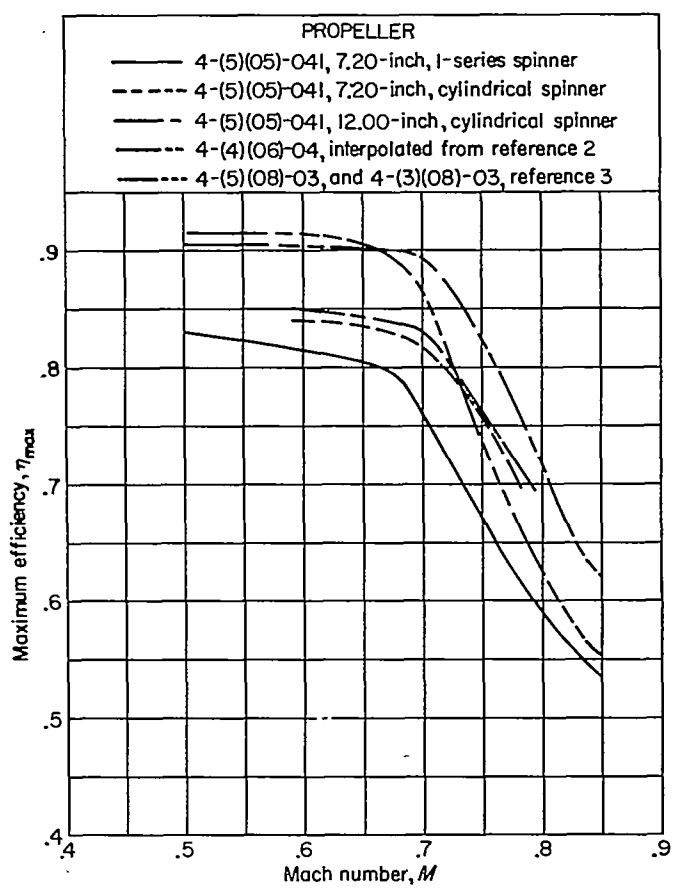

FIGURE 12.—The effect of spinner shape on the maximum efficiency of the NACA 4–(5)(05)–041 four-blade, single-rotation propeller; β=60°.

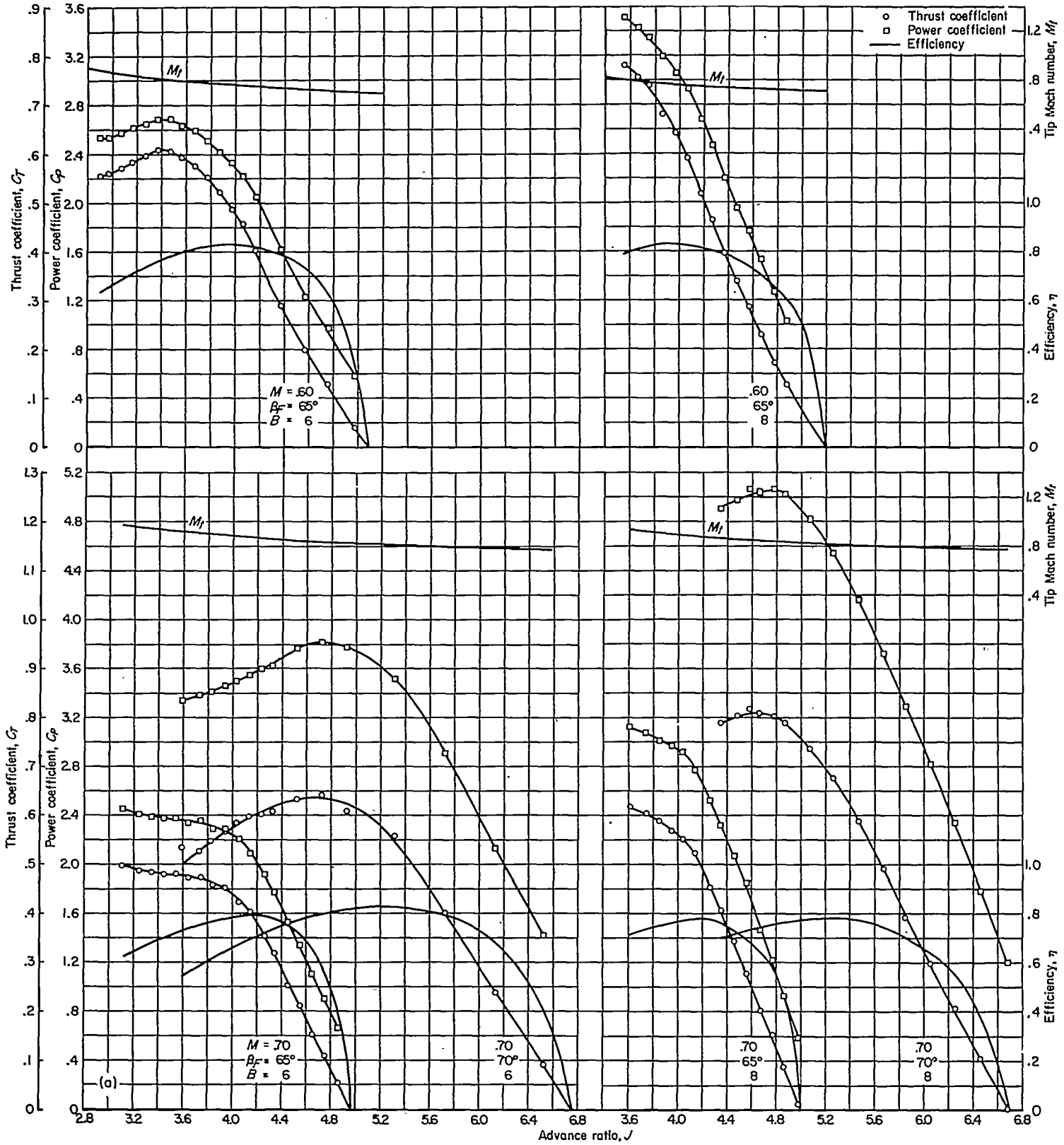

(a) M=0.60 and 0.70

FIGURE 13.—Positive-thrust characteristics of the NACA 4-(5)(05)-037 dual-rotation propellers (design $\Delta\beta$=0.8°) with NACA 1-series spinners.

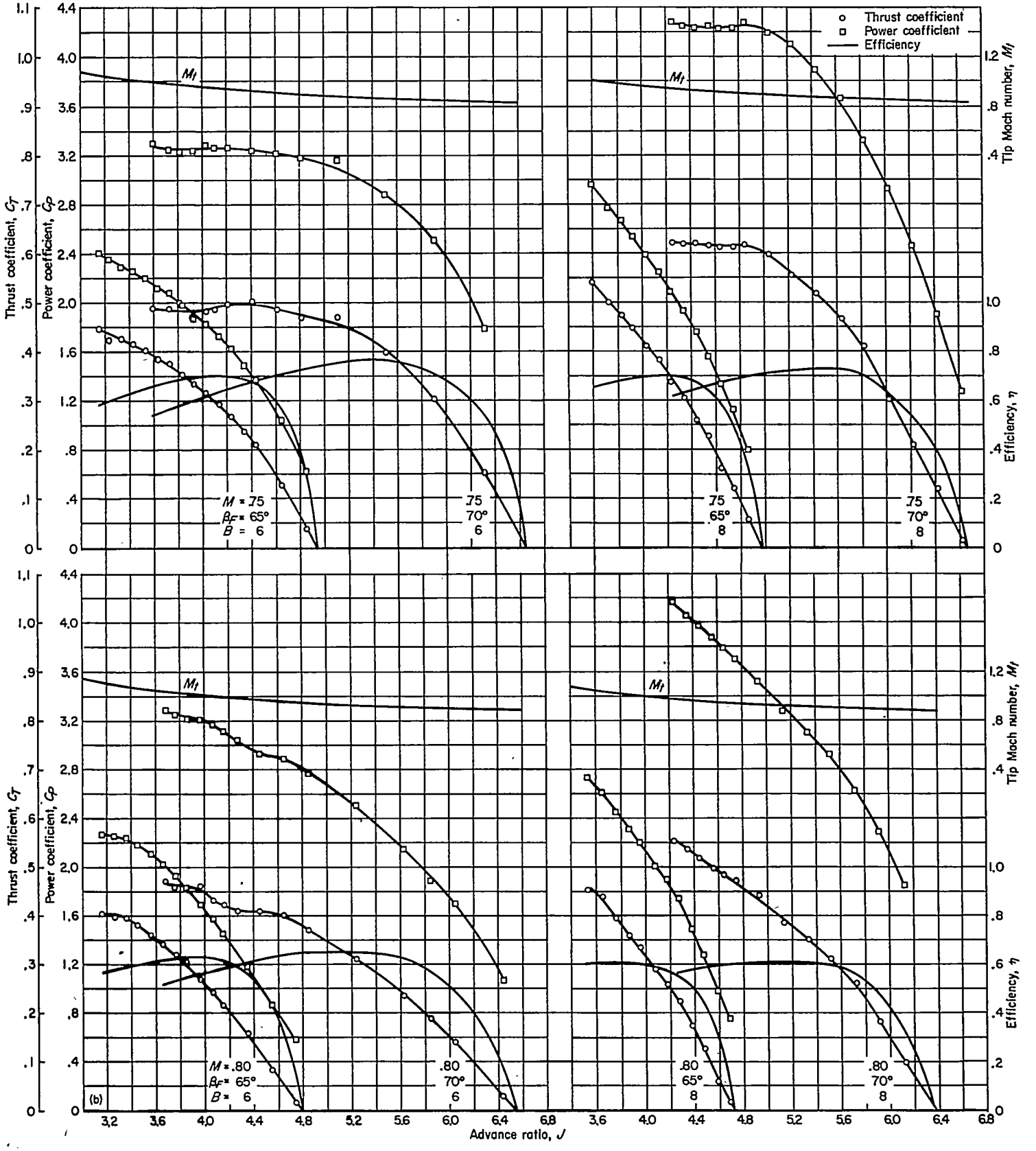

(b) M=0.75 and 0.80

FIGURE 13.—Continued.

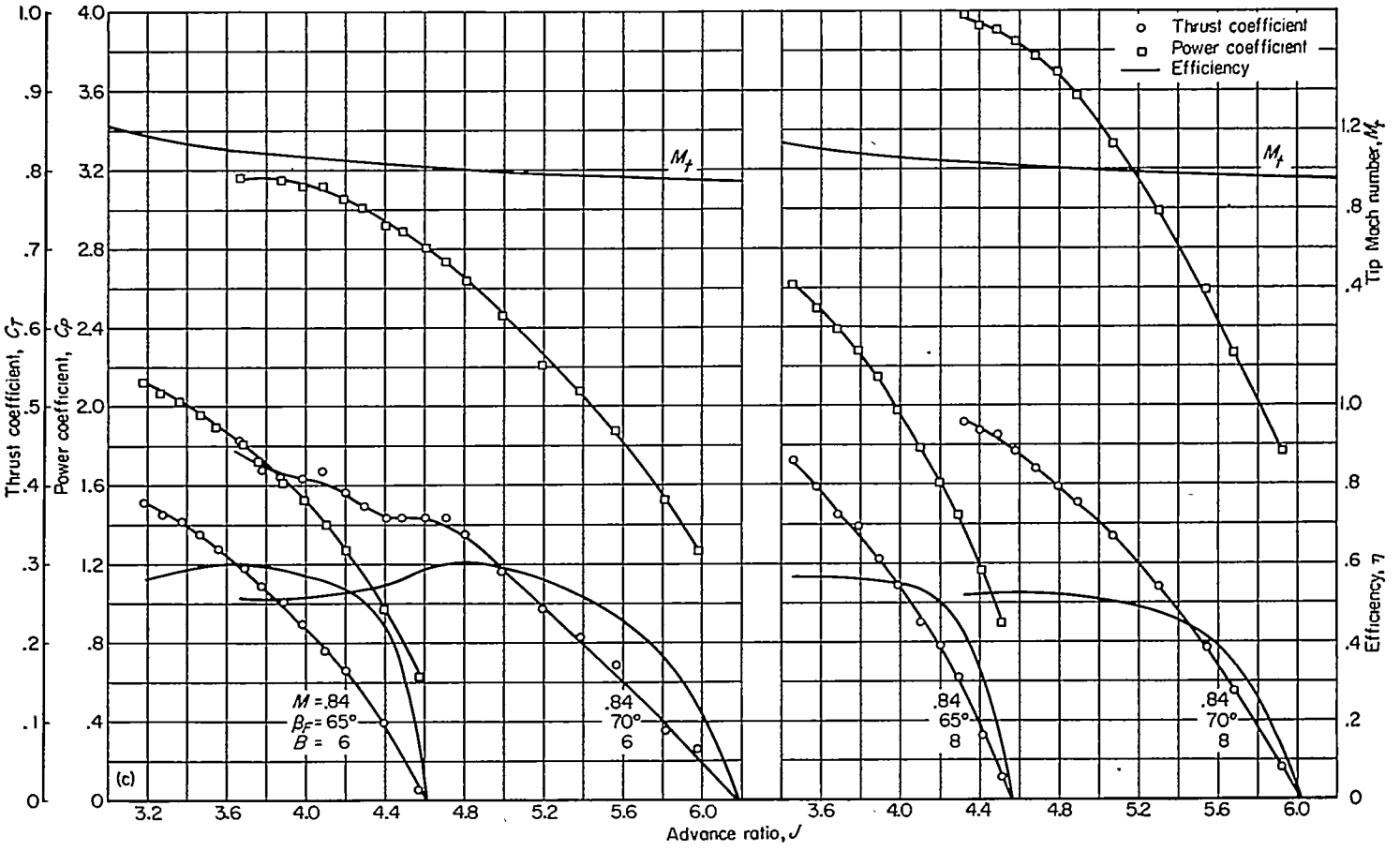

(c) M=0.84

FIGURE 13.—Concluded.

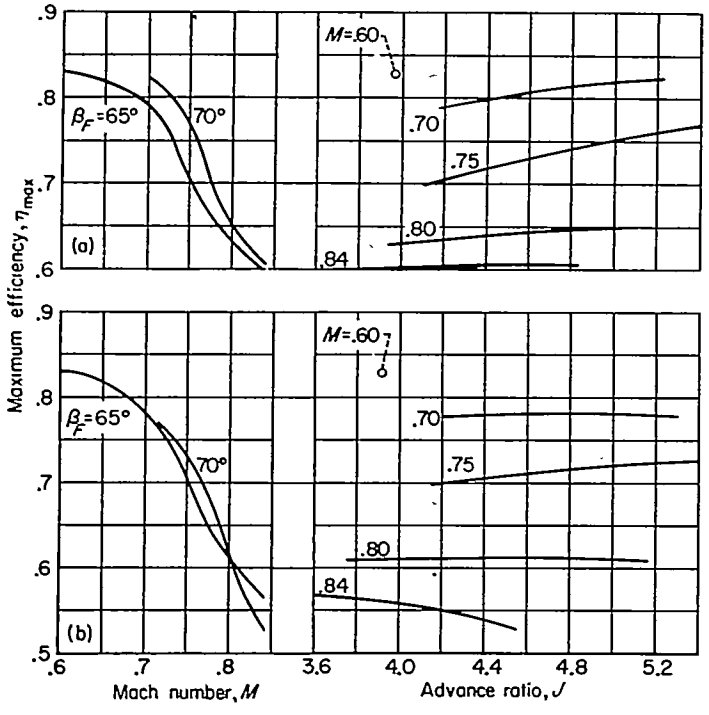

(a) NACA 4–(5)(05)–037 six-blade, dual-rotation propeller.

(b) NACA 4–(5)(05)–037 eight-blade, dual-rotation propeller.

FIGURE 14.—The effect of Mach number and advance ratio on the maximum efficiency of the dual-rotation propellers, at design $\Delta\beta$ (0.8°), with NACA 1-series spinners.

It was demonstrated by the results of surveys of the local Mach numbers in the vicinity of the propeller plane (discussed in the appendix) that with the short 1-series spinner used with the single-rotation propeller, the local velocities on the inner portions of the propeller blades were considerably higher than the free-stream velocities. Calculations, using the method of reference 20, of the thrust and torque loadings on the blades in combination with the 1-series and cylindrical spinners of equal diameter indicated that the lower efficiencies for the propeller with the 1-series spinner are probably due to the higher resultant Mach numbers and the accompanying reduced section angles of attack, and hence to lower lift-drag ratios, for the inboard portions of the blades. Similarly, the differences in the efficiencies of the propeller with the 7.2- and 12.0-inch-diameter, cylindrical spinners are partly attributable to the different radial Mach number distributions in the plane of the propeller with the two spinners, and partly attributable to the enclosure of a portion of the thick inner portions of the propeller blades within the larger spinner.

Limited tests of the NACA 4–(5)(05)–041 four-blade propeller with the NACA 1–46.5–047 spinner and of the NACA 4–(5)(05)–037 six-blade propeller with the NACA 1–46.5–085 spinner (fig. 4) were made as listed in table I. The results of these tests (not presented herein) show that the maximum efficiencies of the four-blade propeller with the NACA 1–46.5–047 spinner were essentially the same (within the

limits of the experimental accuracy of these tests) as those for the four-blade propeller with the 7.2-inch-diameter, 1-series spinner, and that the maximum efficiencies of the six-blade propeller with the NACA 1–46.5–085 spinner were generally about 2 percent lower than those for the six-blade propeller with the 6.51-inch-diameter, 1-series spinner. It is believed that the latter result is again due to the inboard sections of the propeller blades being subjected to higher velocities with the shorter NACA 1–46.5–085 spinner than with the 6.51-inch-diameter, 1-series spinner.

Comparison of the maximum efficiency of the NACA 4–(5)(05)–041 propeller with results of previous investigations.—In figure 12 the variation of maximum efficiency with Mach number for the NACA 4–(5)(05)–041 four-blade propeller, with various spinners, is compared to similar data (refs. 2 and 3) for the NACA 4–(4)(06)–04, 4–(5)(08)–03, and 4–(3)(08)–03 two-blade propellers with 13.0-inch-diameter, cylindrical spinners. The Mach number at which losses in efficiency due to compressibility began was about the same (0.7) for the NACA 4–(5)(05)–041 propeller with the 12.0-inch-diameter, cylindrical spinner and the NACA 4–(4)(06)–04 propeller with a 13.0-inch-diameter, cylindrical spinner, as might be expected in view of the small differences in camber and thickness between the two blades. Also as might be expected for the thinner blades, at Mach numbers greater than about 0.7 the rate of loss of efficiency with increasing Mach number was not so great for the NACA 4–(5)(05)–041 propeller as for either the NACA 4–(4)(06)–04 or 4–(5)(08)–03 propeller. The trend of the data indicates that at some Mach number in excess of 0.8, the NACA 4–(5)(05)–041 propeller with the 12.0-inch-diameter, cylindrical spinner would have a higher maximum efficiency than either the NACA 4–(4)(06)–04 or 4–(5)(08)–03 propeller. At the subcritical Mach numbers at least part of the difference in maximum efficiency between the NACA 4–(5)(05)–041 propeller with the 12.0-inch-diameter, cylindrical spinner and the NACA 4–(4)(06)–04 propeller may be attributable to the difference in total solidity of the two- and four-blade propellers.

Effects of $\Delta\beta$ and of sealing the platform-juncture gap on the maximum efficiency of the dual-rotation propellers.—Comparison of the data in figure 14 with those in figure 9 show that for both the six- and eight-blade propellers at blade angles of 65° and 70° the maximum efficiency obtained with a $\Delta\beta$ of 0.8° was generally lower, by about 2 percent, than with the corresponding optimum $\Delta\beta$ settings of 2.4° and 2.9°. As would be anticipated, at a given advance ratio the effect of increasing the blade angle of the rear component of the dual-rotation propellers, in changing from optimum $\Delta\beta$ to a $\Delta\beta$ of 0.8°, was primarily to increase the power coefficient for the rear component. The power absorbed by the front component of the propeller at a given advance ratio was unaffected by changes in the rear-component blade angles. The total thrust of the dual-rotation propellers was greater with $\Delta\beta$ equal to 0.8 than with the optimum $\Delta\beta$, but the thrust increased by an amount proportionately less than the increase in power absorbed by the rear component of the propeller.

Limited tests of the six-blade, dual-rotation propeller with the 6.51-inch-diameter, 1-series spinner were made at Mach numbers of 0.60, 0.70, and 0.80, with β_F equal to 65° and with the gaps between the propeller blades and the platform junctures (fig. 3) sealed. The results of these tests have not been presented herein, but they indicate that sealing the gaps of the junctures had no significant effect on the propeller characteristics.

NEGATIVE- AND STATIC-THRUST CHARACTERISTICS OF THE PROPELLER-SPINNER COMBINATIONS

Negative thrust.—The effects of Mach number and blade angle on the characteristics of the single- and dual-rotation propellers when operating at negative thrust are presented in figures 15 to 17. The negative-thrust characteristics of the three propellers at a Mach number of 0.15, and of the dual-rotation propellers at the higher Mach numbers, are in good agreement when compared on the basis of equal total solidity. This is shown for the dual-rotation propellers in figure 17. It also may be seen from the data of figure 17, that there was practically no effect of compressibility on the negative-thrust characteristics of the dual-rotation propellers for Mach numbers up to 0.60.

Static thrust.—The characteristics of the four-, six-, and eight-blade propellers at low forward speeds are presented in figure 18. The velocity of the air in the test section for these tests was produced by the model propeller alone and thus varied with propeller rotational speed and blade angle as shown in figure 18. These data were used to determine envelope curves for the variation of thrust per horsepower with power disc loading as shown in figure 19. Included in figure 19 is the theoretical ideal curve for the static condition from actuator-disc theory, computed from the equations of reference 21. For all power-disc loadings, thrust per horsepower increased slightly with increasing number of propeller blades. That the thrust-per-horsepower values for the dual-rotation propellers are higher than those for the single-rotation propellers is probably due in part to lower rotational losses for the dual-rotation propellers. At a power disc loading of about 20 the propellers produced about 3.0 pounds of thrust per horsepower at near static conditions. The experimental thrust per horsepower for the propellers was about 73 percent of the theoretically ideal values, but the data of reference 8 indicate that these values might have been somewhat higher if the data were for a true static condition.

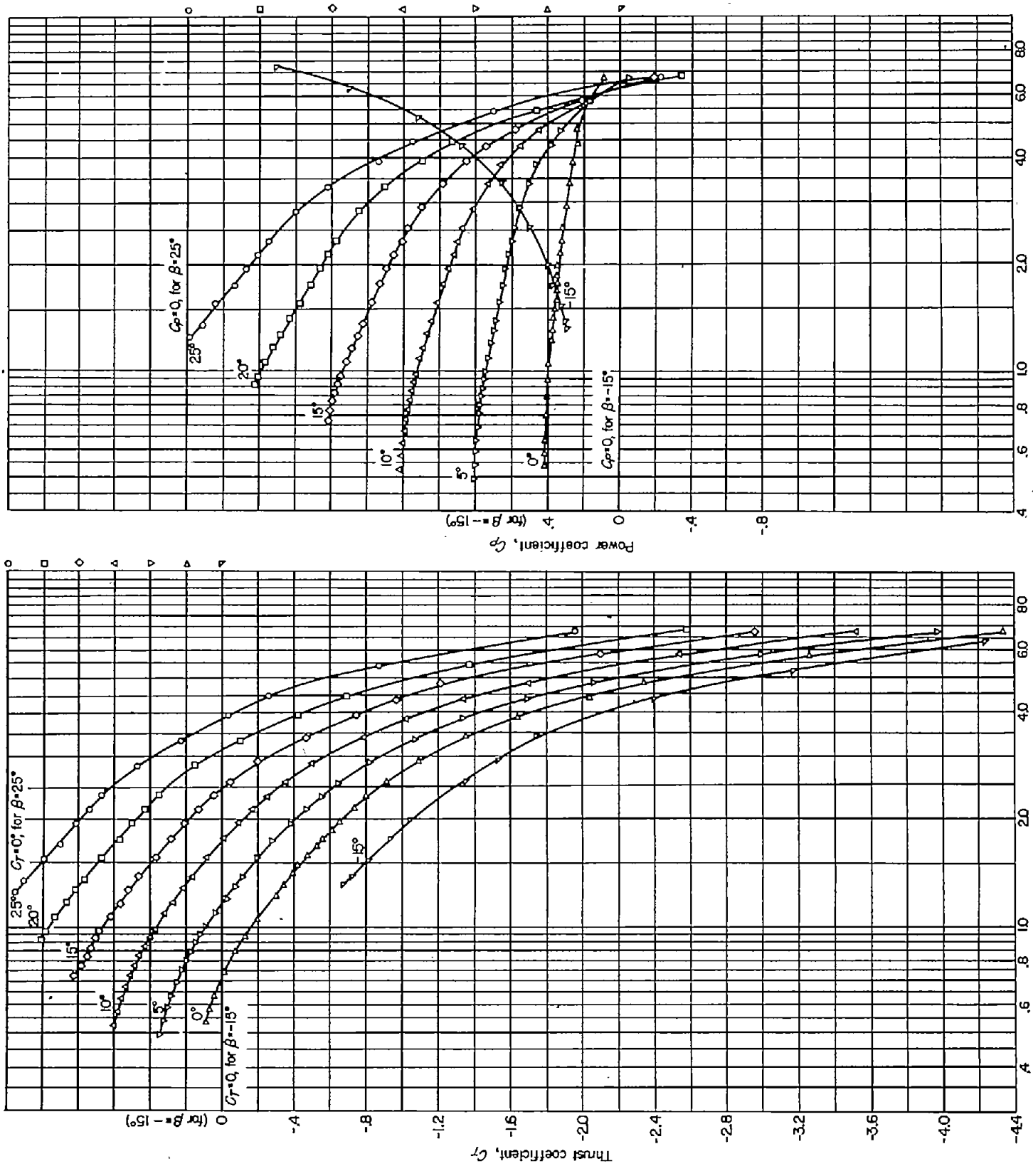

FIGURE 15.—The negative-thrust characteristics of the NACA 4-(5)(05)-041 four-blade, single-rotation propeller, with NACA 1-series spinner, at M=0.15.

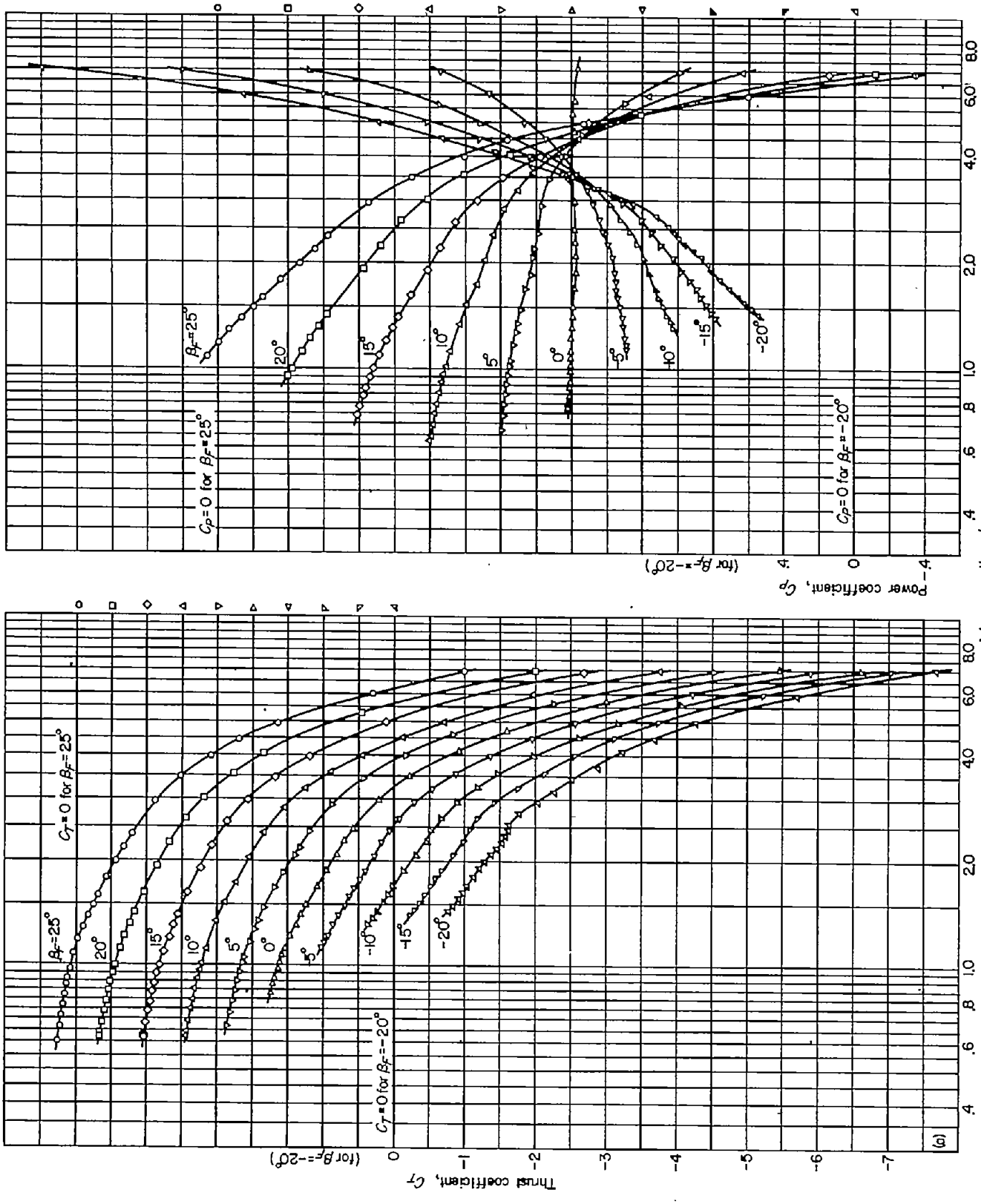

FIGURE 10.— The negative-thrust characteristics of the NACA 4–(5)(06)–037 six-blade, dual-rotation propeller, with NACA 1-series spinner.

(a) $M=0.15$

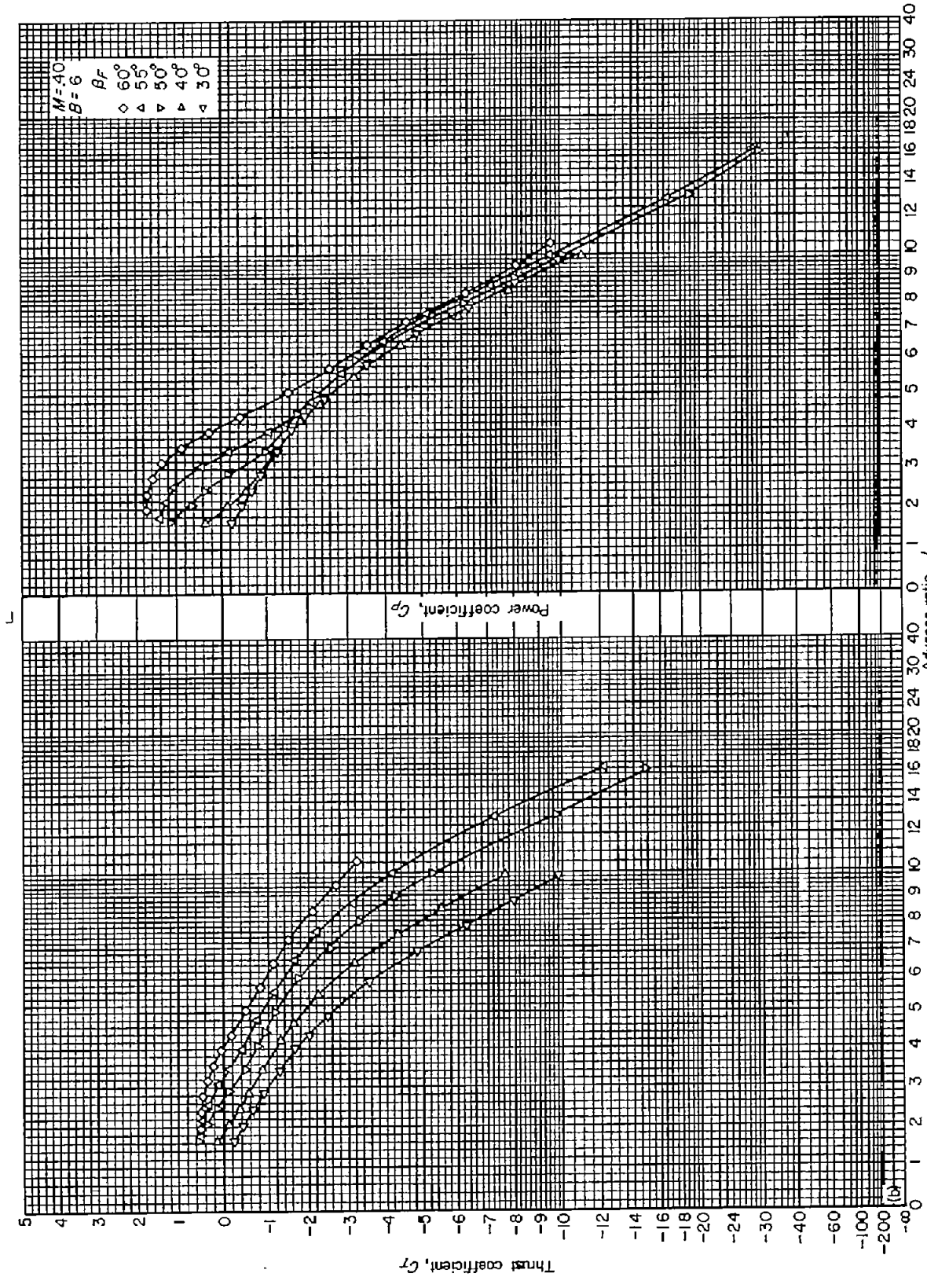

(b) $M=0.40$

FIGURE 16.—Continued.

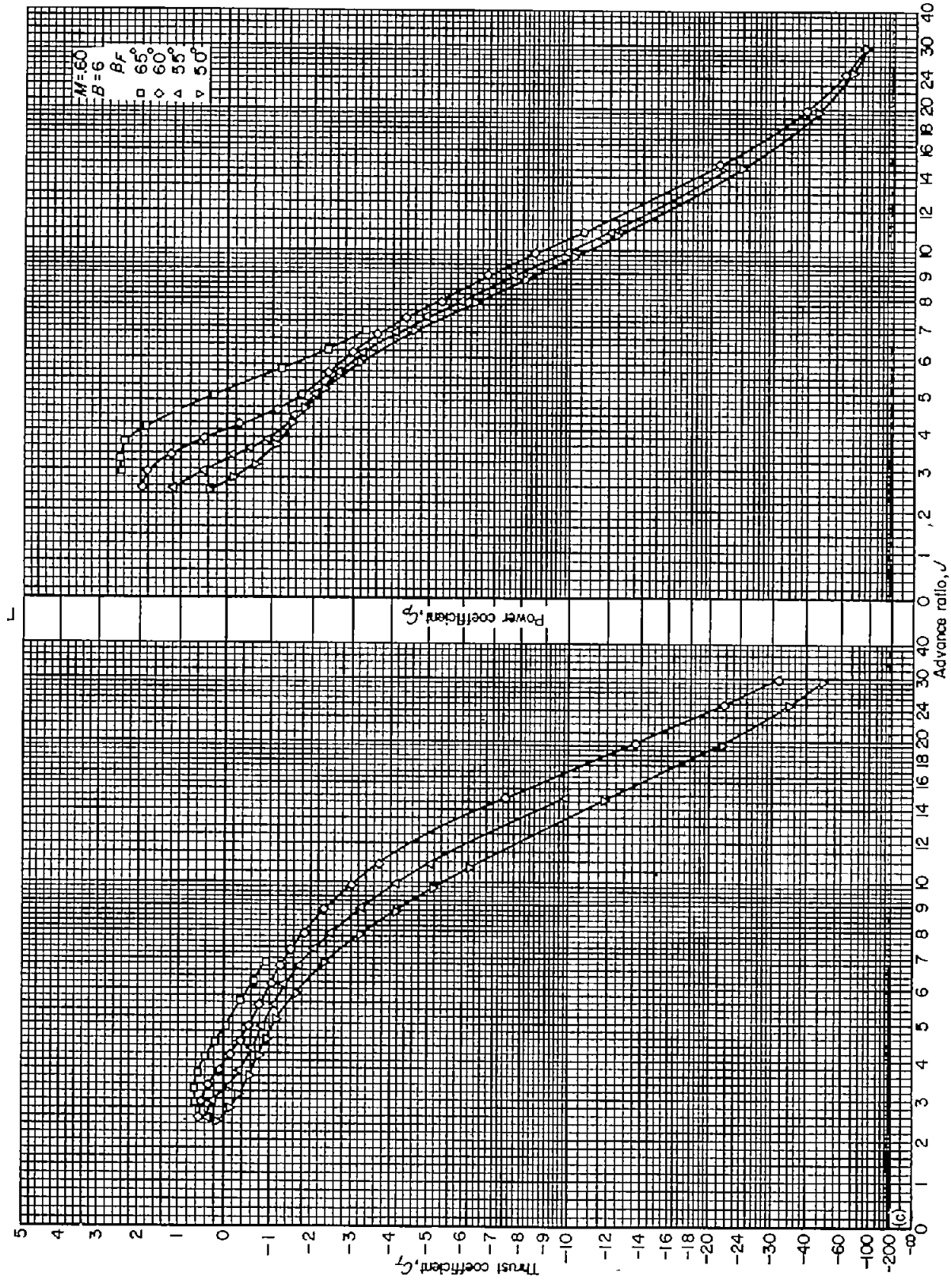

(c) $M = 0.60$

FIGURE 16.— Continued.

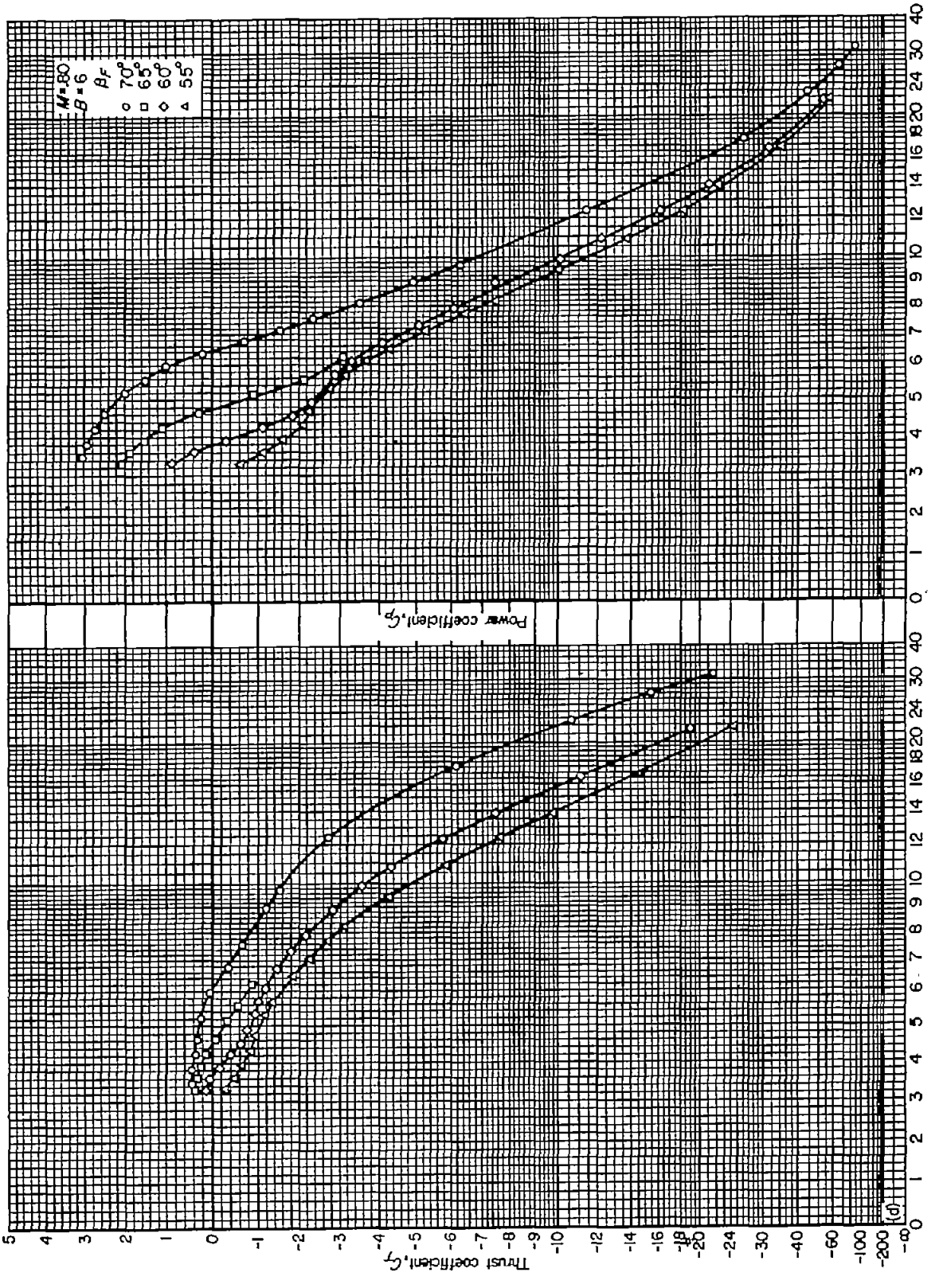

(d) $M=0.80$

FIGURE 18.—Concluded.

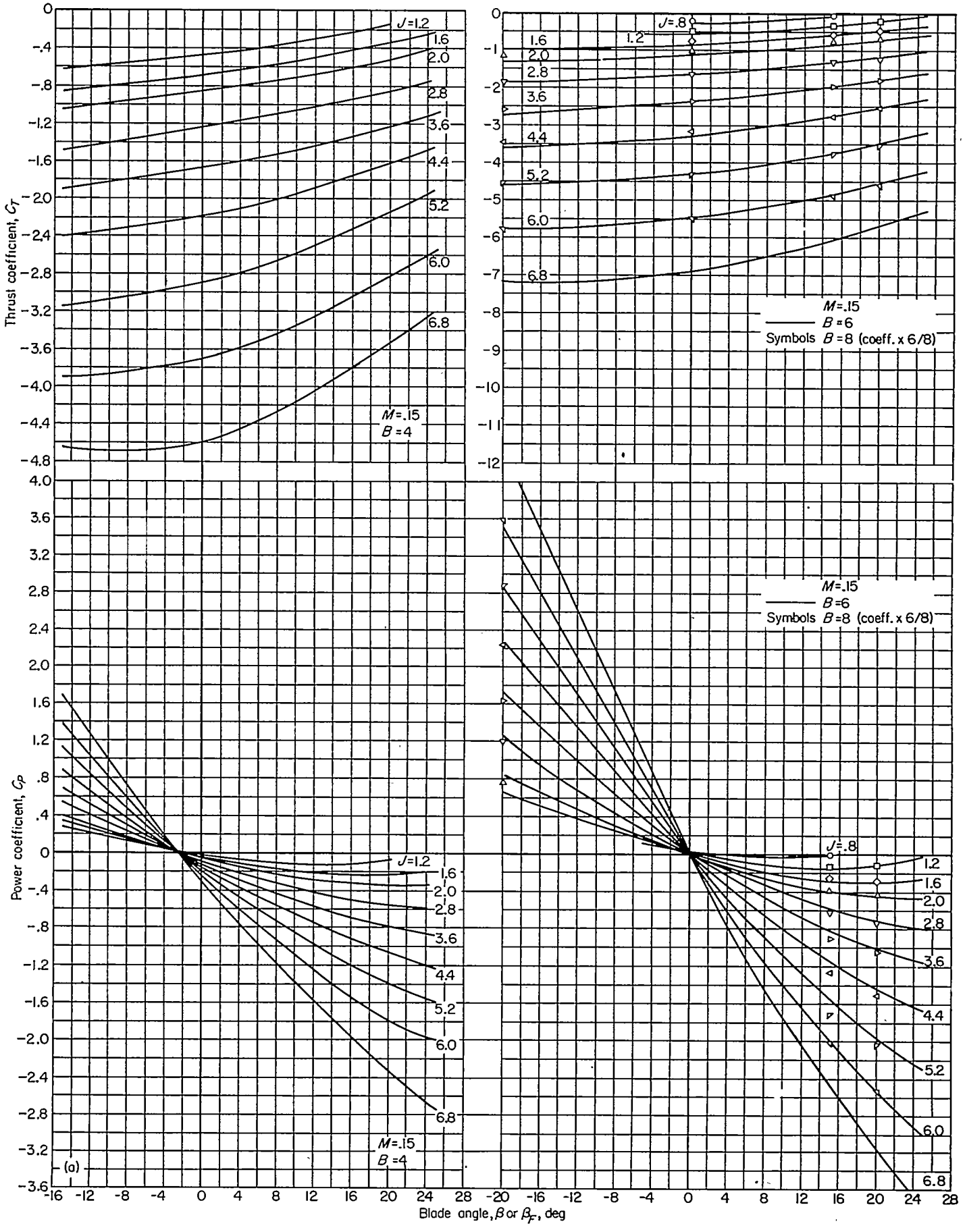

(a) $M=0.15$

FIGURE 17.—The effect of blade angle on the negative-thrust characteristics of the NACA 4-(5)(05)-041 four-blade, single-rotation propeller and the NACA 4-(5)(05)-037 six- and eight-blade, dual-rotation propellers.

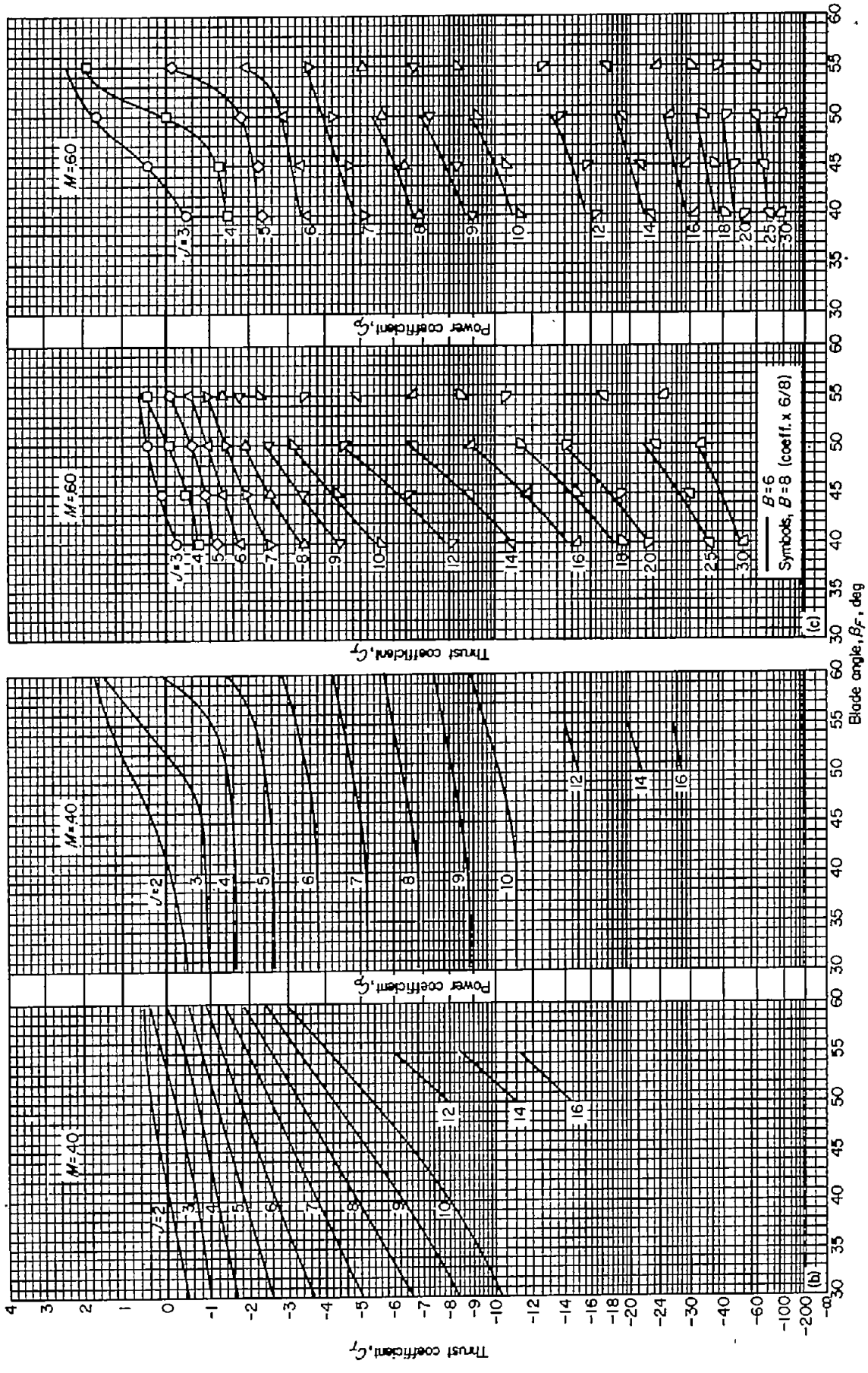

FIGURE 17.—Continued.

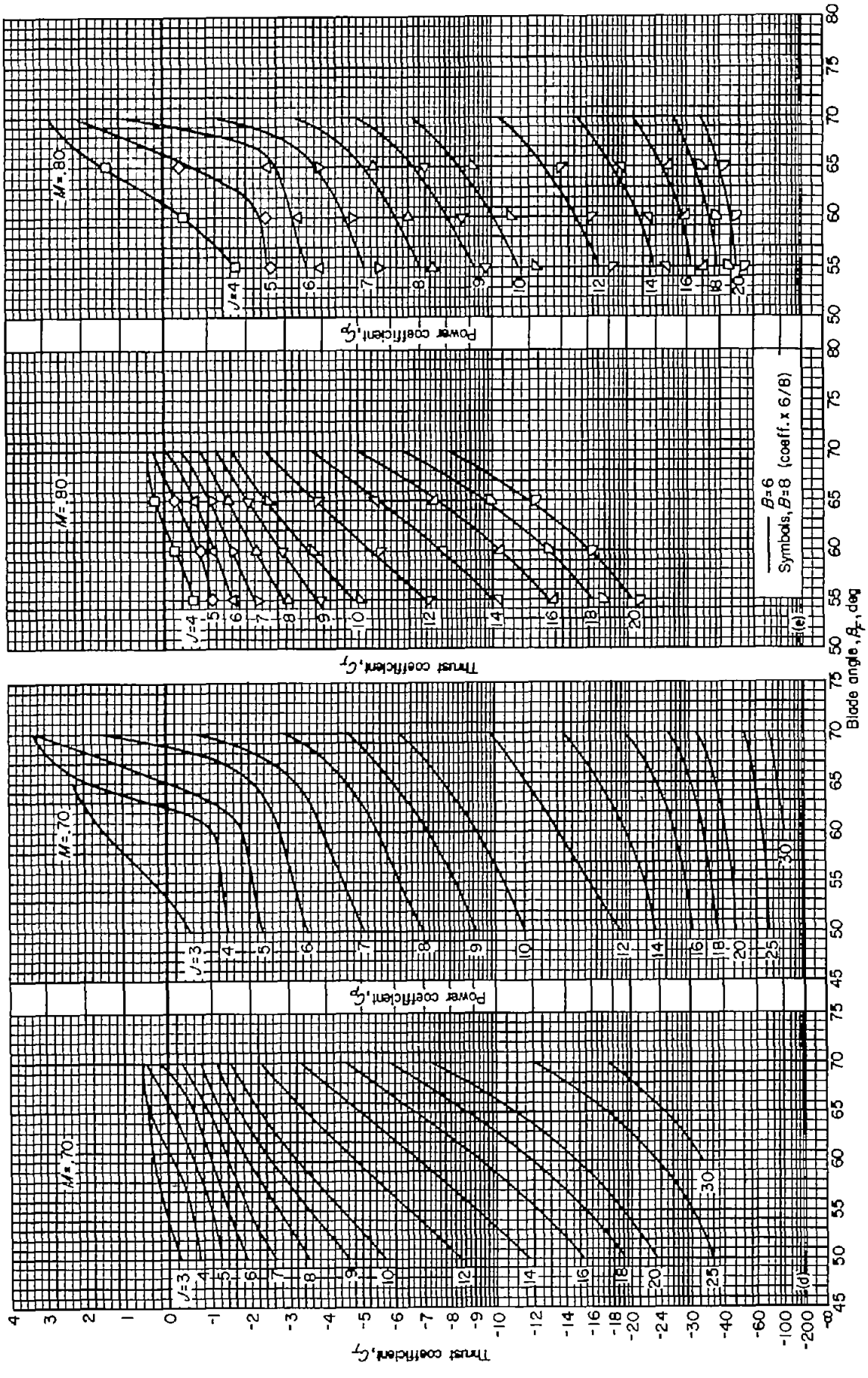

(d) $M=0.70$ (e) $M=0.80$

FIGURE 17.—Concluded.

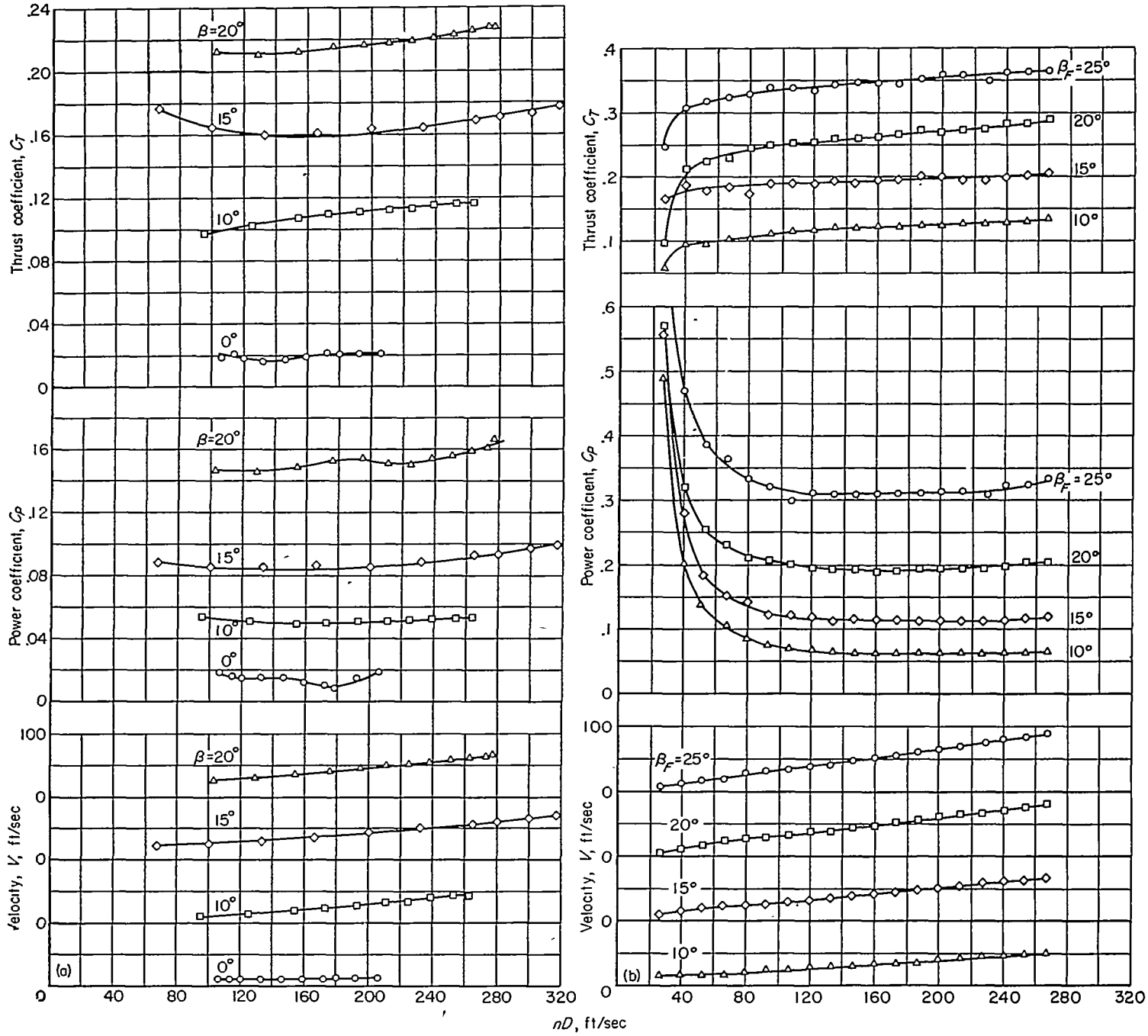

(a) NACA 4-(5)(05)-041 four-blade, single-rotation propeller.
(b) NACA 4-(5)(05)-037 six-blade, dual-rotation propeller, optimum $\Delta\beta$.

FIGURE 18.—Near static-thrust characteristics of the propellers with NACA 1-series spinners.

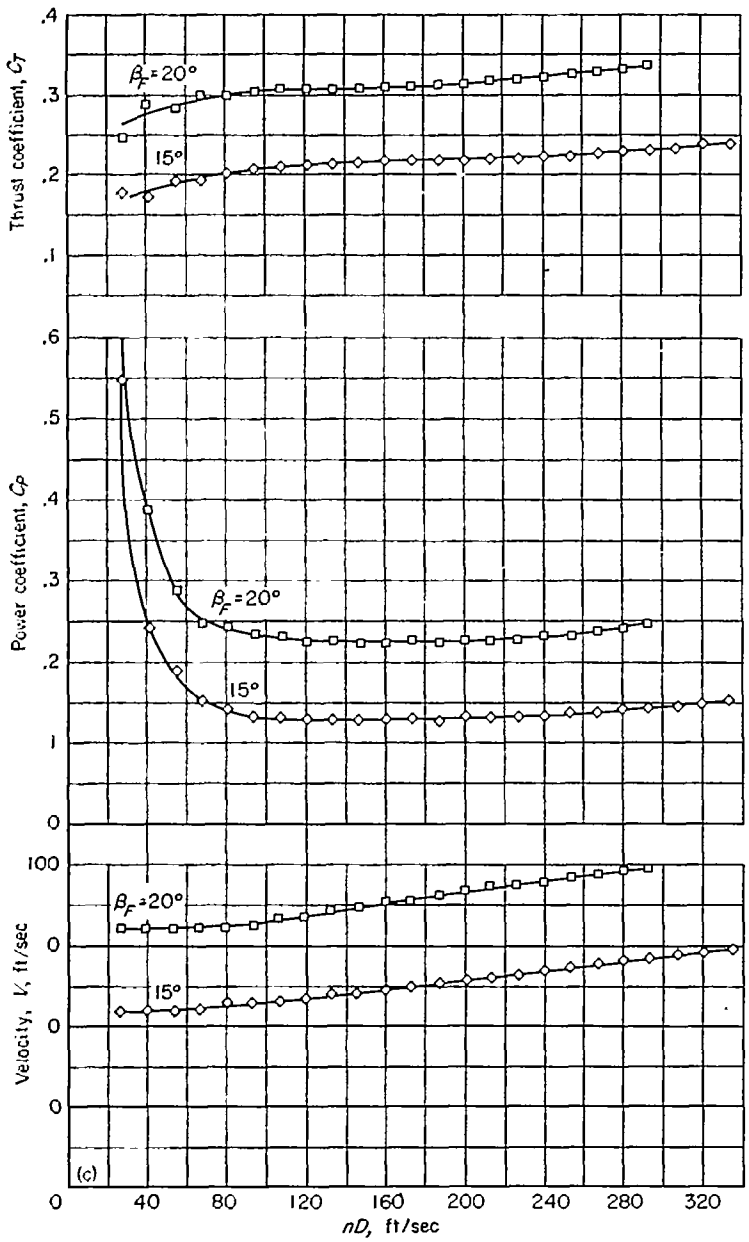

(c) NACA 4-(5)(05)-037 eight-blade, dual-rotation propeller, optimum $\Delta\beta$.

FIGURE 18.—Concluded.

CHARACTERISTICS OF PROPELLER-SPINNER-COWLING COMBINATIONS

Propeller characteristics in positive thrust.—The characteristics of the single- and dual-rotation ($\Delta\beta$=0.8°) propellers operating in the presence of the spinner-cowling combinations

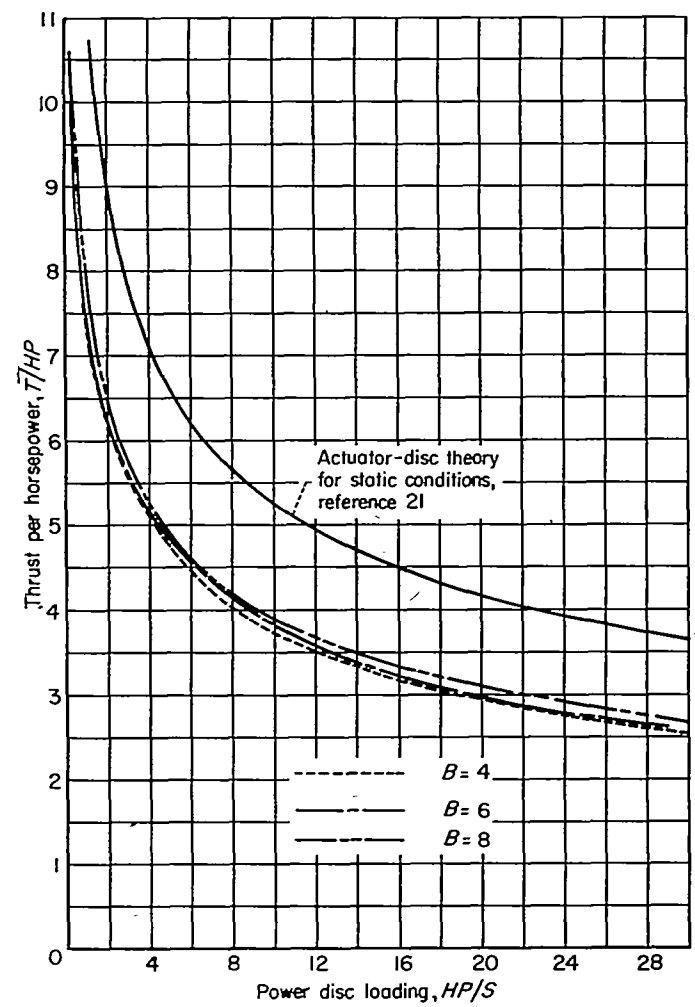

FIGURE 19.—Comparison with actuator-disc theory of the experimentally determined variation of thrust per horsepower with power disc loading for operation of the propellers at near static conditions.

are shown in figure 20. These data are only for cowling inlet-velocity ratios near 0.6 and only for the combinations with platform propeller-spinner junctures, since variation of inlet-velocity ratio within the range of these tests and changes from ideal (or sealed gap) to platform propeller-spinner junctures had only small effects, of the order of the accuracy of these tests, on the propeller characteristics.

A comparison of the maximum efficiency of the propellers operating in the presence of the spinner-cowling combinations, at an inlet-velocity ratio of 0.8, with the maximum efficiency of the propellers in combination with the spinners alone is presented in figure 21. It is readily seen that the

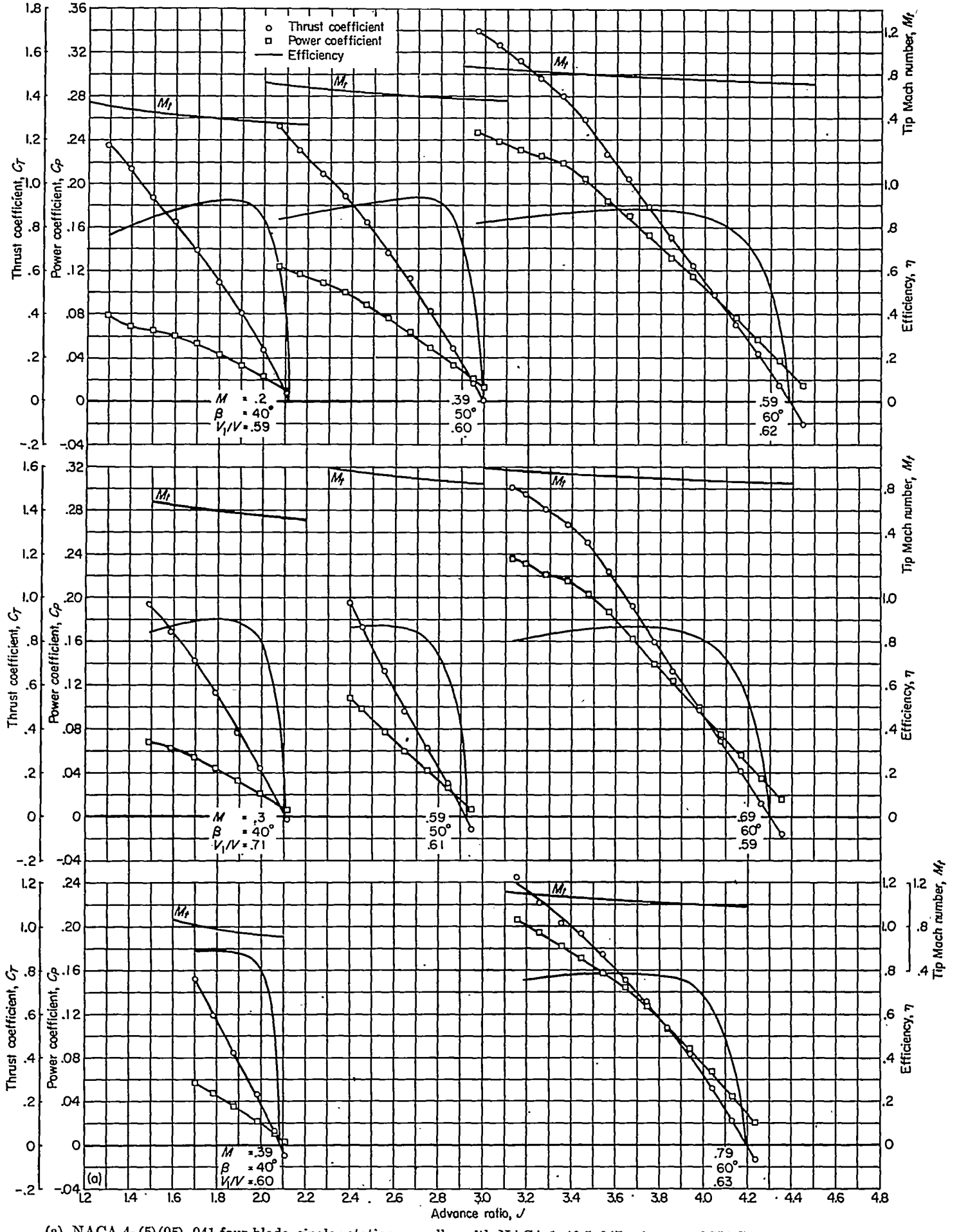

(a) NACA 4-(5)(05)-041 four-blade, single-rotation propeller with NACA 1-46.5-047 spinner and NACA 1-62.8-070 cowling.

FIGURE 20.—Positive-thrust characteristics of the propellers operating in the presence of the spinner-cowling combinations.

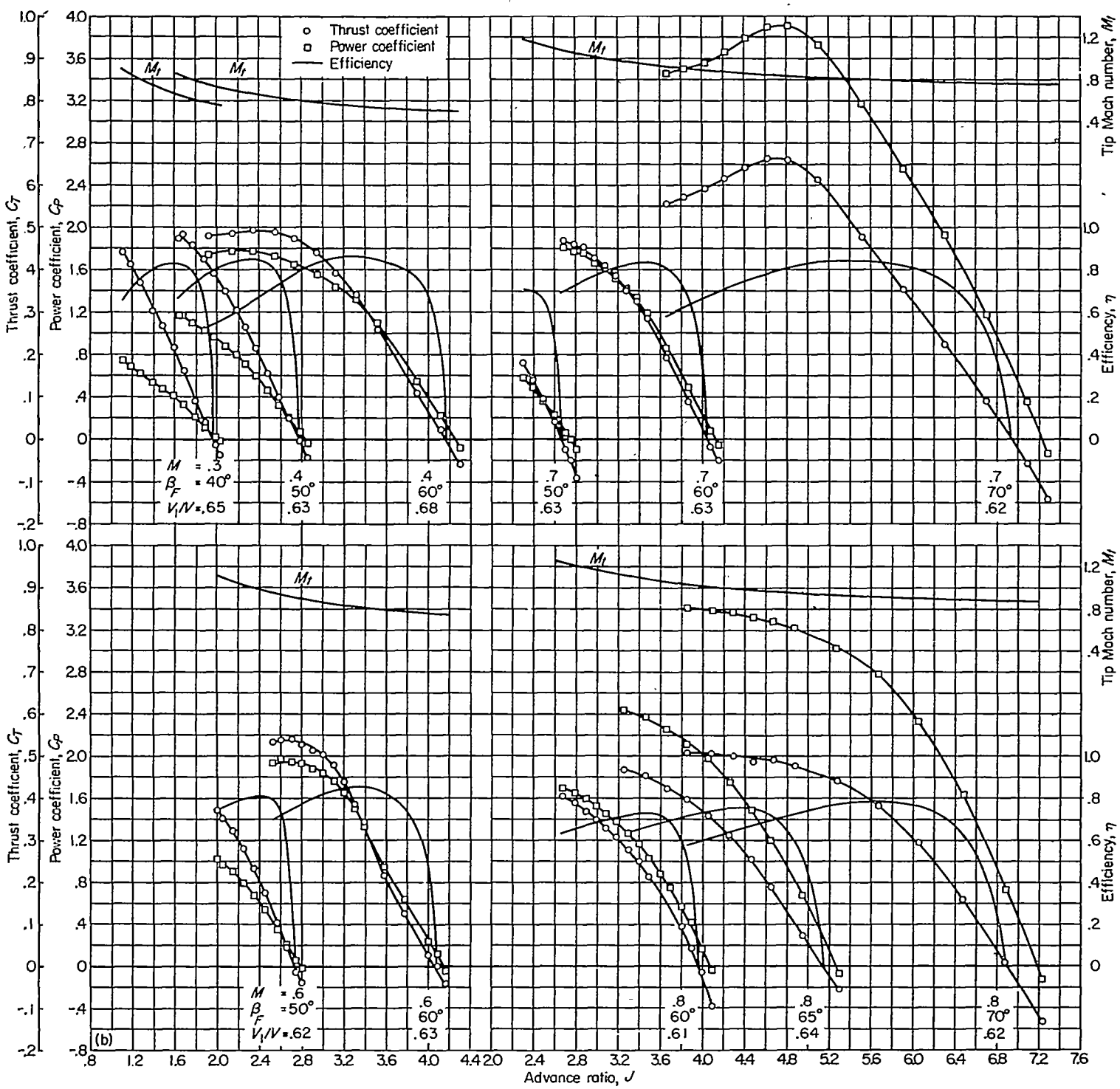

(b) NACA 4–(5)(05)–037 six-blade, dual-rotation propeller with NACA 1–46.5–085 spinner and NACA 1–62.8–070 cowling.

FIGURE 20.—Continued.

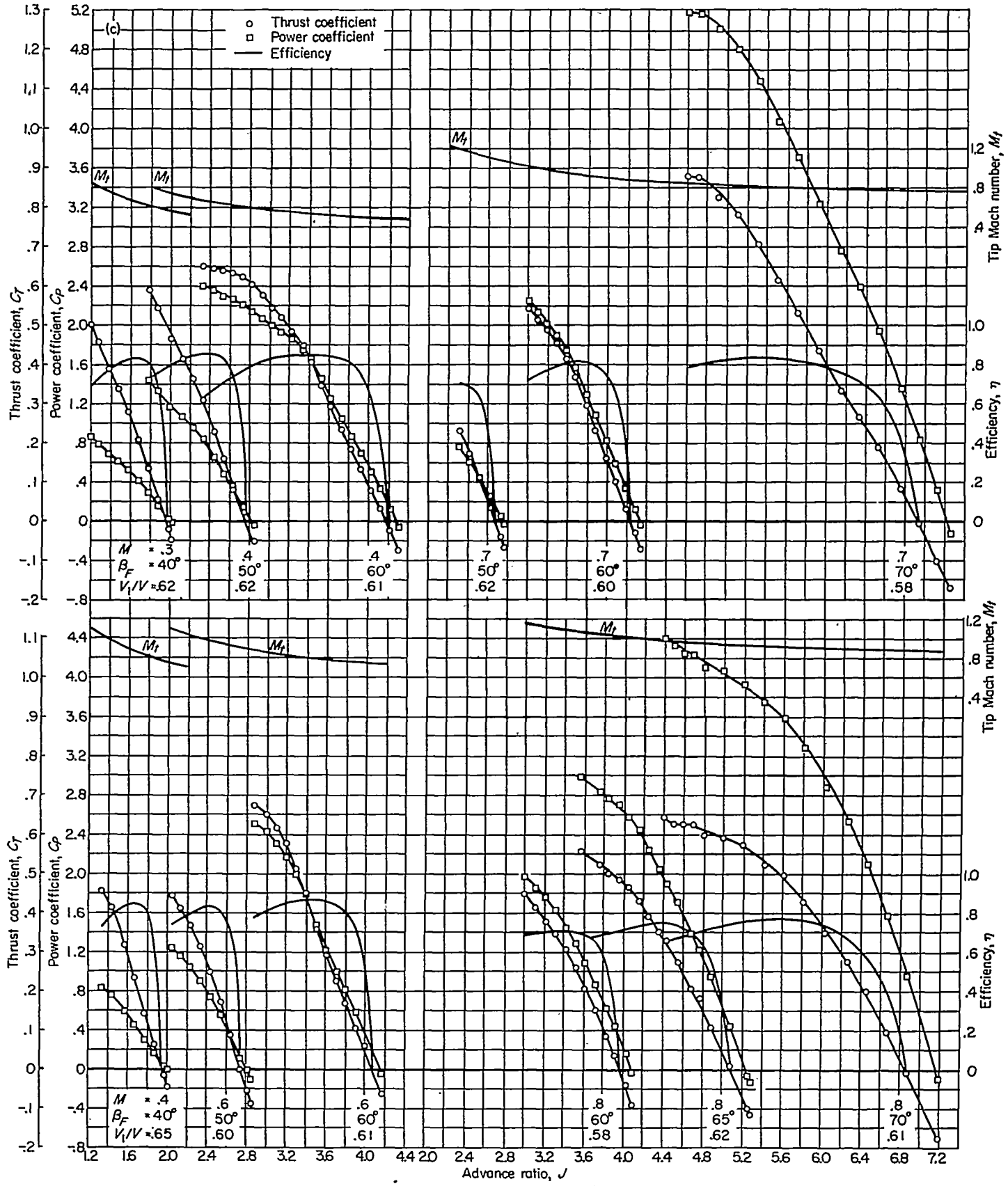

(c) NACA 4–(5)(05)–037 eight-blade, dual-rotation propeller with NACA 1–46.5–085 spinner and NACA 1–62.8–070 cowling.

FIGURE 20.—Concluded.

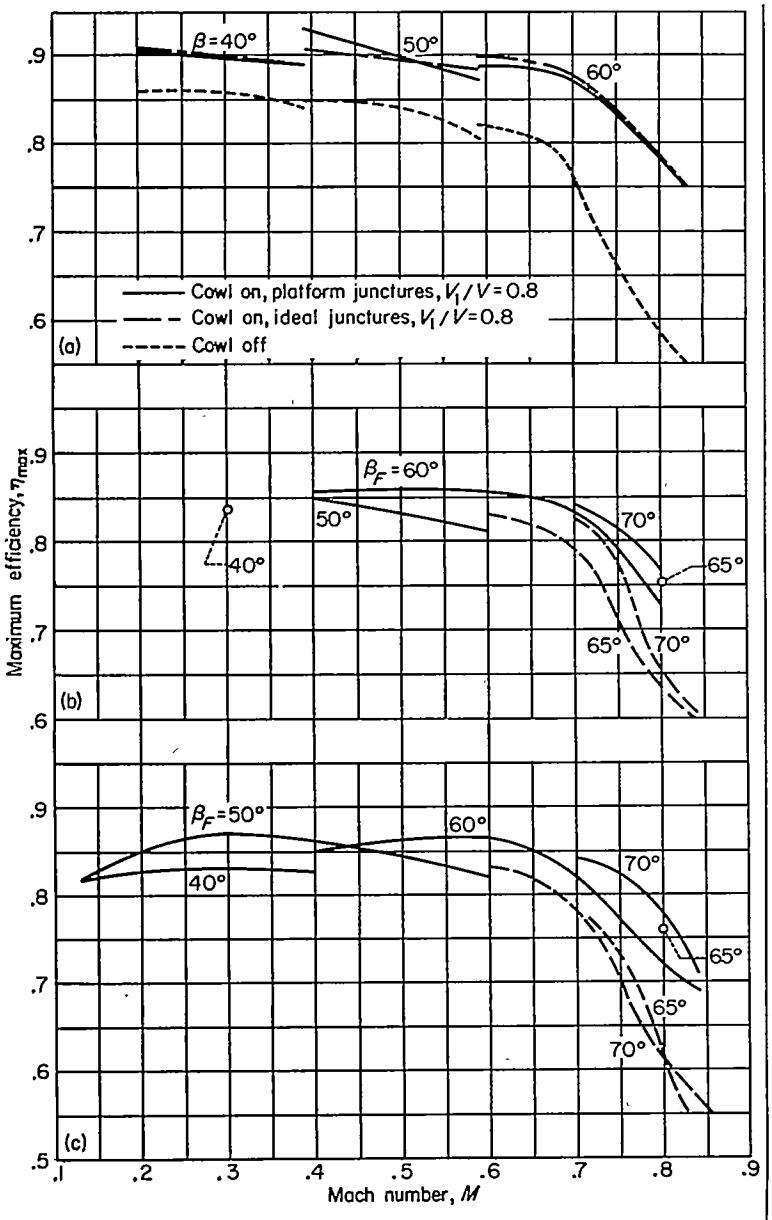

(a) NACA 4–(5)(05)–041 four-blade, single-rotation propeller.
(b) NACA 4–(5)(05)–037 six-blade, dual-rotation propeller.
(c) NACA 4–(5)(05)–037 eight-blade, dual-rotation propeller.

FIGURE 21.—The effect of the cowling on the variation with Mach number of the maximum efficiency of the propellers.

maximum efficiencies obtained for the propellers in the presence of the cowl were higher at all Mach numbers and blade angles than those for the isolated propeller-spinner combinations. For example, the efficiencies of the various configurations at a Mach number of 0.8 are compared in the following tabulation:

Propeller	β	Propeller efficiency	
		With spinner alone	With spinner-cowling combination
NACA 4–(5)(05)–041 four-blade	60°	0.59	0.78
NACA 4–(5)(05)–037 six-blade	65°	.63	.75
NACA 4–(5)(05)–037 eight-blade	65°	.61	.76

This trend would be expected, according to the discussion in reference 22, considering the reduction in air-stream velocities in the region of the propellers due to the interference effects of the cowling, as shown by the results of air-stream surveys in the propeller planes for the spinner-cowling combinations, presented in figure 22 and in table II. With the propeller at a given stream Mach number, blade angle, and rotational speed, these reduced local velocities due to the influence of the cowling lead to higher blade-section angles of attack and hence to an apparent increase in both propeller thrust and torque, compared to the values that would exist for the propeller operating in free air. This effect may be seen by comparing the data of figure 20 (a) with those of figure 7 for the four-blade propeller, and the data of figures 20 (b) and 20 (c) with the respective data in figure 13 for the dual-rotation propellers. Since the determination of propulsive thrust was precluded by the impracticality of measuring the increase in drag of the cowl and dynamometer parts within the influence of the propeller slipstream with the dynamometer arrangement used in the present investigation, and since the useful work done by the propeller is defined as the product of the thrust and the free-stream velocity, efficiencies computed for the propellers using these apparently higher thrust values are thus greater than those for the isolated propellers at equal advance ratios.

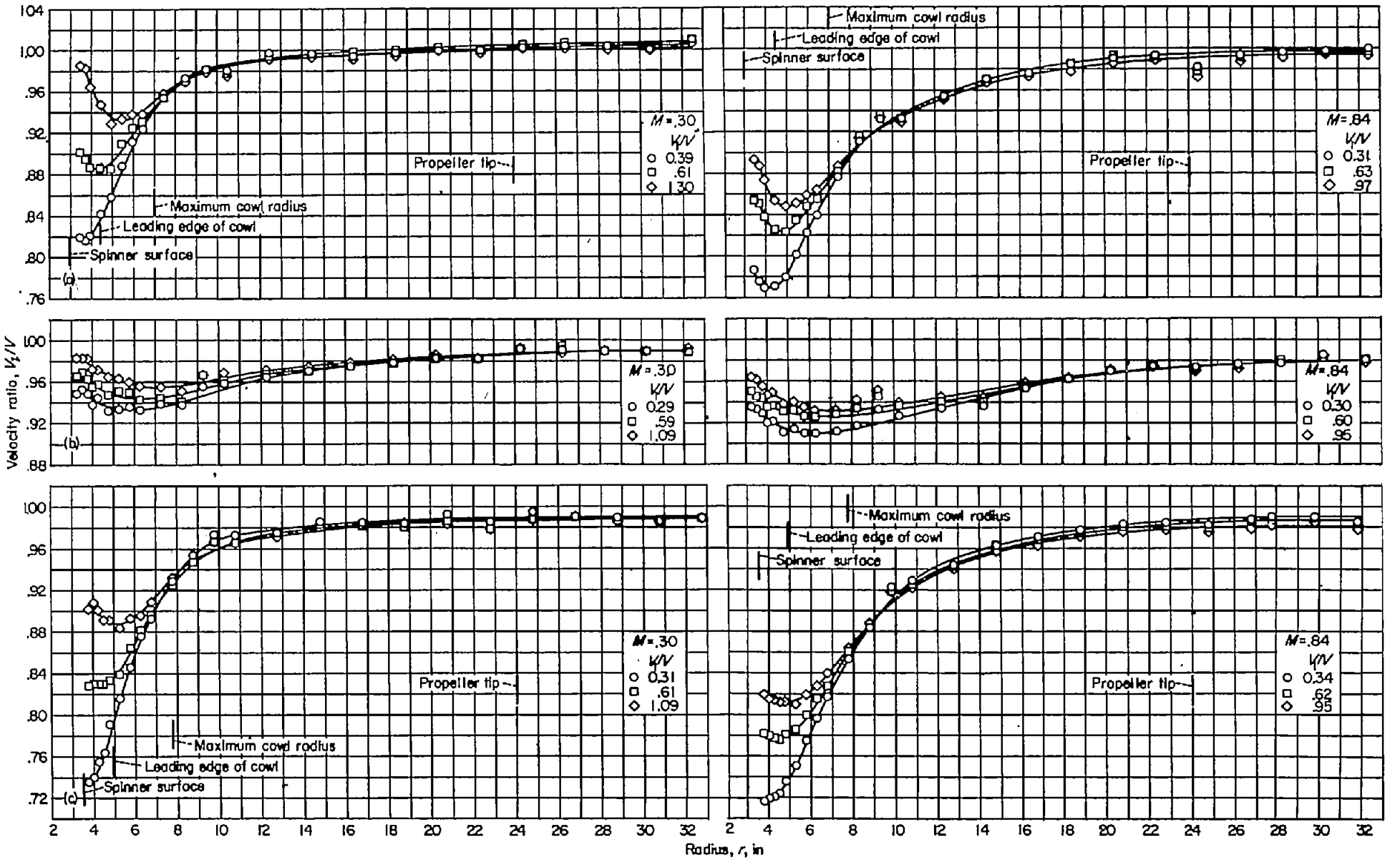

(a) NACA 1–46.5–047 spinner with NACA 1–62.8–070 cowling.
(b) NACA 1–46.5–085 spinner with NACA 1–62.8–070 cowling, front plane of rotation.
(c) NACA 1–46.5–085 spinner with NACA 1–62.8–070 cowling, rear plane of rotation.

FIGURE 22.—Typical radial distributions of the local velocity ratio at the propeller planes of the spinner-cowling combinations.

That the differences between the efficiencies of the propellers with the spinner-cowling combinations and the efficiencies of the isolated propeller-spinner combinations are smaller for the dual-rotation propellers than for the single-rotation propeller may also be explained with the aid of the survey data of figure 22 and table II. It is seen from these data that the interference effects of the cowl on the single-rotation propeller and on the rear component of the dual-rotation propellers were quite pronounced, with local velocities near the surface of the spinners reduced as much as 30 percent from the free-stream velocity at low inlet-velocity ratios. In contrast, the cowl had a much smaller effect on the flow at the front component of the dual-rotation propeller, causing local velocities over the inner portions of the blades to be reduced only about 9 percent. Thus the favorable interference effects of the cowling in alleviating the adverse effects of compressibility on the propeller characteristics would not be expected to be as large for the dual-rotation propeller-spinner-cowling combinations as for the single-rotation combination.

It may be noted that with the design $\Delta\beta$ of 0.8°, the front and rear components of the dual-rotation propellers did not absorb equal power when operating at the advance ratio for maximum efficiency. On the basis of the comparison of the data of figure 14 with those of figure 9, it would be expected that the efficiencies of the dual-rotation propellers would be of the order of 2 percent higher than those measured if the propellers were operated at more nearly optimum blade angles so that the two components of the propeller would absorb equal power at an advance ratio near that for maximum efficiency.

Inlet characteristics.—The effects of Mach number, inlet-velocity ratio, blade angle, advance ratio, and propeller-spinner juncture on the pressure recovery at the inlet of the propeller-spinner-cowling combinations are shown in plots of typical data in figures 23 and 24, and are summarized in the comparisons presented in figure 25.

As shown in figure 25, the pressure-recovery characteristics of the spinner-cowling combinations with the propeller removed were not affected by compressibility within the range of Mach numbers covered in this investigation. Ram-recovery ratios greater than 0.96 were obtained at all inlet-velocity ratios greater than about 0.4 and 0.51, respectively, for the single- and dual-rotation spinner-cowling combinations. Decreasing inlet-velocity ratio below these values led to abrupt and rapid losses in pressure recovery due to thickening of the spinner boundary layer, as shown by the radial distributions of pressure recovery presented in figures 23 (e) and 23 (f). The recoveries obtained for the cowling with the NACA 1–46.5–085 spinner were lower at all test conditions than those obtained with the shorter NACA 1–46.5–047 spinner, as shown in figure 25. Also, the inlet-velocity ratio required to avoid excessive inlet losses was higher for the –085 spinner than for the –047 spinner, that is, 0.51 as compared to 0.45. Comparison of the pressure recoveries presented herein for the NACA 1–46.5–085 spinner in combination with the NACA 1–62.8–070 cowling with those reported in reference 13 for a model of the same geometric proportions shows relatively good agreement in spite of the differences between the two models in the location and extent of the inlet instrumentation and in spinner surface condition (the spinner of ref. 13 had a smooth, continuous, painted surface, whereas the spinner of the present investigation had machined surfaces and a discontinuity at the gap between the front and rear components).

With the addition of the propellers to the spinner-cowling combinations, the recoveries in the cowling inlet were affected not only by the spinner boundary layer, as in the case with the propeller removed, but also by the angle of attack (loading) of the platforms and inner portions of the propeller blades, by the air flow through the gap between the platforms and the propeller blades, and by other propeller interference effects. The comparison, in figure 25, of the pressure recoveries obtained with the various propeller-spinner-cowling combinations at operating conditions near those for maximum propeller efficiency shows that the addition of the propellers, with platform propeller-spinner junctures, to the spinner-cowling combinations resulted in a considerable decrease in pressure recovery due to the interference effects of the propellers. Also, as might be expected, the interference effects of the propellers generally increased with increasing solidity of the propellers. As shown in figure 24, however, for constant inlet-velocity ratios, operation of the propellers at combinations of blade angles, rotational speeds, and forward speeds that increased the angle of attack, and thus the loading, of the platforms and inner portions of the blades resulted in increased recoveries, exceeding a value of 1.0 in the case of the dual-rotation propellers at low Mach numbers and high rotational speeds. For these operating conditions, it is apparent that the pumping action of the platforms and inner portions of the blades added sufficient energy to the inlet flow to overcome the energy losses in the spinner boundary layer. Figure 24 also shows that variation of propeller advance ratio had a considerably greater effect on the pressure recoveries of the dual-rotation, propeller-spinner-cowling combinations than on the recoveries of the single-rotation combination at comparable operating conditions. Several factors may contribute to this behavior, such as the higher solidity, smaller rotational losses, and higher platform-juncture angles of the dual-rotation propellers.

Maximum pressure recoveries for the propeller-spinner-cowling combinations were obtained at inlet-velocity ratios near 1.0, as shown in figure 25. Although decreasing inlet-velocity ratio of the propeller-spinner-cowling combinations, at a constant Mach number, blade angle, and rotational speed, tends to increase the angle of attack of the platforms and inner portions of the blades, it is evident from the data that the resulting losses in energy in the thickened boundary layer were greater than the energy imparted to the inlet flow by the increased loadings on the platforms and inner propeller blade sections. Consequently, as shown in figures 23 to 25, pressure recoveries in the inlets behind operating propellers decreased with decreasing inlet-velocity ratio, as for the spinner-cowling combinations alone, but in a more gradual manner and with less distinct "breaks" in the recoveries at low inlet-velocity ratios. Figures 24 and 25 show that the pressure recoveries for the various combinations were essentially the same at high speeds; for example, the single-

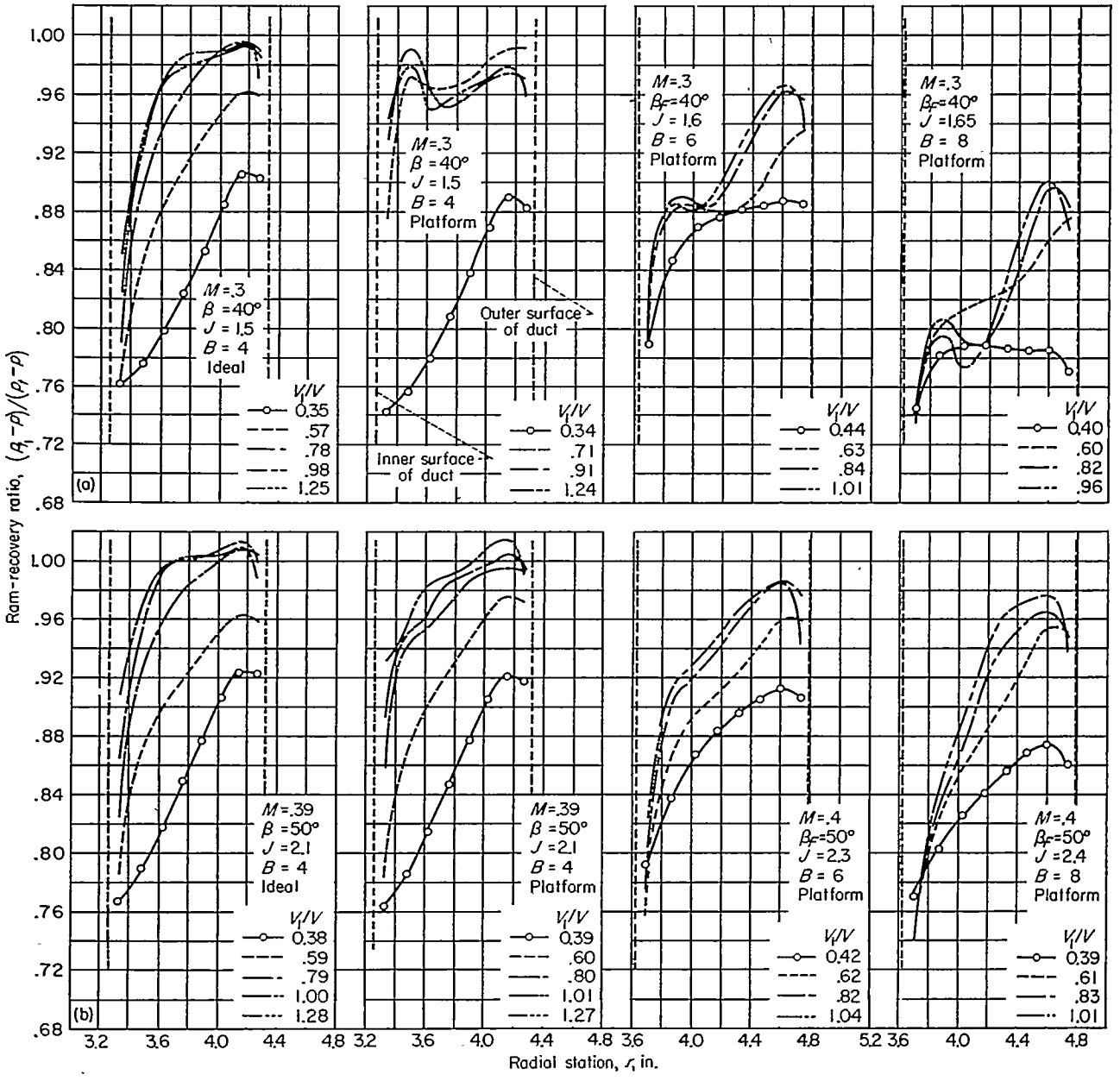

(a) Propeller-spinner-cowling combinations, with ideal and platform junctures, at $M=0.30$.
(b) Propeller-spinner-cowling combinations, with ideal and platform junctures, at $M\cong0.40$.

FIGURE 23.—Typical radial distributions of ram-recovery ratio at the inlet of the spinner-cowling combinations.

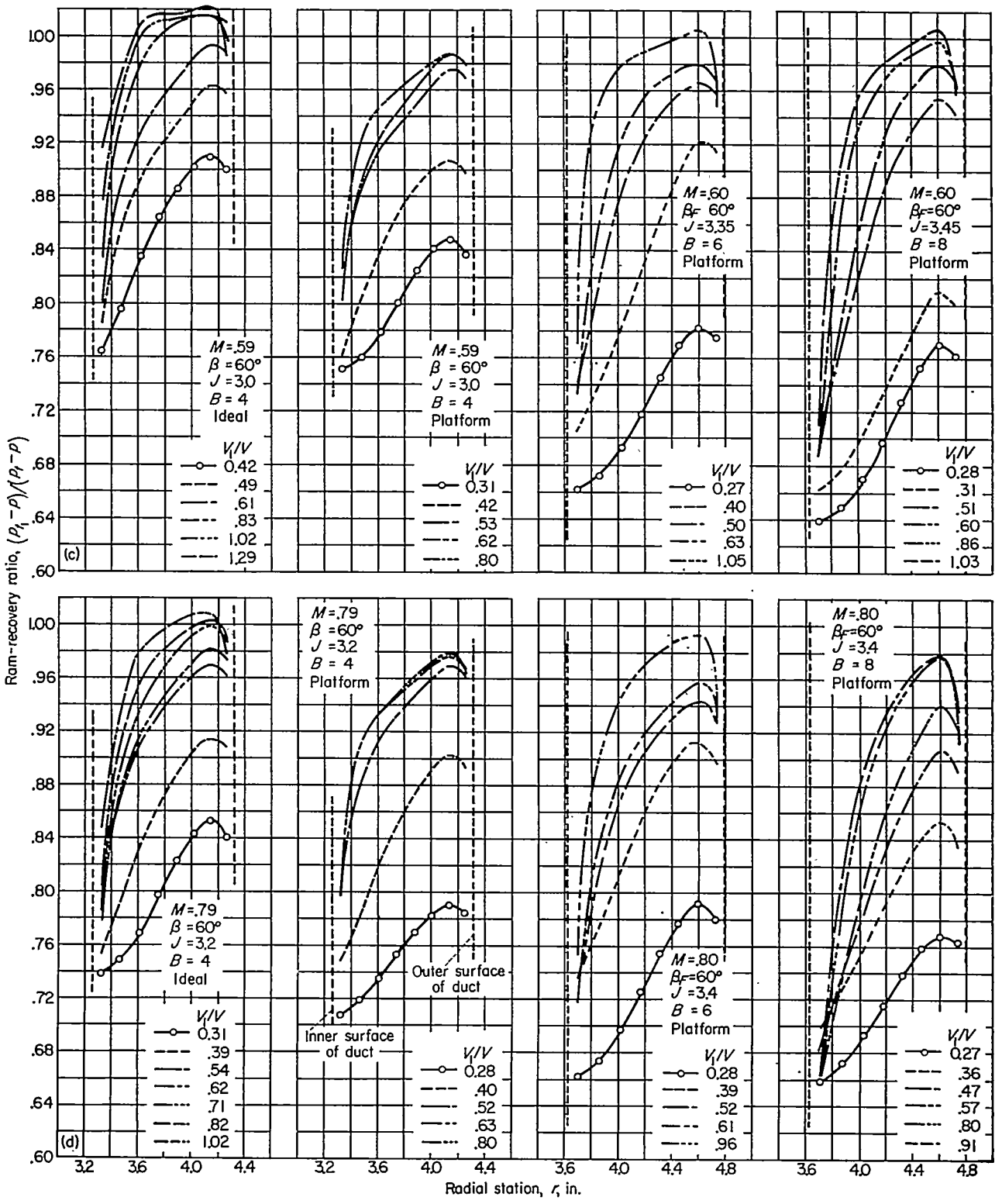

(c) Propeller-spinner-cowling combinations, with ideal and platform junctures, at $M \cong 0.60$.
(d) Propeller-spinner-cowling combinations, with ideal and platform junctures, at $M \cong 0.80$.
FIGURE 23.—Continued.

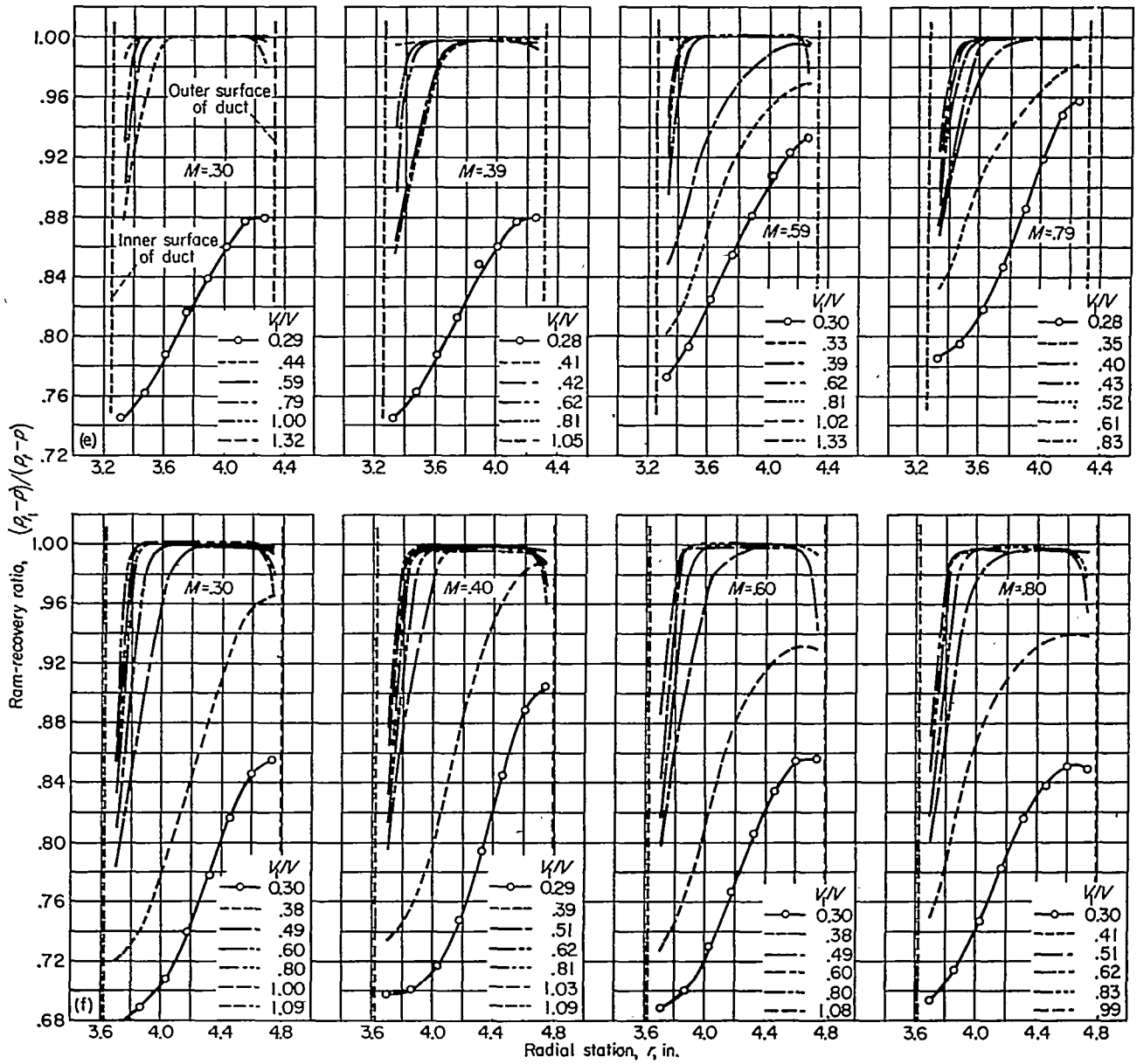

(e) NACA 1–46.5–047 spinner with NACA 1–62.8–070 cowling, propeller removed.
(f) NACA 1–46.5–085 spinner with NACA 1–62.8–070 cowling, propeller removed.

FIGURE 23.—Concluded.

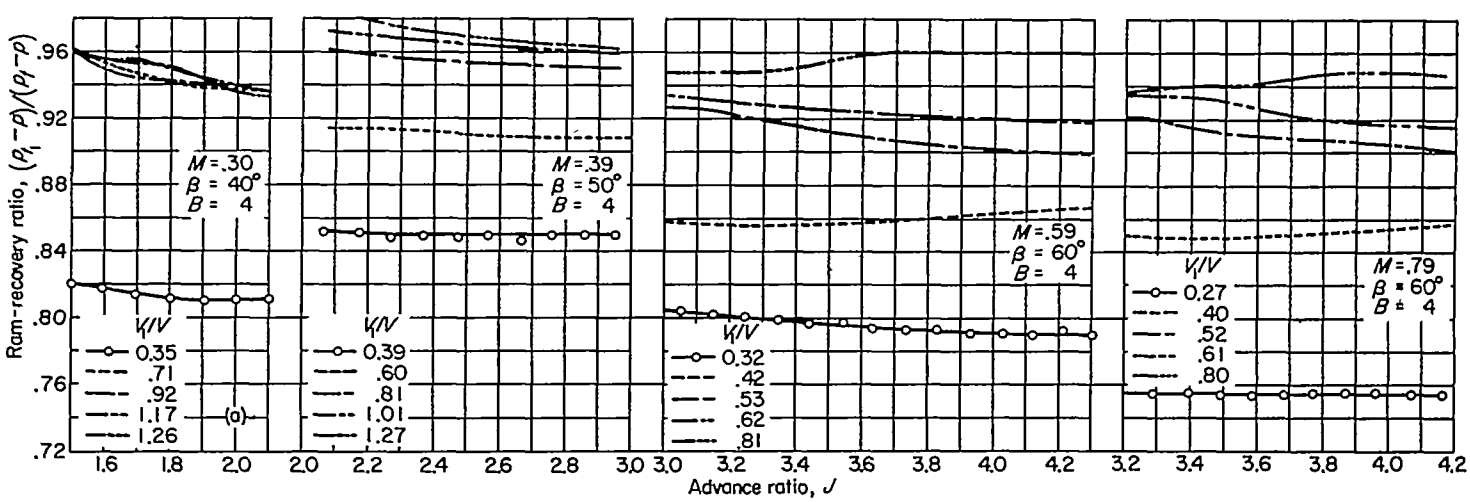

(a) Single-rotation propeller-spinner-cowling combination.

FIGURE 24.—The effect of propeller advance ratio on the average ram-recovery ratio at the spinner-cowling inlet, with platform junctures.

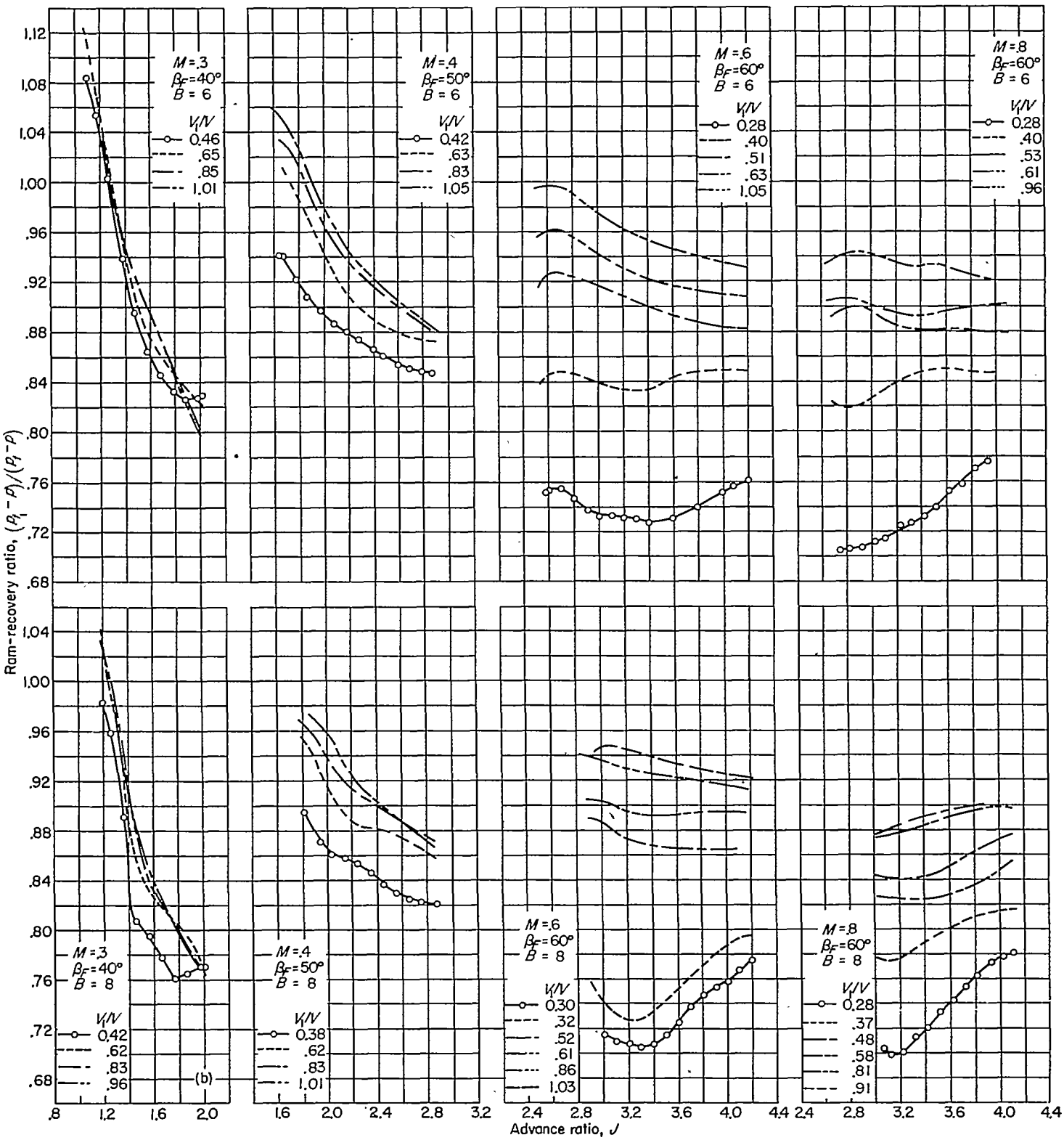

(b) Dual-rotation propeller-spinner-cowling combinations.

FIGURE 24.—Concluded.

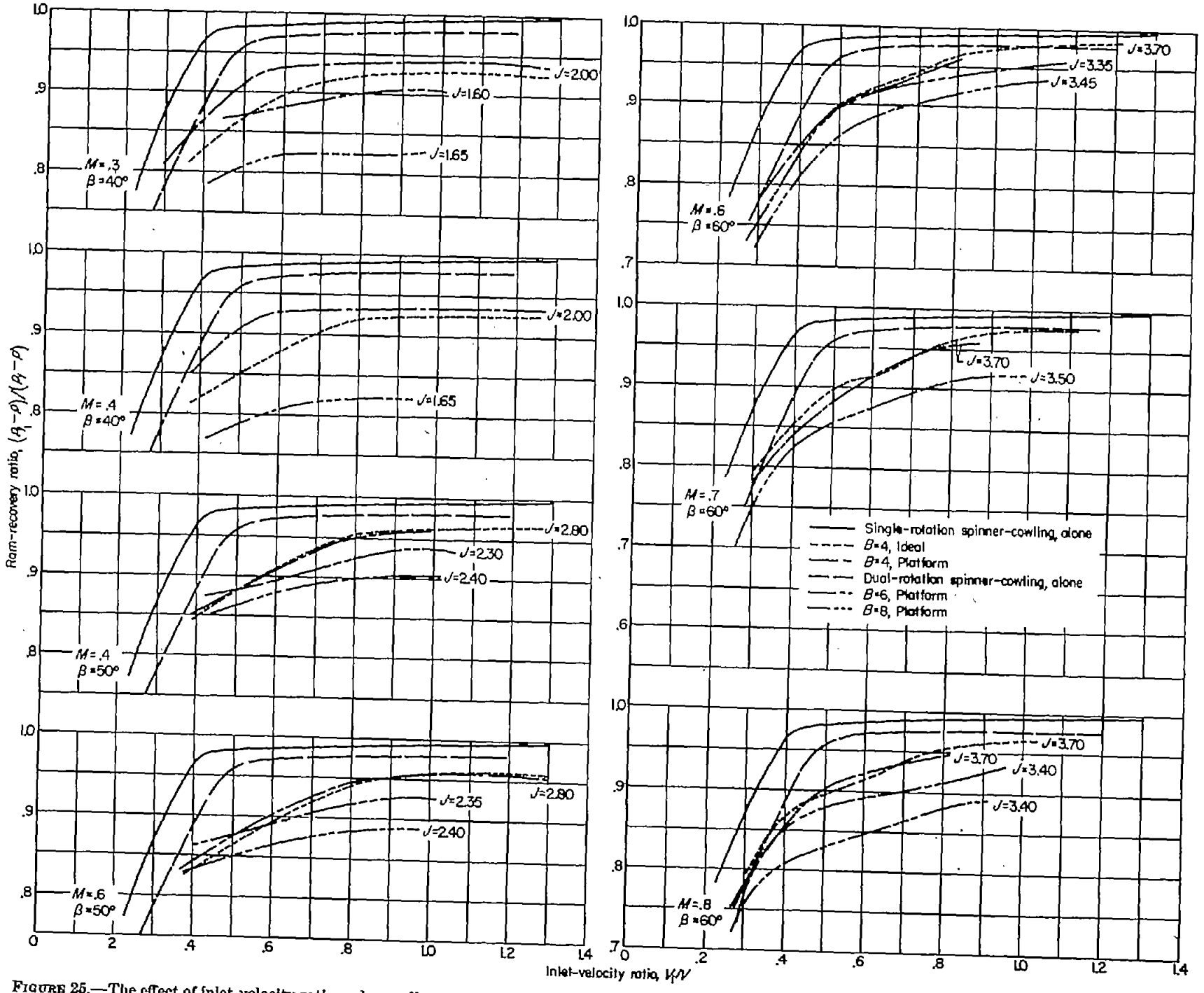

FIGURE 25.—The effect of inlet-velocity ratio and propeller operation on the average ram-recovery ratio at the inlet of the propeller-spinner-cowling combinations.

rotation propeller-spinner-cowling combination at $M=0.8$, $J=3.7$, and $V_1/V=0.42$ had a recovery ratio of 0.87, whereas the dual-rotation combinations at $M=0.8$, $J=4.2$, and $V_1/V=0.50$ attained recovery ratios of 0.88 and 0.86, respectively, with the six- and eight-blade propellers.

The effect of Mach number on the pressure recoveries at the inlets of the propeller-spinner-cowling combinations is shown indirectly in figure 25. Comparison of the pressure recoveries obtained for a spinner-cowling combination with a given propeller, at a constant blade angle and nearly constant advance ratio but at different test Mach numbers, shows that increasing Mach number generally resulted in lower pressure recoveries for both the single- and dual-rotation propeller-spinner-cowling combinations. That this is due to compressibility effects on the platforms and inner portions of the blades is also evidenced by the fact that variation of Mach number had the greatest effect on the recoveries of the dual-rotation combinations. A secondary effect of Mach number, shown most clearly by the data for the dual-rotation propellers, is that with increasing Mach number it was possible to operate the inlet to lower inlet-velocity ratios before the abrupt losses in pressure recovery were encountered.

The pressure recoveries obtained for the single-rotation propeller-spinner-cowling combination with ideal and platform propeller-spinner junctures are also compared in figure 25. Little difference exists between the recoveries obtained with the two types of junctures, except for the lowest blade angle of the tests where the angular discontinuity between the platforms and propeller blades was a maximum. The higher pressure recoveries obtained with the platform-type junctures at this operating condition may be due either to the fact that the platform junctures were being operated at a more favorable angle of attack than the corresponding sections of the ideal junctures, or to the possibility that the spinner boundary layer was energized by a vortex generated at the gap between the platforms and the blades. Evidence of these possibilities is shown (fig. 23 (a)) by the fact that the pressure recoveries obtained near the inner surface of the inlet with the platform junctures were higher than those for the ideal junctures. It may be noted that, as shown in figure 23 (a), the radial variations of pressure recovery across the inlet of the dual-rotation propeller-spinner-cowling combinations with platform junctures showed the same double peak, for a blade angle of 40°, as those for the single-rotation combination. Ideal junctures on the eight-blade, dual-rotation, propeller-spinner-cowling combination were simulated in limited tests made with the propeller blades alined with the platforms at $\beta_F=65°$ and with the juncture gaps sealed. At a Mach number of 0.8 and at inlet-velocity ratios greater than 0.5, the recoveries obtained with the platform gap sealed were about 3 percent higher than those with the gap open.

Spinner-cowling pressure distributions.—The effects of Mach number, inlet-velocity ratio, and propeller operation on the static-pressure distributions on the external and inner-lip surfaces of the single-rotation propeller-spinner-cowling combination are shown in figures 26 to 28. These data show the same general characteristics as those reported in reference 23 for other spinner-cowling combinations employing the NACA 1-series coordinates. In general, operation of the propeller resulted in more positive pressure coefficients on the external surface of the cowling at all inlet-velocity ratios and Mach numbers, as compared with the distributions obtained with the propeller removed. The external pressure distributions were unaffected, at least for the inlet-velocity ratios of these tests, by the change from ideal to platform propeller-spinner junctures.

The effect of inlet-velocity ratio on the critical Mach number of the spinner-cowling combination is shown in figure 29. At an inlet-velocity ratio of 0.42, the measured critical Mach number of 0.79 was somewhat higher than the predicted value of 0.75.

CONCLUSIONS

An investigation of the NACA 4–(5)(05)–041 four-blade, single-rotation propeller and the NACA 4–(5)(05)–037 six- and eight-blade, dual-rotation propellers operating with various spinners and spinner-cowling combinations at Mach numbers up to 0.84 indicated the following:

1. The highest Mach number at which the propellers with NACA 1-series spinners operated without marked compressibility losses was about 0.7. The maximum efficiencies of the propellers at this Mach number were 0.79, 0.83, and 0.82, respectively, for the four-, six-, and eight-blade propellers at a blade angle of 65°. The results indicate that for operation of the propellers at Mach numbers greater than about 0.8, highest efficiencies would be obtained at lower advance ratios and blade angles.

2. Substantially higher efficiencies were obtained for the NACA 4–(5)(05)–041 four-blade, single-rotation propeller in combination with extended cylindrical spinners as compared to those obtained for the propeller with the NACA 1-series spinners, amounting to as much as 15 percent at the highest Mach number and blade angle of these tests.

3. There were no significant effects of compressibility on the negative-thrust characteristics of the dual-rotation propellers up to a Mach number of about 0.6. When compared on the basis of total solidity, the negative-thrust characteristics of the propellers were in good agreement.

4. The thrust per horsepower produced by the propellers at near static conditions varied with power disc loading as calculated by actuator disc theory, but the measured values were about 28 percent lower than the ideal values. At a power disc loading of about 20, the propellers produced about 3.0 pounds of thrust per horsepower at near static conditions.

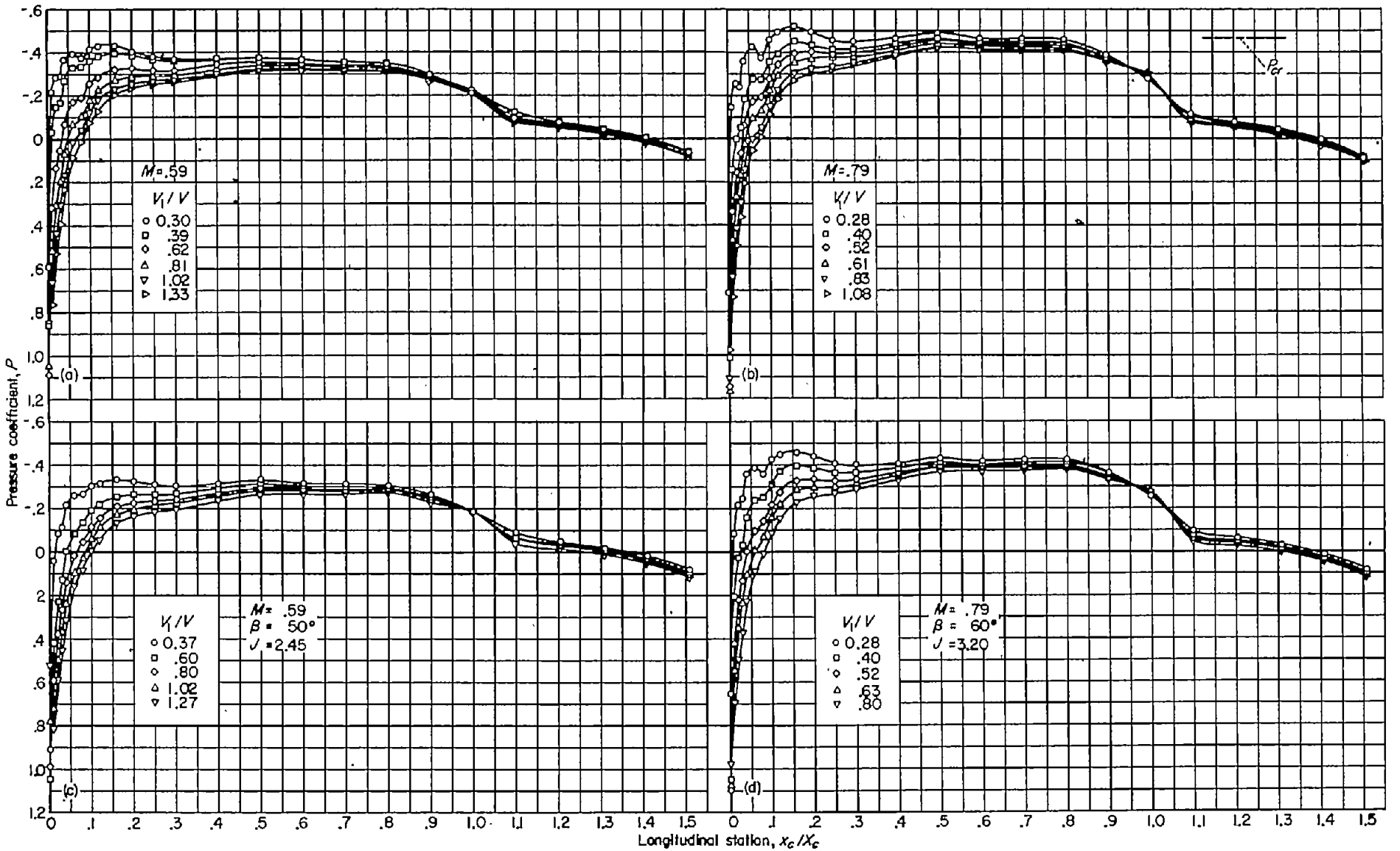

(a) $M=0.59$, propeller removed.
(b) $M=0.79$, propeller removed.
(c) $M=0.59$, propeller operating, platform junctures.
(d) $M=0.79$, propeller operating, platform junctures.

FIGURE 26.—Typical static-pressure distributions on the external surfaces of the NACA 1–62.8–070 cowling, single-rotation propeller-spinner-cowling combination.

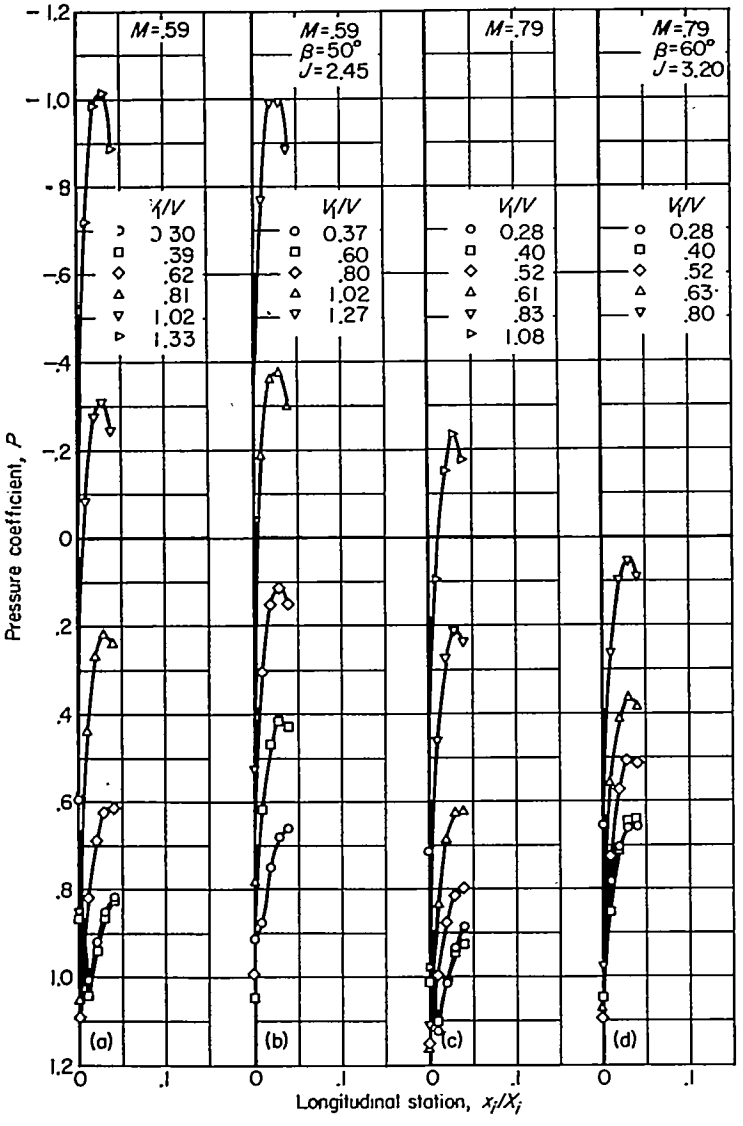

(a) $M=0.59$, propeller removed.
(b) $M=0.59$, propeller operating, platform junctures.
(c) $M=0.79$, propeller removed.
(d) $M=0.79$, propeller operating, platform junctures.

FIGURE 27.—Typical static-pressure distributions on the inner-lip surface of the NACA 1–62.8–070 cowling, single-rotation propeller-spinner-cowling combination.

5. The maximum efficiencies obtained for the propellers operating in the presence of the cowlings were higher at all Mach numbers and blade angles than those for the isolated propeller-spinner combinations, with the difference in efficiencies amounting to as much as 19 percent for the single-rotation propeller at a Mach number of 0.8. Variation of cowling inlet-velocity ratio and changes from ideal- to platform-type propeller-spinner junctures had no significant effects on the characteristics of the propeller.

6. Ram-recovery ratios greater than 0.96 were obtained at inlet-velocity ratios greater than about 0.4 and 0.51, respectively, for the single- and dual-rotation spinner-cowling combinations with the propeller removed. Decreasing inlet-velocity ratio below these values resulted in abrupt and rapid losses in pressure recovery. Addition of the propellers, with platform propeller-spinner junctures, to the spinner-cowling combinations resulted in a considerable decrease in pressure recovery. Except at low blade angles, where the angular discontinuity between the platform and propeller blades was large, only small differences in pressure recovery were noted between operation of the propellers with ideal- and platform-type propeller-spinner junctures.

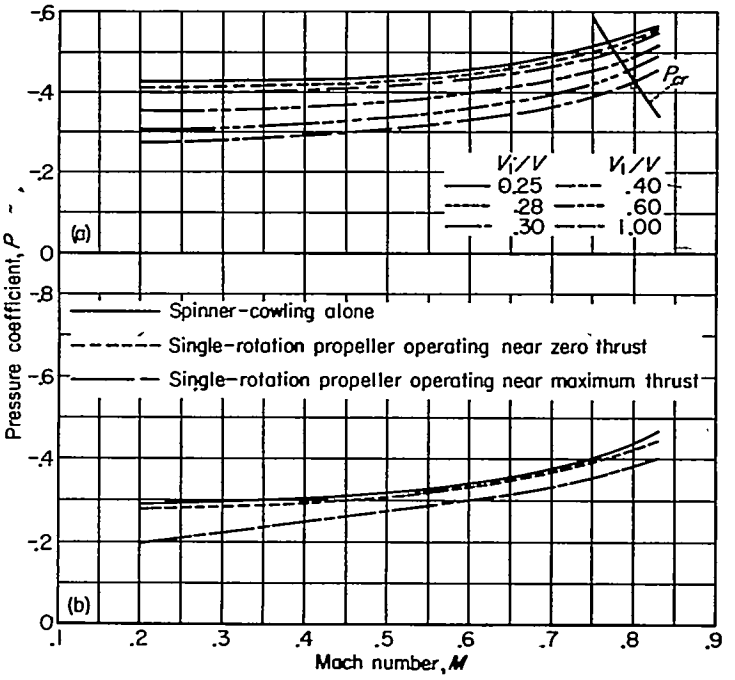

(a) Propeller removed.
(b) Propeller operating, $V_1/V=0.8$.

FIGURE 28.—The effect of Mach number and propeller operation on the minimum pressure coefficient on the external surface of the NACA 1–62.8–070 cowling, single-rotation propeller-spinner-cowling combination.

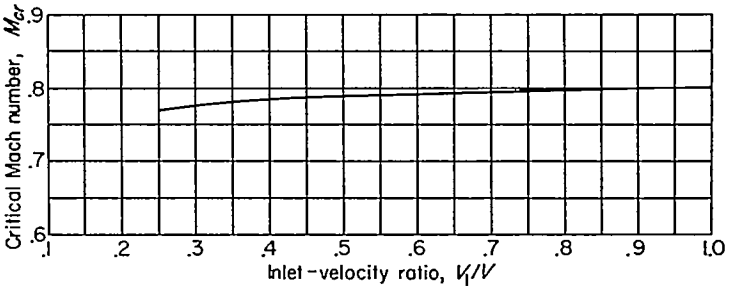

FIGURE 29.—The effect of inlet-velocity ratio on the critical Mach number of the NACA 1–46.5–047 spinner and NACA 1–62.8–070 cowling combination.

AMES AERONAUTICAL LABORATORY
NATIONAL ADVISORY COMMITTEE FOR AERONAUTICS
MOFFETT FIELD, CALIF., *August 14, 1957*

APPENDIX

THE 1000-HORSEPOWER PROPELLER DYNAMOMETER OF THE AMES 12-FOOT PRESSURE WIND TUNNEL

GENERAL ARRANGEMENT

Sketches, coordinates, and photographs of the single-rotation propeller dynamometer are presented in figure 1, and a cutaway view of the internal mechanism is presented in figure 30. The dynamometer has a rating of 1000 horsepower at 6600 revolutions per minute. Speed control of the two-pole induction motor is accomplished by means of a variable-frequency power supply.

For the testing of dual-rotation propellers, the single-rotation dynamometer was modified by the installation of a gear box within the dynamometer housing and separate torquemeters on each of the two concentric propeller drive shafts. The torquemeters were mounted on the drive shafts between the propellers and the gear box so that mechanical losses in the gear box would not be present in the measured torque. The two drive shafts had the same rotational speed.

The dynamometer is made up of two major subassemblies, the fixed external housing and the floating dynamometer unit, interconnected structurally at two flexure-pivot supports. The fixed external housing is comprised of the shroud, main housing, tail cone, support struts, shroud for the box beam, thrust strain-gage members, and motor stator torque-restraining member. The components of the floating dynamometer unit are the spinner, propeller-hub assembly, drive shafts, torquemeters, motor, box beam (for support of electrical, lubricant, air, and coolant leads), inside member of the mercury seal, and the dynamometer housing.

The flexure pivots carry, in tension, the weight of the floating unit and provide restraint against lateral motion. When the flexure pivots and their supports are deflected longitudinally by a thrust load, they produce a moment equal and opposite to the moment produced by the weight of the floating dynamometer unit. This assembly, as supported on the flexure-pivot supports, is thus neutrally stable longitudinally.

Restraint of the floating dynamometer unit against longitudinal motion is accomplished by means of a pair of cantilever beams with strain gages. These beams are fixed to the main housing and linked to the dynamometer housing. The links are parallel to and equidistant from the dynamometer center line.

The manner in which the motor stator is mounted in the dynamometer housing permits nearly frictionless longitudinal motion of the floating dynamometer unit without the motor-stator torque reaction being transmitted through the flexure pivots to the fixed housing. The motor stator is supported on trunnion bearings and is restrained against rotational movement by a pair of forked torque arms which are attached to the motor stator and fit over a corresponding pair of radial ball bearings supported by the fixed structure. The reaction forces in the arms form a couple about the center line of the dynamometer. The inner races of the radial bearings are continuously rotated by a motor drive in

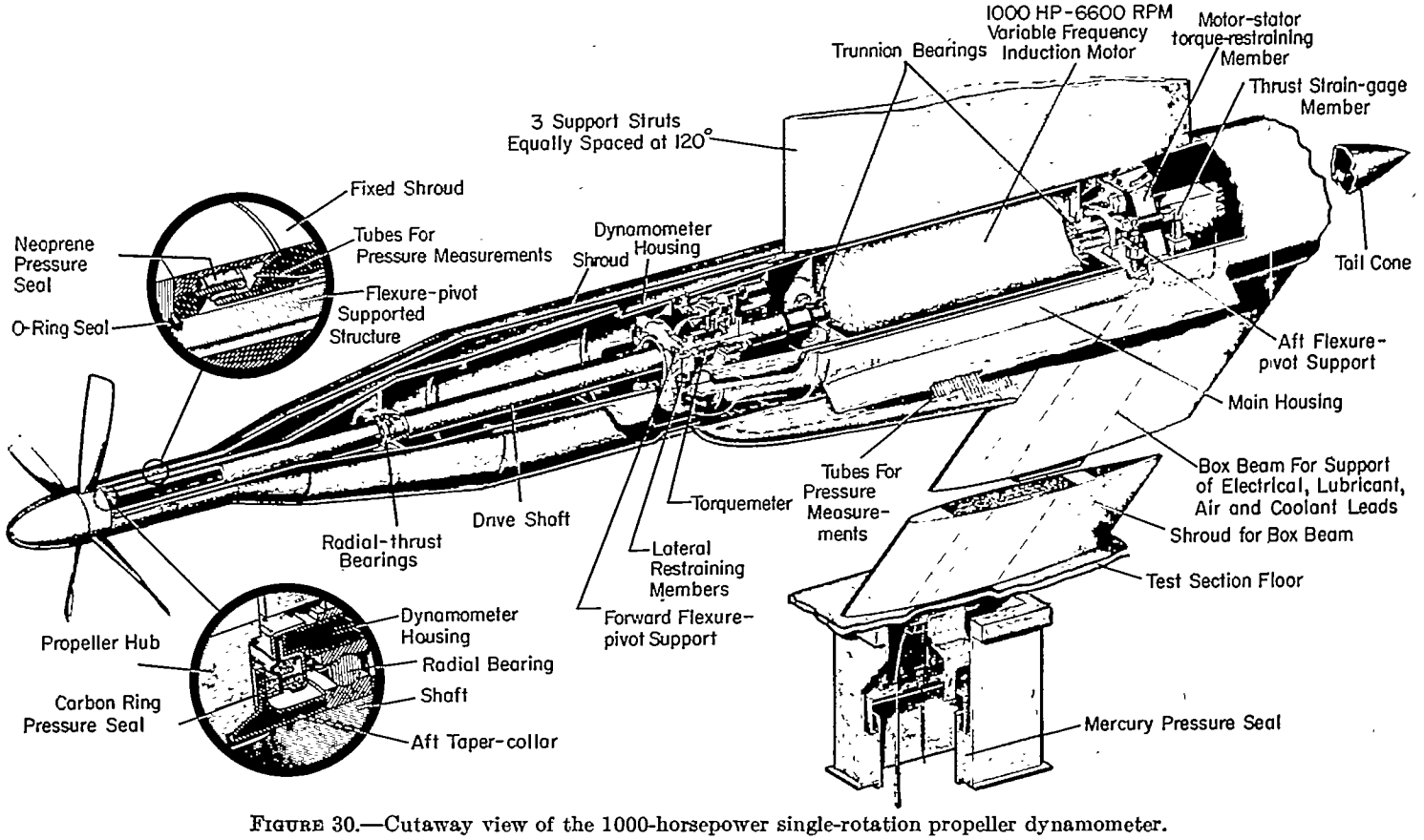

FIGURE 30.—Cutaway view of the 1000-horsepower single-rotation propeller dynamometer.

order that only the difference between the rolling friction of the bearings is present in the thrust system.

Control of the air pressure inside of the dynamometer is maintained during its operation. Air is introduced through the oil-mist lubrication system for the motor and drive shaft bearings. Air and oil mist is scavenged from the dynamometer by vacuum pumps. Three types of pressure seals (see fig. 30) are employed to separate the inside of the dynamometer from the wind tunnel. A flexible, neoprene pressure seal joins the floating dynamometer unit to the fixed shroud a short distance behind the propeller spinner. A carbon ring, bonded to a molded neoprene diaphragm and spring retained against the back face of the rear propeller-hub taper collar provides a pressure seal between the dynamometer housing and the rotating drive shaft. A mercury pressure seal, beneath the box-beam shroud and the floor of the test section, separates the interior of the dynamometer from the wind-tunnel balance chamber. In addition, for installations of the dual-rotation propellers, molded neoprene ring seals, fixed to the rear hub and bearing on a journal on the front hub, sealed the dynamometer at the gap between the dual-rotation propeller hubs.

All electrical, lubricant, air, and coolant leads entering the dynamometer pass through airtight packing glands in the floating member of the mercury pressure seal. The leads swing freely in a long loop from the floating member of the mercury seal to brackets which secure them to stationary structure in the balance chamber.

INSTRUMENTATION AND CALIBRATIONS

THRUST

Propeller thrust, as noted in REDUCTION OF DATA, is the thrust of the propeller-spinner combination indicated by the cantilever-beam strain gages linking the fixed and floating portions of the dynamometer, plus the spinner drag tare force, and minus the thrust due to pressures acting between the floating and fixed members of the dynamometer. The cantilever-beam strain gages, having thrust capacities of either 1500 or 750 pounds per pair, were calibrated together with a self-balancing potentiometer, by applying known thrust loads to the propeller shaft with the dynamometer, complete with all fairings, leads, and hoses, installed in the wind tunnel. All calibration data were treated uniformly by use of the method of least squares, giving straight-line calibrations having errors in indicated thrust of less that 1 percent of the applied load, except for the small-load range (less than 25 pounds) where larger percentage errors would be expected. The spinner drag tare forces were measured by operating the dynamometer, complete except for the propeller blades, in the wind tunnel at velocities, densities, and rotational speeds nearly identical to those for the propeller tests. The pressures exerted on spinner surfaces inside and outside the neoprene pressure seal between the fixed and floating parts of the dynamometer, and inside and outside concentric-ring labyrinths on the extended cylindrical spinners, were measured, and the products of these pressures and the areas on which they acted were applied as corrections to the indicated thrust. Control of the internal dynamometer pressure was maintained by regulation of the vacuum pumps in a manner such that the pressure inside the neoprene seal was always less than the pressure outside the seal. The pressure inside the dynamometer was also measured at three widely separated locations throughout the dynamometer, and no data were recorded until the pressures at these locations and the pressures inside and immediately adjacent to the neoprene pressure seal were equalized. Because of this pressure seal arrangement, it was necessary to use some reference pressure for the spinner base pressure in order to obtain a value for the spinner drag tare. The choice of reference pressure is immaterial insofar as the propeller thrust is concerned since, in applying the spinner drag tare to the thrust of a propeller-spinner combination, the reference pressure appears in both terms but of opposite sign, and hence is eliminated. Free-stream static pressure was therefore assumed as the spinner base pressure, primarily for computational convenience. The spinner drag tare forces for all the spinners except the 12.0-inch-diameter, extended cylindrical spinner include the skin-friction drag of the cylindrical portion of the dynamometer behind the spinner, back to and including the cover plates over the neoprene pressure seal. The spinner drag tare forces as evaluated from the tare runs were found to be independent of rotational speed and, for constant Reynolds number, dependent on tunnel Mach number and inlet-velocity ratio only.

TORQUE

The torque produced in the propeller shafts is measured by means of General Electric Company variable-reluctance-type torquemeters with capacities of 800 and 400 pound-feet, respectively, for the single- and dual-rotation dynamometers. Calibrations of the torquemeters together with potentiometers were made to determine the characteristics of the torquemeters when subjected to torque loads while stationary (static calibrations) and while rotating (dynamic calibrations). All calibrations, both static and dynamic at constant rotational speeds, were treated uniformly by the method of least squares, giving linear calibrations having errors in indicated torque of less than ½ percent of the applied torque, except in the small-load range. Repeated dynamic calibrations at constant rotational speeds agreed with one another within probable errors of ¼ percent for each installation of the dynamometer. The calibration constants for zero rotational speed as extrapolated from the dynamic calibrations showed fair agreement with the slopes obtained in the static calibrations. There were no significant differences between dynamic calibrations made with the propeller shafts rotating under combined thrust and torque loads and dynamic calibrations made with no thrust loads.

ROTATIONAL SPEED

A frequency meter, having as an input the current produced by a variable-reluctance alternating-current generator mounted on the motor shaft, indicates the rotational speed of the propeller drive shafts within an accuracy of ⅛₀ percent in the speed range between 240 and 6600 revolutions per minute.

AIR-STREAM VELOCITY

Surveys of the local Mach number in the vicinity of the propeller plane were made with the dynamometer installed in the wind tunnel. At radii of 0.17, 0.33, 0.63, and 1.04 propeller diameters from the dynamometer center line, local Mach numbers were measured at seven stations spaced over a longitudinal distance from 0.35 propeller diameters ahead of the propeller plane to 0.77 propeller diameters behind the propeller plane for both the 1-series and extended cylindrical spinners. Local Mach numbers along the tunnel wall were obtained at 25 orifices spaced over a distance from 1.6 propeller diameters ahead of the propeller plane to 2.5 propeller diameters behind the propeller plane. Also, local Mach number distributions on the surface of the 7.2-inch-diameter, 1-series spinner and the forebody of the dynamometer were measured on a mock-up of the dynamometer. Some typical results of these surveys are shown in figure 31, and a summary of the radial variation of local Mach number at the propeller plane of rotation for the various spinners is presented in figure 32.

The reference Mach numbers given in these figures are averages of the local Mach numbers at the five wall orifices on one side of the dynamometer and immediately adjacent to the propeller plane.

In order to obtain a theoretical confirmation of the radial and longitudinal Mach number gradients measured by tunnel air-stream surveys, the dynamometer body was represented by a longitudinal source-sink distribution of varying strength in a uniform flow field. Calculations of the radial and longitudinal Mach number gradients induced in various planes by the assumed source-sink distribution were made using the equations developed in reference 24, modified for compressibility effects as indicated in reference 25. The results of these calculations confirm the general magnitude and trend of the radial and longitudinal Mach number gradients and indicate that the radial variation of Mach number in the plane of the propeller, for the extended cylindrical spinner, was due to the presence of the dynamometer body downstream of the propeller.

Because it was felt that any differences in propeller performance due to local effects of the 1-series spinners on the propeller flow field should be chargeable to the propeller-spinner combination, the choice was made to base the test Mach number on the radial distributions of local Mach number obtained with the 7.2-inch-diameter, extended cylindrical spinner. Accordingly, the test Mach number was taken as the average Mach number over the propeller disc area, obtained by integration, within the limits of the spinner surface and the propeller tip, of the local Mach numbers shown in figure 32 (b) replotted versus the square of the radius.

REFERENCES

1. Delano, James B., and Carmel, Melvin M.: Investigation of the NACA 4–(5)(08)–03 Two-Blade Propeller at Forward Mach Numbers to 0.925. NACA RM L9G06a, 1949.
2. Delano, James B., and Harrison, Daniel E.: Investigation of the NACA 4–(4)(06)–04 Two-Blade Propeller at Forward Mach Numbers to 0.925. NACA RM L9I07, 1949.
3. Delano, James B., and Morgan, Francis G., Jr.: Investigation of the NACA 4–(3)(08)–03 Two-Blade Propeller at Forward Mach Numbers to 0.925. NACA RM L9I06, 1949.
4. Carmel, Melvin M., and Milillo, Joseph R.: Investigation of the NACA 4–(0)(03)–045 Two-Blade Propeller at Forward Mach Numbers to 0.925. NACA RM L50A31a, 1950.
5. Carmel, Melvin M., Morgan, Francis G., Jr., and Coppolino, Domenic A.: Effect of Compressibility and Camber as Determined From an Investigation of the NACA 4–(3)(08)–03 and 4–(5)(08)–03 Two-Blade Propellers Up to Forward Mach Numbers of 0.925. NACA RM L50D28, 1950.
6. Platt, Robert J., Jr., and Shumaker, Robert A.: Investigation of the NACA 3–(3)(05)–05 Eight-Blade Dual-Rotating Propeller at Forward Mach Numbers to 0.925. NACA RM L50D21, 1950.
7. Swihart, John M.: Experimental and Calculated Static Characteristics of a Two-Blade NACA 10–(3)(062)–045 Propeller. NACA RM L54A19, 1954.
8. Webb, Dana A., and Willer, Jack E.: Propeller Performance at Zero Forward Speed. WADC TR 52–152, Wright Air Development Center, July 1952.
9. Gray, W. H., and Gilman, Jean, Jr.: Characteristics of Several Single- and Dual-Rotating Propellers in Negative Thrust. NACA WR L–634, 1945. (Supersedes NACA MR L5C07)
10. Hanson, Frederick H., Jr., and Mossman, Emmet A.: Effect of Pressure Recovery on the Performance of a Jet-Propelled Airplane. NACA TN 1695, 1948.
11. Nichols, Mark R., and Keith, Arvid L., Jr.: Investigation of a Systematic Group of NACA 1-Series Cowlings With and Without Spinners. NACA Rep. 950, 1949. (Formerly NACA RM L8A15)
12. Pendley, Robert E., and Smith, Norman F.: An Investigation of the Characteristics of Three NACA 1-Series Nose Inlets at Subcritical and Supercritical Mach Numbers. NACA RM L8L06, 1949.
13. Keith, Arvid L., Jr., Bingham, Gene J., and Rubin, Arnold J.: Effects of Propeller-Shank Geometry and Propeller-Spinner-Juncture Configuration on Characteristics of an NACA 1-Series Cowling-Spinner Combination With an Eight-Blade Dual-Rotation Propeller. NACA RM L51F26, 1951.
14. Bingham, Gene J., and Keith, Arvid L., Jr.: Effects of Compressibility at Mach Numbers Up to 0.8 on Internal-Flow Characteristics of a Cowling-Spinner Combination Equipped With an Eight-Blade Dual-Rotation Propeller. NACA RM L53E12, 1953.
15. Crigler, John L., and Talkin, Herbert W.: Charts for Determining Propeller Efficiency. NACA WR L–144, 1944. (Formerly NACA ACR L4I29)
16. Uddenberg, R. C.: Characteristics and Design of Shielded Total-Head Tubes. Rep. D–4265, Boeing Aircraft Co., Aug. 28, 1942.
17. Herriot, John G.: Blockage Corrections for Three-Dimensional-Flow Closed-Throat Wind Tunnels, With Consideration of the Effect of Compressibility. NACA Rep. 995, 1950. (Formerly NACA RM A7B28)
18. Young, A. D.: Note on the Application of the Linear Perturbation Theory to Determine the Effect of Compressibility on the Wind Tunnel Constraint on a Propeller. TN No. Aero. 1539, RAE (British) 1944.
19. Smith, Norman F.: Numerical Evaluation of Mass-Flow Coefficient and Associated Parameters from Wake-Survey Equations. NACA TN 1381, 1947.
20. Crigler, John L.: Comparison of Calculated and Experimental Propeller Characteristics for Four-, Six-, and Eight-Blade Single-Rotating Propellers. NACA WR L–362, 1944. (Supersedes NACA ACR 4B04)
21. Gilman, Jean, Jr.: Analytical Study of Static and Low-Speed Performance of Thin Propellers Using Two-Speed Gear Ratios to Obtain Optimum Rotational Speeds. NACA RM L52I09, 1952.
22. Glauert, H.: Airplane Propellers. Body and Wing Interference, Vol. IV, div. L, ch. VIII of Aerodynamic Theory, W. F. Durand, ed., Julius Springer (Berlin), 1935. (CIT reprint, 1943)

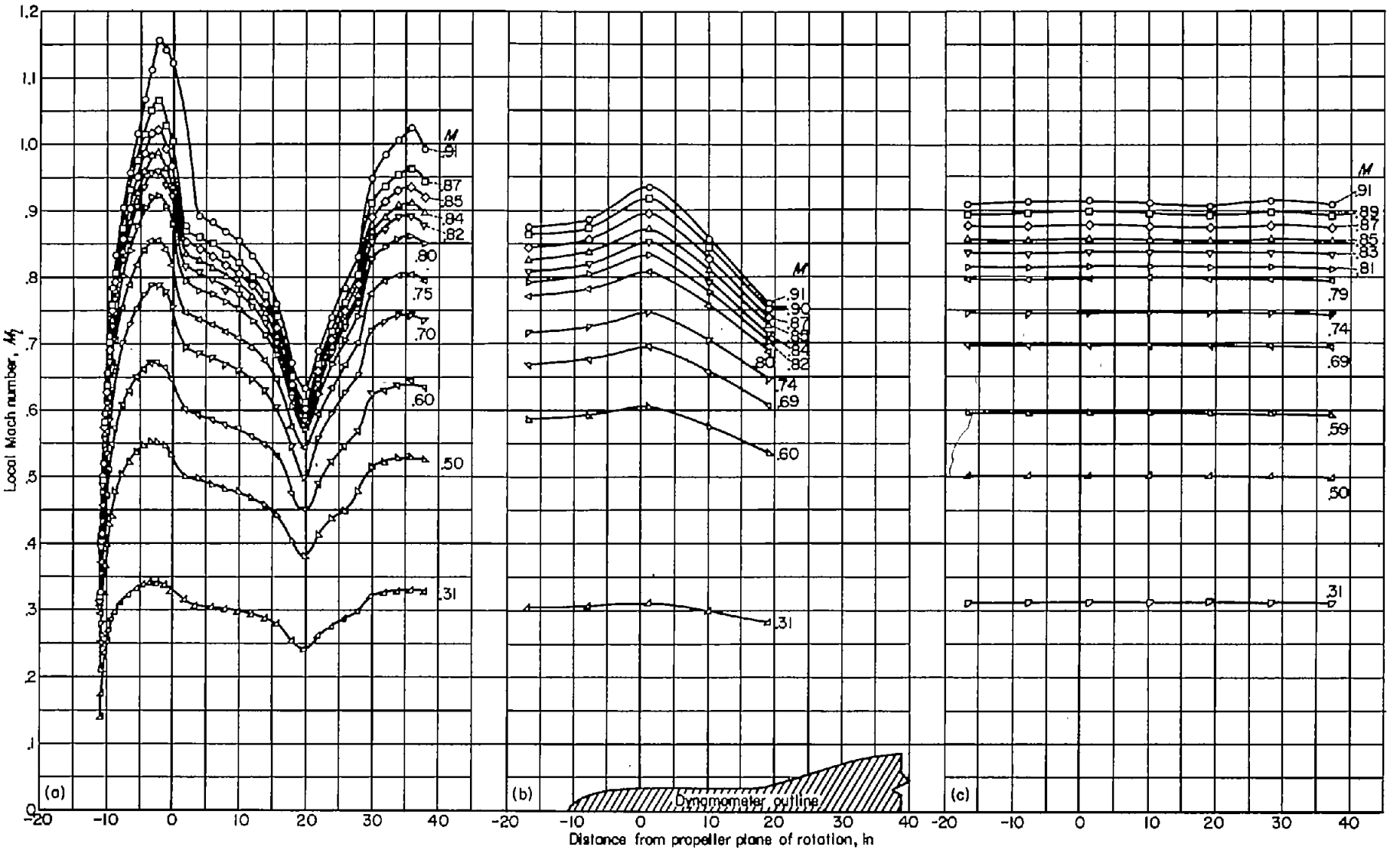

(a) At the dynamometer surface.
(b) 8 inches from the dynamometer center line.
(c) 50 inches from the dynamometer center line.

Figure 31.—The longitudinal variation of the local Mach number for the dynamometer with the 7.2-inch-diameter, 1-series spinner.

23. Boswinkle, Robert W., Jr., and Keith, Arvid L., Jr.: Surface-Pressure Distributions on a Systematic Group of NACA 1–Series Cowlings With and Without Spinners. NACA RM L8I24, 1948.
24. Prandtl, L.: Applications of Modern Hydrodynamics to Aeronautics. NACA Rep. 116, 1921.
25. Boltz, Frederick W., and Beam, Benjamin H.: The Effects of Compressibility on the Pressures on a Body of Revolution and on the Aerodynamic Characteristics of a Wing-Nacelle Combination Consisting of the Body of Revolution Mounted on a Swept-Back Wing. NACA RM A50E09, 1950.

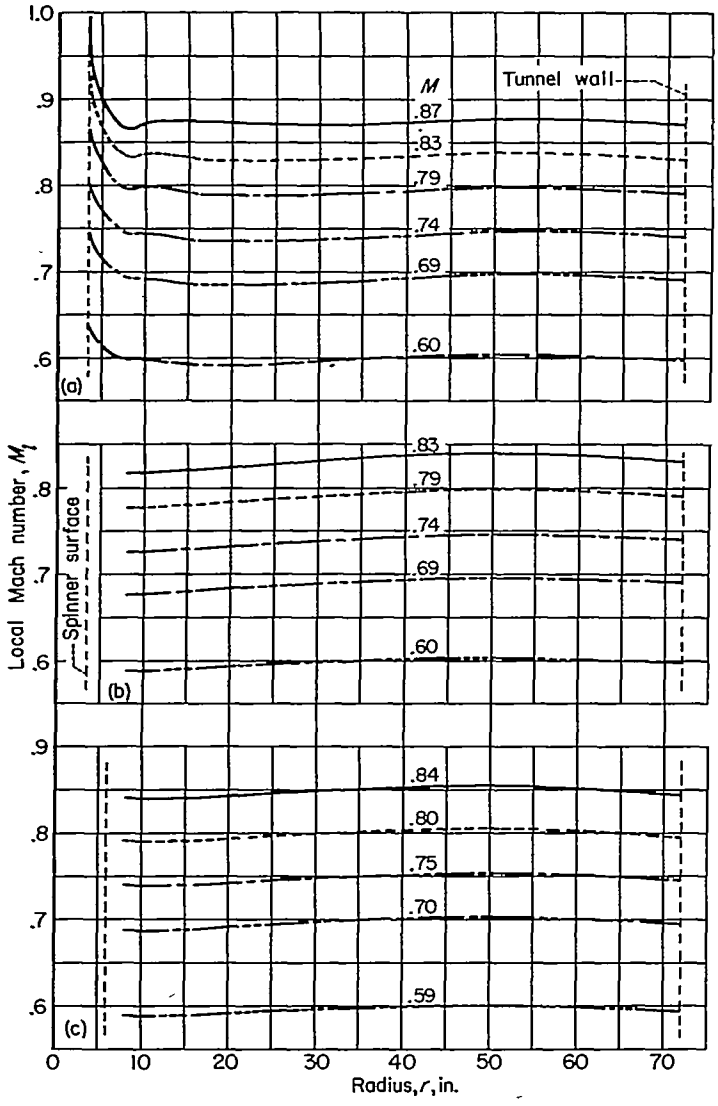

(a) 7.2-inch-diameter, 1-series spinner.
(b) 7.2-inch-diameter, extended cylindrical spinner.
(c) 12.0-inch-diameter, extended cylindrical spinner.

FIGURE 32.—The radial variation of the local Mach number at the propeller plane of rotation for various spinners.

TABLE I.—TEST CONDITIONS FOR PROPELLER-SPINNER-COWLING COMBINATIONS

Propeller	Spinner	Cowl	Propeller-spinner juncture	Mach number range	Reynolds number per foot, million	β or β_r, deg	$\Delta\beta$	Advance-ratio range	Inlet-velocity ratio range	Thrust	Measured quantities
Single-rotation, B=4	7.20-in.-diam., 1-series	Off	Ideal	0.10 to 0.90	1.5	15 to 70	----------	0.4 to 7.2	----------	Positive	Propeller thrust, torque, and rotational speed
	7.20- and 12.00-in.-diam., extended cylindrical			.59 to .83		55, 60, 65	----------	2.6 to 5.6	----------		
	7.20-in.-diam., 1-series			----------	----------	0, 10, 15, 20	----------	----------	----------	Static	
	NACA 1-46.5-047			.10 to .20	1.0	−15 to 25	----------	.5 to 7.0	----------	Negative	
				.20 to .82	1.5	40, 50, 60	----------	1.3 to 4.3	----------	Positive	
		NACA 1-62.8-070	Ideal and platform	.20 to .83		ditto	----------	1.3 to 4.4	0.27 to 1.30	Positive	Propeller thrust, torque, and rotational speed Inlet pressure recovery and mass flow Cowling surface pressure distributions
Off			----------	.20 to .83		----------	----------	----------	.26 to 1.33	----------	Inlet pressure recovery and mass flow Velocity surveys in propeller planes
Dual-rotation, B=6	6.51-in.-diam., 1-series	Off	Ideal	.60 to .80	1.0	65	Optimum	2.8 to 4.9	----------	Positive	Propeller thrust, torque, and rotational speed
			Platform	.15 to .84		15 to 70		0.6 to 6.3			
				.60 to .90		65, 70	0.8	2.9 to 6.7	----------	Positive	
				.15 to .84		−20 to 70	Optimum	.6 to 31.5	----------	Negative	
				.60 to .90		65, 70	0.8	4.6 to 32.4	----------	Negative	
				----------	----------	10, 15, 20, 25	Optimum	----------	----------	Static	
	NACA 1-46.5-085			.60 to .90	1.0	65	0.8	2.9 to 5.0	----------	Positive	
		NACA 1-62.8-070		.30 to .80		40 to 70	0.8	1.1 to 6.9	.28 to 1.08	Positive	Propeller thrust, torque, and rotational speed Inlet pressure recovery and mass flow
Off			----------	.30 to .84		----------	----------	----------	.28 to 1.09	----------	Inlet pressure recovery and mass flow Velocity surveys in propeller planes
Dual-rotation, B=8	6.51-in.-diam., 1-series	Off	Platform	.15 to .84	1.0	15 to 65	Optimum	0.5 to 5.1	----------	Positive	Propeller thrust, torque, and rotational speed
				.60 to .90		65, 70	0.8	3.4 to 6.7	----------	Positive	
				.15 to .84		−20 to 65	Optimum	.5 to 34.6	----------	Negative	
				.60 to .80		65, 70	0.8	4.8 to 13.7	----------	Negative	
				----------	----------	15, 20	0	----------	----------	Static	
	NACA 1-46.5-085	NACA 1-62.8-070		.30 to .84	1.0	40 to 70	0.8	1.2 to 6.9	.27 to 1.06	Positive	Propeller thrust, torque, and rotational speed Inlet pressure recovery and mass flow
			Ideal	.80		65		3.6 to 5.3	.31 to .96		

TABLE II.—LOCAL VELOCITY RATIO, V_l/V

(a) NACA 1–46.5–047 single-rotation spinner

Radial station, in.	M=0.30					M=0.40					M=0.60						
	Inlet-velocity ratio, V_l/V					Inlet-velocity ratio, V_l/V					Inlet-velocity ratio, V_l/V						
	0.39	0.61	0.80	1.00	1.30	0.39	0.63	0.81	1.03	1.30	0.29	0.35	0.50	0.59	0.78	1.00	1.32
3.47	0.820	0.902	0.929	0.956	0.986	0.815	0.904	0.927	0.952	0.983	0.836	0.852	0.871	0.883	0.912	0.936	0.959
3.72	.817	.895	.932	.949	.983	.810	.894	.917	.945	.973	.828	.845	.862	.876	.898	.928	.948
3.97	.822	.887	.914	.938	.965	.818	.888	.909	.933	.962	.826	.840	.855	.867	.893	.916	.936
4.47	.843	.887	.908	.925	.948	.838	.886	.901	.919	.942	.829	.838	.850	.859	.881	.900	.915
4.97	.859	.896	.900	.914	.930	.855	.895	.898	.908	.926	.841	.849	.855	.864	.878	.892	.907
5.47	.859	.910	.917	.924	.934	.853	.903	.908	.916	.928	.865	.869	.873	.876	.888	.895	.907
5.97	.912	.926	.929	.933	.939	.906	.915	.921	.926	.933	.890	.890	.892	.893	.902	.909	.914
6.47	.925	.932	.936	.936	.939	.921	.928	.928	.931	.939	.903	.902	.905	.907	.912	.912	.919
7.47	.955	.955	.959	.959	.959	.948	.950	.950	.948	.950	.934	.933	.931	.931	.933	.936	.936
8.47	.974	.971	.971	.968	.971	.971	.968	.968	.968	.971	.957	.955	.955	.954	.955	.955	.955
9.47	.983	.983	.980	.984	.980	.985	.982	.980	.980	.980	.974	.973	.971	.971	.969	.969	.969
10.47	.982	.979	.979	.976	.976	.982	.980	.977	.980	.980	.974	.972	.971	.969	.967	.969	.967
12.47	.998	.995	.992	.995	.992	.995	.993	.990	.990	.990	.987	.987	.986	.988	.984	.984	.984
14.47	.997	.997	.997	.997	.994	1.002	1.000	.997	.994	.997	.996	.994	.996	.992	.992	.991	.991
16.47	.995	.999	.995	.999	.992	.999	.999	.996	.993	.996	.997	.997	.995	.995	.993	.993	.993
18.47	.998	1.001	1.001	.998	.994	.999	.999	.996	.999	.996	1.000	.998	.998	.998	.998	.997	.997
20.47	1.000	1.004	1.003	1.003	1.000	1.008	1.005	1.003	1.005	1.005	1.006	1.004	1.002	1.002	.999	1.001	1.001
22.47	1.000	1.000	1.000	1.000	.997	1.007	1.004	1.002	1.002	1.004	1.005	1.005	1.003	1.001	1.001	1.001	1.001
24.47	1.003	1.006	1.002	1.006	1.002	1.006	1.003	1.003	1.003	1.006	.995	.995	.995	.992	.994	.992	.992
26.47	1.005	1.008	1.005	1.005	1.001	1.005	1.007	1.005	1.005	1.005	1.008	1.008	1.008	1.006	1.006	1.005	1.006
28.47	1.004	1.004	1.000	1.004	1.000	1.004	1.004	1.004	1.004	1.004	1.008	1.006	1.006	1.006	1.004	1.004	1.004
30.47	1.001	1.001	1.004	1.004	1.000	1.003	1.005	1.003	1.003	1.003	1.005	1.003	1.003	1.000	1.002	1.002	1.002
32.47	1.010	1.010	1.010	1.009	1.006	1.007	1.004	1.004	1.004	1.004	1.007	1.007	1.006	1.004	1.005	1.005	1.005

Radial station, in.	M=0.70						M=0.80						M=0.84					
	Inlet-velocity ratio, V_l/V						Inlet-velocity ratio, V_l/V						Inlet-velocity ratio, V_l/V					
	0.30	0.38	0.47	0.62	0.80	1.16	0.31	0.39	0.50	0.60	0.80	1.03	0.31	0.40	0.51	0.63	0.85	0.97
3.47	0.824	0.843	0.860	0.875	0.907	0.937	0.799	0.826	0.845	0.864	0.892	0.909	0.787	0.813	0.836	0.854	0.883	0.893
3.72	.815	.836	.851	.866	.900	.930	.789	.817	.836	.853	.884	.899	.776	.807	.828	.851	.877	.887
3.97	.812	.827	.843	.857	.888	.895	.784	.811	.826	.844	.872	.887	.770	.798	.818	.838	.864	.873
4.47	.810	.824	.834	.848	.874	.895	.782	.803	.819	.830	.855	.869	.771	.791	.808	.826	.846	.854
4.97	.824	.833	.840	.848	.867	.885	.794	.811	.821	.830	.849	.862	.780	.797	.809	.824	.841	.848
5.47	.848	.852	.858	.860	.879	.892	.819	.829	.834	.844	.857	.868	.802	.812	.825	.835	.848	.851
5.97	.871	.874	.880	.881	.891	.898	.841	.848	.852	.857	.867	.873	.823	.830	.837	.848	.855	.859
6.47	.895	.898	.891	.890	.897	.903	.857	.860	.862	.866	.874	.879	.840	.844	.850	.855	.860	.864
7.47	.918	.918	.919	.918	.921	.924	.892	.894	.894	.897	.900	.902	.877	.877	.879	.883	.887	.888
8.47	.948	.945	.946	.946	.946	.949	.926	.925	.925	.926	.928	.927	.911	.910	.911	.916	.915	.915
9.47	.964	.964	.963	.963	.963	.963	.948	.947	.946	.946	.948	.946	.933	.931	.933	.937	.937	.934
10.47	.963	.961	.961	.961	.961	.960	.944	.944	.943	.943	.943	.942	.933	.930	.931	.933	.931	.930
12.47	.981	.979	.979	.978	.978	.978	.967	.966	.964	.964	.963	.962	.955	.954	.953	.954	.953	.952
14.47	.984	.990	.990	.988	.988	.987	.980	.979	.977	.979	.979	.978	.971	.966	.969	.971	.968	.967
16.47	.994	.994	.993	.993	.993	.993	.985	.987	.983	.983	.984	.983	.977	.976	.976	.977	.975	.973
18.47	.997	.997	.997	.995	.996	.994	.992	.989	.989	.987	.989	.988	.986	.985	.982	.981	.980	.978
20.47	1.002	1.002	1.002	1.000	1.002	.999	.999	.996	.996	.993	.992	.993	.991	.990	.989	.987	.986	.985
22.47	1.004	1.004	1.004	1.001	1.004	1.001	.999	.999	.998	.998	.998	.995	.994	.992	.990	.993	.989	.989
24.47	.992	.992	.992	.992	.992	.989	.986	.986	.983	.982	.983	.981	.983	.979	.978	.978	.977	.973
26.47	1.006	1.006	1.006	1.004	1.006	1.002	.999	.999	.999	.999	.999	.995	.994	.992	.992	.992	.991	.987
28.47	1.007	1.007	1.007	1.005	1.005	1.002	1.002	1.002	1.000	1.002	.999	.996	.997	.994	.993	.997	.993	.991
30.47	1.003	1.003	1.005	1.003	1.005	1.002	1.004	1.002	1.001	1.001	1.000	.994	.998	.997	.996	.997	.995	.995
32.47	1.003	1.000	1.003	1.002	1.003	1.002	1.003	1.000	1.000	1.000	1.002	.998	1.000	.999	.996	.996	.996	.994

TABLE II.—LOCAL VELOCITY RATIO, V_l/V—Continued.

(b) NACA 1–46.5–085 dual-rotation spinner, front plane of rotation

Radial station, in.	M=0.30						M=0.40						M=0.60					
	Inlet-velocity ratio, V_l/V						Inlet-velocity ratio, V_l/V						Inlet-velocity ratio, V_l/V					
	0.29	0.39	0.52	0.59	0.80	1.09	0.31	0.41	0.51	0.62	0.82	1.09	0.32	0.40	0.50	0.58	0.80	1.05
3.26	0.949	0.959	0.963	0.966	0.976	0.983	0.945	0.957	0.962	0.965	0.972	0.978	0.952	0.952	0.957	0.969	0.971	0.974
3.51	.953	.963	.966	.969	.980	.983	.947	.959	.962	.967	.975	.980	.950	.949	.954	.962	.971	.978
3.76	.949	.959	.963	.963	.973	.983	.945	.952	.959	.962	.967	.975	.947	.950	.954	.959	.964	.971
4.01	.938	.945	.952	.955	.962	.972	.933	.944	.950	.952	.956	.967	.935	.940	.945	.952	.954	.959
4.26	.945	.948	.952	.958	.965	.972	.937	.949	.952	.954	.962	.967	.938	.940	.945	.952	.955	.962
4.76	.932	.942	.948	.948	.958	.965	.925	.938	.941	.943	.951	.959	.930	.933	.936	.943	.950	.954
5.26	.934	.944	.951	.951	.954	.964	.928	.940	.943	.946	.951	.959	.931	.933	.936	.943	.947	.954
5.76	.936	.943	.946	.950	.953	.960	.928	.940	.941	.943	.951	.956	.933	.933	.936	.940	.949	.952
6.26	.933	.940	.943	.943	.950	.956	.928	.938	.941	.943	.948	.956	.933	.933	.936	.940	.947	.948
7.26	.939	.942	.945	.945	.952	.955	.930	.937	.940	.942	.947	.953	.933	.935	.936	.941	.943	.948
8.26	.938	.941	.941	.941	.944	.951	.932	.937	.940	.942	.947	.953	.928	.928	.931	.933	.938	.938
9.26	.956	.964	.964	.967	.970	.967	.952	.959	.964	.962	.964	.967	.952	.952	.954	.959	.962	.962
10.26	.959	.963	.963	.962	.963	.969	.957	.962	.962	.962	.964	.967	.952	.954	.954	.955	.957	.957
12.26	.965	.968	.968	.968	.972	.971	.962	.965	.965	.967	.967	.970	.960	.960	.958	.961	.963	.963
14.26	.971	.971	.971	.970	.971	.974	.965	.967	.970	.970	.972	.975	.962	.960	.961	.961	.965	.963
16.26	.975	.975	.975	.975	.975	.979	.968	.973	.976	.973	.973	.971	.975	.970	.972	.975	.975	.972
18.26	.979	.982	.982	.978	.982	.982	.976	.976	.978	.978	.978	.976	.979	.976	.978	.977	.976	.978
20.26	.983	.987	.987	.983	.987	.987	.981	.984	.987	.984	.984	.979	.989	.987	.989	.989	.987	.987
22.26	.983	.983	.983	.983	.990	.983	.981	.984	.989	.986	.986	.987	.989	.988	.986	.988	.988	.986
24.26	.992	.996	.992	.992	.989	.992	.986	.988	.991	.990	.990	.991	.992	.988	.988	.990	.990	.988
26.26	.991	.995	.995	.995	.991	.988	.987	.989	.992	.987	.989	.992	.996	.991	.993	.992	.993	.991
28.26	.990	.990	.990	.990	.990	.990	.986	.988	.991	.991	.988	.991	.994	.992	.991	.992	.992	.991
30.26	.990	.990	.990	.990	.987	.990	.985	.990	.993	.990	.990	.990	.993	.990	.990	.991	.991	.990
32.26	.989	.993	.989	.989	.989	.993	.984	.988	.989	.986	.986	.987	.991	.991	.991	.991	.989	.989

Radial station, in.	M=0.70						M=0.80						M=0.84					
	Inlet-velocity ratio, V_l/V						Inlet-velocity ratio, V_l/V						Inlet-velocity ratio, V_l/V					
	0.29	0.40	0.50	0.59	0.82	1.06	0.32	0.41	0.48	0.62	0.81	1.00	0.30	0.42	0.47	0.60	0.83	0.95
3.26	0.940	0.950	0.956	0.963	0.969	0.970	0.940	0.945	0.955	0.961	0.965	0.969	0.935	0.944	0.949	0.950	0.961	0.964
3.51	.941	.950	.956	.961	.967	.968	.938	.945	.947	.953	.959	.964	.933	.940	.947	.945	.961	.961
3.76	.934	.944	.950	.955	.961	.964	.934	.941	.947	.952	.960	.963	.929	.936	.942	.944	.955	.955
4.01	.928	.935	.943	.946	.952	.955	.925	.930	.938	.944	.949	.953	.919	.927	.931	.935	.946	.946
4.26	.928	.938	.943	.955	.956	.965	.926	.932	.939	.944	.952	.956	.921	.930	.936	.936	.947	.949
4.76	.919	.929	.932	.939	.945	.947	.916	.924	.928	.935	.941	.947	.911	.919	.925	.931	.936	.938
5.26	.920	.931	.934	.939	.945	.947	.918	.924	.930	.943	.944	.947	.914	.922	.926	.932	.938	.940
5.76	.919	.928	.934	.939	.945	.943	.917	.921	.930	.932	.939	.941	.910	.917	.921	.926	.932	.935
6.26	.917	.926	.934	.937	.942	.943	.917	.921	.928	.931	.937	.940	.910	.918	.922	.926	.932	.932
7.26	.920	.928	.932	.937	.940	.943	.917	.921	.926	.931	.937	.940	.912	.919	.922	.927	.931	.932
8.26	.926	.932	.937	.940	.945	.943	.922	.928	.932	.935	.943	.943	.917	.925	.929	.934	.941	.942
9.26	.943	.949	.952	.955	.957	.965	.937	.940	.948	.948	.955	.956	.933	.937	.938	.945	.952	.951
10.26	.940	.943	.947	.951	.951	.952	.934	.937	.942	.943	.947	.948	.926	.931	.933	.936	.941	.938
12.26	.949	.952	.955	.957	.958	.959	.942	.942	.946	.948	.951	.951	.934	.939	.939	.940	.946	.945
14.26	.953	.955	.955	.957	.963	.965	.942	.944	.946	.947	.949	.951	.936	.940	.939	.940	.946	.944
16.26	.967	.968	.968	.972	.969	.968	.961	.961	.962	.963	.965	.967	.953	.955	.957	.955	.958	.958
18.26	.974	.974	.974	.976	.975	.973	.968	.968	.967	.969	.969	.971	.962	.962	.963	.962	.964	.963
20.26	.983	.985	.985	.987	.985	.982	.978	.980	.980	.979	.980	.980	.970	.972	.971	.970	.972	.971
22.26	.985	.985	.985	.987	.986	.982	.981	.981	.982	.982	.983	.983	.975	.978	.975	.975	.975	.976
24.26	.984	.986	.984	.986	.985	.981	.979	.979	.980	.979	.981	.981	.974	.975	.974	.973	.971	.971
26.26	.991	.994	.991	.993	.990	.992	.985	.985	.984	.984	.985	.984	.977	.977	.979	.976	.976	.973
28.26	.992	.992	.992	.992	.992	.989	.988	.988	.989	.988	.990	.988	.978	.982	.983	.981	.980	.980
30.26	.988	.990	.990	.992	.990	.988	.989	.989	.988	.989	.990	.990	.986	.986	.986	.984	.981	.985
32.26	.988	.988	.988	.990	.988	.985	.988	.986	.986	.985	.987	.987	.981	.982	.982	.981	.980	.979

TABLE II.—LOCAL VELOCITY RATIO, V_l/V—Concluded.

(c) NACA 1–46.5–085 dual-rotation spinner, rear plane of rotation

Radial station, in.	M=0.30						M=0.40						M=0.60					
	Inlet-velocity ratio, V_l/V						Inlet-velocity ratio, V_l/V						Inlet-velocity ratio, V_l/V					
	0.31	0.41	0.52	0.61	0.81	1.09	0.32	0.40	0.48	0.63	0.82	1.08	0.33	0.42	0.50	0.59	0.80	1.08
3.78	0.735	0.802	0.818	0.828	0.862	0.902	0.737	0.787	0.805	0.828	0.855	0.897	0.719	0.755	0.799	0.814	0.847	0.883
4.03	.740	.817	.817	.830	.864	.908	.744	.792	.810	.830	.860	.897	.724	.757	.802	.814	.850	.885
4.28	.757	.807	.820	.830	.861	.901	.754	.794	.813	.830	.855	.892	.738	.764	.800	.814	.843	.878
4.53	.764	.814	.820	.830	.854	.891	.762	.794	.813	.830	.853	.889	.745	.771	.802	.812	.842	.874
4.78	.791	.824	.830	.834	.864	.891	.785	.810	.823	.833	.850	.884	.768	.785	.809	.819	.845	.874
5.28	.816	.830	.836	.839	.870	.894	.807	.824	.829	.837	.857	.878	.788	.802	.816	.826	.847	.873
5.78	.846	.859	.862	.865	.879	.893	.842	.849	.850	.860	.870	.893	.831	.828	.836	.842	.859	.876
6.28	.876	.879	.883	.882	.889	.896	.867	.872	.873	.880	.885	.898	.850	.852	.857	.862	.874	.887
6.78	.893	.893	.896	.896	.902	.909	.890	.890	.890	.895	.898	.898	.869	.873	.874	.876	.885	.895
7.78	.929	.929	.922	.925	.932	.932	.922	.917	.917	.917	.914	.920	.907	.905	.905	.905	.911	.916
8.78	.954	.951	.947	.947	.951	.948	.943	.944	.942	.944	.944	.942	.931	.928	.928	.928	.928	.931
9.78	.974	.967	.970	.967	.970	.967	.962	.964	.959	.962	.962	.957	.961	.957	.957	.957	.955	.961
10.78	.973	.973	.972	.966	.969	.966	.971	.968	.969	.963	.963	.961	.967	.964	.964	.964	.962	.960
12.78	.975	.978	.975	.975	.975	.971	.973	.973	.973	.973	.975	.970	.975	.973	.973	.972	.972	.974
14.78	.986	.986	.986	.983	.983	.983	.984	.982	.982	.984	.982	.982	.985	.984	.984	.984	.984	.987
16.78	.985	.985	.985	.982	.982	.982	.981	.983	.978	.981	.978	.978	.984	.983	.983	.983	.983	.986
18.78	.984	.984	.984	.984	.984	.984	.982	.980	.980	.980	.982	.977	.988	.990	.986	.986	.986	.990
20.78	.993	.990	.987	.987	.987	.983	.989	.989	.986	.989	.986	.984	.996	.994	.992	.990	.992	.990
22.78	.986	.982	.982	.979	.982	.979	.985	.983	.983	.985	.983	.983	.991	.989	.989	.991	.989	.995
24.78	.995	.995	.991	.988	.991	.988	.989	.987	.987	.989	.987	.987	.997	.992	.994	.994	.994	.997
26.78	.991	.995	.995	.991	.995	.991	.989	.989	.989	.992	.989	.984	.995	.995	.995	.995	.995	.997
28.78	.990	.990	.990	.987	.994	.987	.988	.991	.988	.991	.988	.986	.996	.994	.994	.994	.990	.997
30.78	.986	.986	.986	.986	.989	.986	.990	.990	.987	.987	.987	.985	.992	.990	.990	.992	.992	.995
32.78	.989	.989	.989	.989	.989	.989	.986	.986	.984	.984	.984	.981	.990	.990	.990	.990	.990	.995

Radial station, in.	M=0.70						M=0.80						M=0.84					
	Inlet-velocity ratio, V_l/V						Inlet-velocity ratio, V_l/V						Inlet-velocity ratio, V_l/V					
	0.27	0.39	0.49	0.61	0.83	1.05	0.30	0.41	0.50	0.61	0.81	1.00	0.34	0.43	0.50	0.62	0.83	0.95
3.78	0.701	0.745	0.784	0.808	0.839	0.864	0.704	0.754	0.770	0.789	0.817	0.834	0.716	0.745	0.755	0.782	0.810	0.819
4.03	.706	.750	.775	.808	.841	.864	.708	.756	.769	.785	.815	.833	.719	.745	.755	.780	.808	.815
4.28	.718	.751	.786	.805	.835	.858	.714	.754	.770	.785	.815	.827	.721	.745	.753	.778	.807	.814
4.53	.727	.756	.786	.804	.832	.853	.718	.754	.769	.783	.811	.826	.724	.745	.752	.776	.804	.812
4.78	.746	.769	.793	.808	.833	.855	.735	.762	.774	.790	.814	.827	.736	.755	.761	.781	.804	.812
5.28	.770	.786	.799	.814	.835	.850	.753	.772	.782	.793	.815	.826	.751	.762	.769	.786	.804	.810
5.78	.802	.808	.820	.826	.845	.856	.783	.795	.799	.809	.825	.831	.775	.783	.785	.799	.815	.819
6.28	.830	.834	.841	.846	.857	.865	.807	.815	.818	.825	.835	.841	.796	.803	.805	.815	.826	.828
6.78	.853	.855	.855	.861	.869	.876	.827	.833	.837	.838	.849	.853	.817	.820	.821	.827	.838	.840
7.78	.893	.891	.891	.892	.895	.898	.872	.869	.870	.870	.876	.875	.854	.855	.854	.860	.864	.864
8.78	.919	.910	.912	.912	.911	.916	.894	.894	.895	.892	.898	.899	.884	.884	.882	.880	.890	.888
9.78	.952	.943	.948	.945	.947	.948	.932	.932	.931	.927	.931	.930	.921	.920	.918	.919	.922	.919
10.78	.956	.954	.948	.952	.953	.952	.939	.936	.936	.935	.936	.935	.929	.927	.925	.925	.927	.922
12.78	.970	.966	.964	.964	.964	.964	.954	.954	.952	.950	.950	.948	.944	.943	.941	.943	.941	.941
14.78	.983	.979	.981	.981	.977	.976	.972	.969	.968	.967	.966	.966	.963	.964	.960	.963	.962	.957
16.78	.985	.982	.981	.981	.980	.978	.976	.975	.975	.970	.972	.970	.971	.968	.967	.968	.967	.963
18.78	.989	.987	.985	.987	.985	.985	.982	.981	.982	.978	.979	.978	.978	.977	.974	.975	.975	.972
20.78	.997	.990	.993	.991	.989	.990	.991	.988	.988	.983	.986	.982	.984	.982	.978	.981	.980	.976
22.78	.994	.990	.992	.989	.991	.989	.990	.988	.990	.986	.986	.985	.985	.982	.980	.981	.980	.978
24.78	.995	.991	.992	.989	.990	.991	.988	.988	.988	.983	.984	.984	.983	.984	.980	.980	.982	.976
26.78	.997	.994	.994	.993	.995	.994	.988	.991	.990	.988	.987	.987	.988	.986	.980	.987	.982	.976
28.78	.998	.997	.995	.995	.993	.994	.992	.993	.993	.989	.989	.988	.991	.989	.985	.987	.987	.982
30.78	.997	.994	.992	.992	.990	.992	.996	.996	.993	.991	.992	.991	.991	.992	.989	.990	.991	.985
32.78	.993	.992	.990	.993	.990	.989	.991	.990	.991	.985	.986	.985	.986	.985	.984	.985	.984	.978